Profiling Finger-Hand Function of Rheumatoid Arthritis Patients Using a Telerehabilitation Gaming System

by

Daniel Lockery

A Thesis submitted to the Faculty of Graduate Studies of

The University of Manitoba

in partial fulfilment of the requirements of the degree of

DOCTOR OF PHILOSOPHY

Department of Electrical and Computer Engineering

University of Manitoba

Winnipeg

Abstract

The problem considered in this thesis is developing a set of digital features relevant in describing finger-hand function of early-onset rheumatoid arthritis (RA) patients. The premise is based on a novel telerehabilitation gaming system that operates on a store-and-forward design. The solution to this problem was to develop a full-scale gaming platform to examine client movement performance for precision aiming tasks based on a set of digital features. To complement the movement performance, still imagery in three unique poses are captured during a session to detect visual symptoms during disease activity and early warning signs of deformities that can arise from joint damage. Resulting data is gathered in a clinic or housed in a content management system where features are extracted and analyzed, providing reports/queries for care providers and allowing remote monitoring. The goal is to help automate monitoring patient finger-hand function between office visits from a remote location, on a smaller scale and with minimal supervision. The contributions presented in this work include development of a detailed set of digital features derived from a custom built gaming platform to highlight client movement performance and algorithms to extract hand structure to approximate goniometry measurements of joint angles monitoring for potential changes during progression of the disease. The significance of this contribution is that it provides a readily accessible, experimental platform for the provision of physical therapy tailored to the individual RA patient through the use of a telerehabilitation gaming platform.

Keywords: Telerehabilitation, rheumatoid arthritis, finger-hand function, serious games, feature values, movement performance analysis, image analysis, goniometry.

Acknowledgements

There are many people that have been a great help to me on this journey and it has been my privilege to know and work with all of them. A special thanks to my advisor, Dr. J.F. Peters has been a constant source of encouragement with great vision and without which, none of this would have been possible. Many thanks to my advisory committee, Dr. McLeod, Dr. Hossein and Dr. Szturm, I appreciate your suggestions and also your time and effort in support of this endeavour. Similarly, I'd like to thank my external examiner Dr. Jain, I appreciate your time and consideration of my work. Also, I need to thank CILab friends, both past and present for putting up with me and helping suggest ideas when I back myself into a corner. In addition, I would like to thank the Canadian Institute of Health Research (CIHR) and the Canadian Arthritis Network (CAN) for their generous support, without which this also would not have been possible. Finally, a huge thanks to my family and friends for putting up with me and also for making do without me during the busier times and to those that did not make it to the end with me, you will be missed.

Contents

List of Tables

List of Figures

1 Introduction

Current methods for treatment of rheumatoid arthritis (RA) patients upon diagnosis are early and aggressive as delays can greatly affect the long term prognosis and quality of life [3, 69, 84]. Rheumatoid arthritis is a disease that affects joints in the human body, some of the most commonly reported in early onset stages are in the feet, wrist and hands, specific to the hands are metacarpophalangeal (MCP) and proximal interphalangeal (PIP) joints in the fingers [3,76,99]. Long term treatment of the disease is an ongoing process that requires periodic re-assessment [84]. As with most healthcare treatment plans, periodic re-assessment requires in-office or clinical visits to determine the current prognosis and decide upon the next steps in treatment. The work presented in this thesis presents a novel idea for a telerehabilitation gaming platform, targeting hand movement that is able to measure and rate movement performance of precision goal-directed aiming tasks during a game session and capture supporting visual information of the hands to report on both, from either home/remote or in a clinical setting.

1.1 Motivation

Rheumatoid arthritis is an autoimmune disease that is not fully understood from the perspective of causation or a cure [84]. The more general category of arthritis, which RA belongs to is reported as a leading cause of disability and a burden on the healthcare system to an estimated cost of 33 billion dollars a year in Canada [136]. Treatment typically consists of a multi-faceted approach through educating patients on their condition, drug treatment plans and physical therapy [84]. This implies that treatment of the disease is an ongoing process. The early stages of treatment upon diagnosis typically follow an aggressive plan that includes drugs that can have some serious side effects and can also take a significant amount of time for uptake, in the range of 2 to 24 weeks [3, 69, 84]. Recommended periodic patient evaluation is often every 2-3 months [84] to assess disease activity, response

to drugs and overall health. Studies have noted that in the early stages of the disease, left untreated, damage can occur to the joints within the first year that can significantly affect long term prognosis [92]. The arguments for early treatment are significant as not everyone responds to drug treatment the same way [84]. The time it takes to manifest tangible benefits or side-effects and then potentially requirement of a change to alternative treatment can be vital considering that damage to joints can be ongoing without proper management (and can occur without pain) [84].

A potential supplement or back-channel of information between office-visits could be provided through the use of a telerehabilitation system that is able to gather key details about patient condition. This includes reporting on several dimensions, movement performance, self-reported condition and visual elements of the hands. The hands were selected as they have been reported to contain some of the most commonly affected joints (MCP,PIP) in early onset RA patients [76] and also they are a good indicator of quality of life based on their importance in daily activities. Considering the sensitivity of the early onset treatment period, providing regular automated updates or only when problematic conditions occur would likely be of benefit to all involved in customizing treatment plans and potentially reducing any potential damage that may occur if left unmonitored over longer periods of time.

1.2 Goals and objectives

The objective of this research is to describe the design and operation of a telerehabilitation gaming platform intended for use by RA patients to monitor performance and progress as part of a physiotherapy treatment program during the early onset stages of the disease. The key hypothesis is that I believe it is possible to describe patient condition well enough to help support a treatment plan through development of a set of digital features extracted from a telerehabilitation gaming session. This will be achieved through development of a custom built gaming platform that has a novel reporting system that provides movement

performance data directly relating to precision aiming tasks during game play. Through post processing and analysis of the data, it is possible to monitor progress of the individual to discover if common tasks are becoming more difficult or easier for them through continued use of the system. In addition, visual features in the form of computer assisted goniometry measures and joint characteristics will be measured from still imagery in specific hand poses to look for common problems and symptoms that can occur in RA as part of the inflammation process and potential complications that can arise from joint damage that can lead to deformities. Verification and experimental work will be done to prove the concepts and utility of the system as a means to keep track of patients in between office visits during the critical early stages of treatment. Resulting output data can either be processed by interested parties to examine their patient data or an alternative content management system (CMS) will be built to house the data and automate the process. For out of control values, automatic notifications can be provided alerting both the patient and primary care-giver that a potential problem has been found in the data and that action to prevent damage needs to be taken. Results from the verification and experimental work will be evaluated to select the most robust features to describe patient condition.

1.3 Scope

The scope of this thesis covers development of the telerehabilitation gaming platform in support of a physical therapy treatment program for RA patients. This will be achieved through extracting movement performance information from a game session and providing verbose analysis on the precision aiming tasks asked of the patient during game play. In addition, still imagery from several hand poses are captured to report on visual aspects of hand condition including joint angles, range of motion (ROM), redness, texture, and size.

1.4 Novelty and contributions

This section briefly describes where the work discussed in this thesis fits within the scope of telerehabilitation for RA patients, movement performance measures in a serious gaming setting, monitoring hand structure and signs of inflammation. In the context of telerehabilitation, there are only a handful of studies reported in the literature pertaining to our target demographic, RA patients. They tend to focus more on patient education [148] and a more general overall encouragement of gross movement to help preserve joint integrity through maintaining muscle strength, mobility and range of motion [87]. More recently there has been work reported using custom built equipment to measure hand function for rheumatic patients remotely, where measurements of a set of hand function tests are either stored or reported via network connections when available [103]. Where the methods described in this thesis differ is that any object can be used for input control when instrumented, implying that it supports a broad range of physical activity to match therapeutic exercises recommended for the individual based on their ability. This includes a wide range of movements from gross to fine control with high fidelity. Also a custom-built gaming platform is provided as a method to motivate and help maintain user interest in the form of providing a challenge. Part of that platform contains a comprehensive suite of movement measurement profiling captured during gameplay, which draws upon a wealth of knowledge from goal-directed aiming tasks [10, 39, 88, 94, 95] to report on movement performance in either a supervised (clinical) or unsupervised (home) setting. Using a fully customizable set of difficulty parameters, the game-play experience can be adjusted to suit the individual. In addition, we use our gaming platform for a short duration (no more than 3 minutes), leaving the remaining time from the session for clients to select alternate games of their choosing to encourage continued use with the specified input control object and its associated therapeutic value. The final element of contribution relates to evaluating hand structure. Traditionally, this is achieved through the use of goniometers to measure joint angles and provide insight into flexibility and range of motion [44]. The possibility of using digital

imagery to replace traditional goniometry has been reported on in [8]. Studies have been done on reliability of goniometry and one area that is reported frequently as a source of error is inter-rater, where repeatability of measurements can incur additional error [85, 149]. The methods described in this document eliminate this source of error as the same algorithm is employed for all hand images, placing the landmarks and building hand structure in the same fashion on each occasion. There are other studies reported in the literature of automated goniometry, however the target area on the body has consisted predominantly of a single joint (e.g. knee, elbow) [37] or a subsection of a more complicated structure such as a part of one finger when considering the hand [135]. This thesis discusses hand structure from three different poses, examining a relaxed posture, extended posture and a lateral view to examine potential manifestation of problems leading to deformities in any joint contained in the fingers/thumb. In addition, visual condition of joints are examined from a perspective of redness, texture and size to detect early warning signs of inflammation associated with RA. In conjunction with the work and encouragement of Peters [111], a novel application using near-sets techniques was employed to refine joint selection and for feature measurement (see Sec. 2.6). Collectively, the different aspects provide a comprehensive suite of reported features to profile finger-hand function for clients and their care providers as part of a treatment plan for RA.

1.5 Organization of document

This thesis is divided into six sections. The second chapter contains background information to help describe the major components involved in the work described herein. This is followed by a description of the system architecture in the third chapter that describes the elements that make up the telerehabilitation gaming system. The fourth chapter contains the details for system verification where each unique aspect of the system is described in more detail and verified through experimental work to demonstrate proof of concept and aid in the confirmation of final selection for system components presented in the discus-

sion on architecture. Next, results are presented in chapter 5 to demonstrate use of the telerehabilitation gaming system by both RA patients and normative cases. The resulting movement performance data is presented, demonstrating the possibility of rating task difficulty for precision aiming tasks. Finally the last chapter contains concluding remarks that discuss in more detail elements that worked, those that did not, my plans for the system moving forward and also future work and areas to expand upon this stream of research.

2 Background

2.1 Telerehabilitation

Telerehabilitation is defined as the provision of rehabilitation services remotely through the use of telecommunications equipment or the Internet. This is a relatively young research area, one of its first official appearances coincided with the awarding of a rehabilitation engineering research centre in 1997 focused on telerehabilitation [152]. Since its inception, telerehabilitation has gone through a number of changes and matured as a unique field under the broad scope of telemedicine. This included the formation of a special interest group as part of the American Telemedicine Association (ATA) [5], tasked with developing core standards and guidelines for telerehabilitation systems in an international capacity. As the concept of telemedicine and telerehabilitation gain in popularity and acceptance, there have been more research units reporting worldwide on healthcare migrating to this medium [30, 40, 65, 147]. In addition, it has since garnered attention from major players in industry with statements of intent toward research and development in the field (i.e. a joint venture between Intel and G.E.) [66]. Support for telehealth or telemedicine has started to find its way into government mandates as evidenced by the push to move into using Electronic Health Records [64] and providing updated and improved regulations for privacy of health information [2]. Healthcare providers and insurance companies are beginning to include reimbursements for treatment via this technology as feasibility tests and

reports increase and improve in both quantity and quality [63]. Closer to home, Manitoba eHealth [32] and Manitoba Telehealth [143] are both active in developing telehealth opportunities, infrastructure and standards to provide improved healthcare in both urban and rural settings. Coupling this together with Canada Health Infoway and their mandates for establishing an Electronic Health Record system [64], a more complete basis for telemedicine is in the process of being established in both Manitoba and Canada.

As telerehabilitation research has progressed, a number of application areas have been reported for various types of system implementations, client demographics and feasibility studies. This has continued and expanded into a wide array of approaches to telerehabilitation that fall under the Process Oriented Model presented by Winters [152]. The four main types of systems considered to be part of telerehabilitation include, teleconsultation, telehomecare, telemonitoring and teletherapy [152]. Teleconsultation is described as consultation when necessary between distant healthcare practitioners with regards to a patient's diagnosis and a treatment plan using telecommunications technology to share data and ideas [152]. This is often seen as a means to communicate between rural and metropolitan areas where rural healthcare providers may not have the expertise necessary to treat a specific case and require expert advice on the matter. The telehomecare classification is more general and has a bit of overlap as a system definition, *Pare et al.* [104] provide two definitions. The first definition consists of systems that are commonly known as home telemonitoring where patients use electronic devices to monitor their clinical condition [104]. The second definition targets home healthcare providers in giving tools for effectively managing their clinical condition [104]. The overlap or similarity can be seen with the next area of telerehabilitation, telemonitoring. The definition of telemonitoring is where a primary care giver remotely monitors a patient's health status through the use of sensory equipment [152]. This type of monitoring typically takes the form of sensor systems on or around the body depending on what is being monitored and can range in importance from critical sensory information for vital statistics that update often or less

important information that can be updated periodically or as needed/used. The last type of telerehabilitation systems fall into the teletherapy category which corresponds to patients that interact with a system or with therapists that are able to monitor their performance at a distance. The work presented in this thesis falls into the category of teletherapy or delivery of remote rehabilitation through the use of a telerehabilitation system.

Telerehabilitation is often thought of as teletherapy as it corresponds to patients that exercise in some form at home or in remote settings with therapists monitoring performance and being able to adjust settings and parameters from an alternate location [152]. There are a number of different systems that exist that offer varying degrees of clinical control over the remote system operation. Most of the earlier efforts tended to make use of audio-visual feedback as a means of communication between a patient and therapist [28]. More recent efforts and interest in studying haptics or tactile sensation [55] has resulted in multi-sensory systems that can include audio, visual and haptic feedback [57, 105]. Different types of technology have been used to provide varying levels of patient immersion in the rehabilitation process. These include telerobotics [16, 29, 59, 105], virtual reality [13, 47, 57] and a game-based approach [15, 47, 78, 80] to name a few. Just as the technology is diverse, so are the target populations and problems that the systems have been built for, some examples include neurorehabilitation [15, 47, 72], post-surgical rehabilitation [57], gait analysis [7] and physical activity intervention for rheumatoid arthritis patients [80, 148]. In most cases, teletherapy examples provide channels of communication between a therapist and patient as part of a rehabilitation program. Using this technology affords a more individualized recovery program that can be situated in either a home or remote community health care environment in addition to the usual clinical setting.

Telerehabilitation has a number of benefits associated with its use as a replacement or additional course of delivering therapy to end users. Common benefits often brought up in discussions about telerehabilitation include saving money, time and providing expert care to patients that live in remote, rural communities that would otherwise require a signifi-

cant cost in travel related expense for the individual as part of the healthcare process. As Canadians, living in a country with the second largest land mass in the world, the idea of providing health care to remote communities is a concern. The bulk of the population can be found along the Southern border of the country, implying that for those that live away from the more densely populated regions, limited access to expert healthcare without travel may be a reality. The largest percentage of telehealth visits in Canadian provinces and territories reported from 2010 consisted of individuals located in more remote and/or northern communities, with the highest concentrations located in Nunavut, Northwest Territories, Yukon and Newfoundland respectively [63]. This type of technology opens up a significant improvement in healthcare options that are not present for those residents otherwise. Considering it avoids or limits travel expenses, the associated time, potential loss of wages, extra stress on the individual being away from home and can potentially reduce the amount of office visits required depending upon the individual needs, it presents an appealing alternative and/or augmentation to traditional healthcare. These types of systems are generally simple to use and often require less time on the part of the care provider, resulting in the possibility of taking on more patients or spending more time with their existing clients.

Although there are a number of appealing reasons to adopt telerehabilitation systems as an alternative to mainstream forms of healthcare delivery, there are some limitations and problems that remain. One common problem that has been noted in the literature from the first ten years of publications is a lack of comprehensive studies and recommendations for administrators and policy makers to adopt this type of technology as part of the clinical practice [122]. Similarly, issues of standardization from one system to the next are a concern when it comes to sharing data [122]. Also, on the notion of data sharing, both privacy and security concerns are a potential stumbling block in the adoption of telerehabilitation systems (which has seen more activity from government and organization to help in standardization [2, 5]). In addition, since telerehabilitation is often seen as a less expensive alternative to the existing healthcare model, it is interesting to see that a number of re-

ported findings from studies present equipment and setups that require expensive specialty equipment and software to get started [47, 57, 86, 137]. These types of systems are better suited to rural community health centres or locations where a larger budget will be in place to purchase, support and have well trained staff on hand to help operate. When it comes to in-home setups there are potential pitfalls starting with cost to the end user, insurance coverage issues and also safety requirements and patient training to ensure proper operation and also provision of support to help keep remotely installed equipment running smoothly. These issues have been addressed in the core standard and the more specific telerehabilitation standards from the ATA [5]. In addition, reports of larger populations or larger study sizes have started to materialize and it appears that motivation to keep users interested and have them continue to participate in a program is yet another challenge to overcome [148]. As rehabilitation can be a lengthy process, it is important to consider a means to maintain patient interest throughout the course of their treatment program to ensure the optimal outcome. One final potential concern for telerehabilitation systems is the need to support a wide range of skill levels depending on degree of disability of the patients. With custom interfaces that have less flexibility this can be a problem as it can exclude certain individuals who may have benefited from treatment programs otherwise. The reason for more specific interfaces is generally for systems that are tailored towards a specific rehabilitation problem. More recently reported efforts are geared towards interchangeable systems that can work with multiple target areas of the body for rehabilitation and have more flexible interfaces depending on the individual.

Often cited important areas of telerehabilitation research include development of systems that provide the same or similar assessment and therapy compared to in-office visits and also developing systems that collect and quantify data that is meaningful for therapists [28, 106, 125, 152]. The work described in the upcoming chapters falls into the latter category and is intended to provide a reasonable degree of flexibility and simplicity in both the user interface and cost outlay to make it accessible to the end user.

2.2 Rheumatoid arthritis

The target demographic focuses on individuals during early-onset of rheumatoid arthritis (RA), which is a disease that affects approximately 1% of the population [76, 99, 136]. Arthritis is a condition that commonly affects joints in the body, the word itself is derived from Greek origins, with *Arthro* meaning joint and *itis* referring to inflammation [136]. For the case of RA, it is a systemic, autoimmune disease that is not unlike other forms of inflammatory arthritis that will affect joints in the body with the mechanism of attacking the tissue in the joint lining but it can also affect other organs in the body causing complications with the eyes, lungs, heart or blood for example [136]. Early onset of the disease symptomatically varies somewhat, although it tends to appear most commonly in the age range of 30-50 [136]. The most likely affected joints in early onset are the metacarpophalangeal (MCP), proximal interphalangeal (PIP), metatarsophalangeal joints and the wrist [76, 84, 136], of particular interest to this proposal are those joints contained in the hand (see Fig. 1). This section includes a brief discussion of some of the signs of early onset RA, why early diagnosis and treatment are important and how the disease is commonly treated.

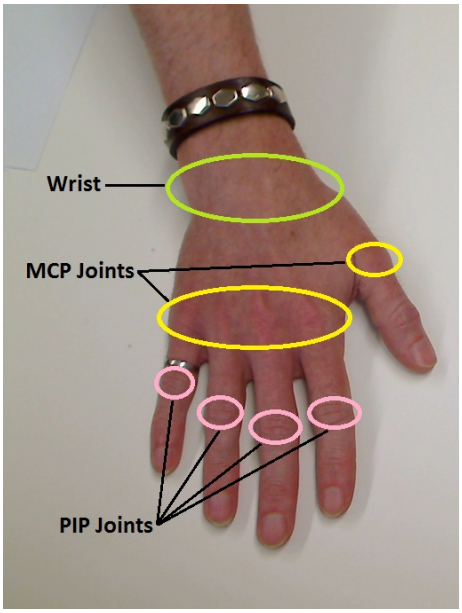

Figure 1: Joints of interest

Rheumatoid arthritis is a disease that can be difficult to diagnose in the early stages as it has a range of symptoms that may not always follow the same pattern. Some of the early symptoms are reported as fatigue, weight loss, a low grade fever, musculoskeletal pain, joint stiffness in the morning or after rest periods and swollen joints (synovitis) in the hands [76, 136]. Evidence of joint degradation is generally not visible in early onset via x-ray although it will accumulate over time [3]. Joint stiffness in the mornings is one of the key symptoms for inflammatory arthritis as it often is a result of fluid in the joints that accumulates as a product of inflammation [76]. The fluid that accumulates in the joints will often take on a gel-like consistency that will dissipate after about 30 minutes from waking and moving around, hence the stiffness [76]. Coupled together with pain and inflammation in the joints is increased warmth and redness of the affected areas [136]. Although in the later stages of the disease, joints are affected in a more symmetric fashion, early onset can result in only a few joints affected, often asymmetric in nature [76]. Typically, a primary care physician will order lab tests to support their diagnosis when RA is suspected. According to the 2010 Rheumatoid Arthritis Classification Criteria [3], at least one serologic test and one acute-phase response measure must be obtained. The acute-phase tests that are commonly employed are the erythrocyte sedimentation rate (ESR) and the C-reactive protein test (CRP) [3]. These are used to look for signs of inflammation in the blood [136]. The ESR is a measure of how quickly red blood cells fall to the bottom of a test tube, if the sedimentation rate is above a certain threshold (30mm/hr) [76], this is considered likely in the presence of inflammation. Similarly, the CRP test is a marker of inflammation, greater than a level of 0.7pg/mL in the blood indicates a higher than normal amount that also signifies the presence of inflammation [76, 136]. The serologic tests look for the presence of autoantibodies, including rheumatoid factor (RF) and the anti-citrullinated protein antibody (ACPA) [3]. The presence of these antibodies is often found in RA patients (70-80% for RF and 80-90% for ACPA [76]). Although for the case of RF, this can be present in normal individuals or those with other rheumatic diseases or long term infections [76, 136]. For

ACPA, it can also be present in other diseases, but is seen as a potential successor to RF in diagnosis [76]. The individual symptoms are not necessarily indicative of the disease, similarly positive blood work does not always indicate RA either [136]. A complete history of the patient, bloodwork and an informed expert opinion is required for a proper diagnosis at early onset.

Early diagnosis and treatment of RA is essential to provide the best possible prognosis for the disease [3, 69, 136]. Some common symptoms in early onset of the disease result in swelling of the joints, pain and warmth, all of which contribute to degradation of affected joints [136]. Joint damage can occur without significant pain, which can manifest later on, causing both pain and disability [136]. Any damage to the joints is undesirable as it is permanent. Left untreated, the damage can become serious, spreading to other joints, typically in a symmetric fashion, including knees, shoulders, ankles, feet, elbows, hips, temperomandibular, spine and sternoclavicular joints [76]. In addition to damage occurring unknowingly, it is not uncommon for patients to go through stages of spontaneous remission where the disease appears inactive (in the order of 30-40% of RA patients reported in [76]). Left untreated, the disease will continue to damage the tissue in the joint linings, which can result in more serious effects and a far worse prognosis. Often the result of long-term disease activity shows up in deformity of various joints. Specifically relating to the hand, ulnar deviation of the MCP joints are encountered [76]. The reason behind this deformity is due to the disease affecting and weakening the wrist structure and causing a radial deviation in the carpal bones [76]. This results in an ulnar deviation of the fingers to compensate and keep the tendons leading to the phalanges in a normal line [76]. The swan-neck deformity is another possible problem occurring in the hand. This results in a hyper-extension of the PIP joint and flexion of the MCP and DIP joints [76]. The other common deformity is the boutonniere, which is similar to the swan neck but opposite in that it results in flexion of the PIP joint and a hyperextension in the DIP joint (see Fig. 2) [76]. These are the most common deformities associated with RA in the hand from a visual per-

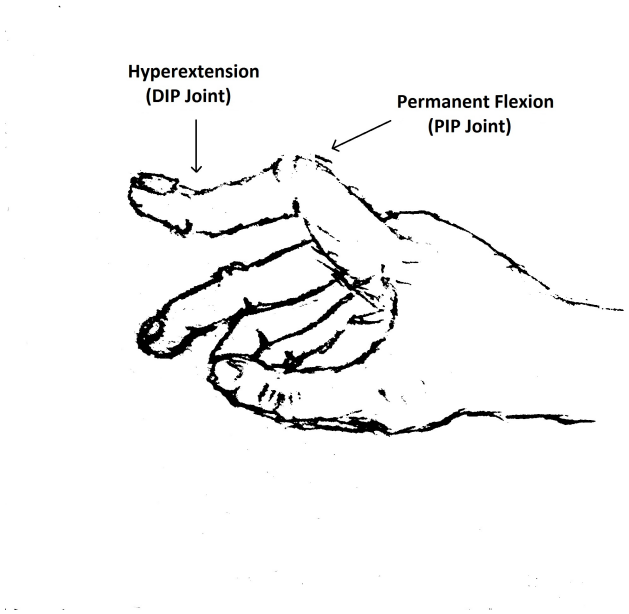

Figure 2: Boutonniere deformity of index finger

spective. There are other complications but they are typically not as visible and therefore not included in this discussion as the proposed work deals with visual cues. Similarly, there are other sites in the body that RA can occur although although only details regarding the hands are considered for the context of this work. When damage and resulting deformities occur relating to joints in the body, this is very undesirable as the process is not reversible and surgery is typically a last resort only when joints are severely damaged and no longer functional [136]. Catching the disease in the early stages and treating it at that point often improves the long-term prognosis and can help reduce joint damage [136].

When a positive diagnosis of RA has been confirmed, early treatment for the patient is aggressive to prevent or limit the disease progression and any associated disability [128, 139, 154]. There have been many supporting studies that report that it is never too early to treat an RA diagnosis and also never too late [46]. Typically, disease modifying anti-rheumatic drugs (DMARDs) are one of the first steps in treating RA [46]. There are several different types of DMARDs (often referred to as small molecule treatment), including methotrexate, hydroxychloroquine, sulfasalzine, and leflunomide to name a few [46]. These have often been the first choice for treatment of RA when looking at a mono ther-

apy approach [46]. Selection of appropriate DMARDs is done on a case by case basis as not all patients will respond to a given DMARD or potentially manifest undesirable side effects [46]. More recently, research has been moving towards biologic DMARDs (biologics) in combination with the more traditional small molecule treatment [46]. Similarly, there are several varieties to consider with the biologics, one of the most successful reported biologic treatments is a combination of tumour necrosis factor (TNF) inhibitors along with methotrexate [46]. There are several varieties of TNF inhibitors and also other biologic agents that can be considered during treatment [46]. The various drugs, their mechanisms of operation, side effects, etc. are outside the scope of this work and are mentioned with the intent of providing a brief look into the many possibilities for treatment. The various medications do not necessarily activate instantaneously and can take a significant amount of time in some cases (anywhere from weeks to months before positive effects are realized) [46]. Since treatment can be time consuming, it is imperative to select a treatment plan wisely as it can greatly affect the long term prognosis of the individual [92, 139]. Regular, consistent monitoring of the RA patient is vital to ensure that they are responding well to the given treatment plan and also to afford a chance to augment dosage, alter the drug plan or use a combination of DMARDs to maximize the benefits and minimize side effects [46]. In addition to the aggressive treatment using DMARDs, there are also adjunct treatment drugs that can help ease the symptoms for the short duration (such as glucocorticoids or a non-steroidal anti-inflammatory drug (NSAID)) [46]. In addition to pharmaceutical treatment, there are other aspects to consider including patient education, counselling, rest, exercise, diet, occupational and physical therapy [46, 84, 136].

Well rounded treatment requires a good support structure to implement, monitor and adjust in the hopes of providing the best outcome for the individual with RA. As not everyone responds the same way to the various drug and rehabilitation treatments, it can take time and requires more frequent monitoring of a patient, especially during the early stages, soon after a positive diagnosis [84, 92, 139]. Traditionally, more frequent monitoring re-

sults in more trips to doctors and specialists for the patient. Depending on their ability to travel, this can be a significant inconvenience. However, when weighing the cost vs. the benefits for early treatment and monitoring, it appears well worth taking the time to support a program that frequently monitors RA patient condition and their response to treatment.

2.2.1 Inflammation

To accompany the discussion of RA, it is important to consider inflammation and how it manifests itself relating to joints and tissue in the hands. This dedicated subsection is intended to fill in more background detail on the inflammation process and provide some insight into feature selection when describing inflammation from a visual perspective.

Rheumatoid arthritis is an inflammatory disease so it is natural to consider the inflammation process when looking for features to describe joint conditions from a visual perspective. The first documented knowledge relating to inflammation was provided by the Roman physician/writer, Aulus Cornelius Celsus, dating back to the 1st century AD [127]. The classical definition of inflammation as described by Celsus consists of four parts, heat, redness, swelling and pain (*Calor, Rubor, Tumor, Dolor* in Latin). Since that first definition, the knowledge base relating to inflammation has expanded significantly examining the original or classical definition all the way to a molecular/cellular level and also for a multitude of different causes (trauma/injury, disease, etc.) [36, 126, 127].

For the purposes of the work detailed in the following chapters, inflammation is considered from a visual perspective so the classical definition is well suited for our needs. The symptoms were further narrowed to two of the four classical symptoms, swelling and redness. These are the best suited symptoms for visual inspection and can both arise from the inflammation process. To provide some insight into inflammation, the mechanism is briefly discussed for completeness.

Inflammation in the body is its response to what is perceived as an invading organism [77, 119]. This can be a result of pathogens, infections or damaged tissues in the

body [77, 119]. The inflammatory response to what is perceived as a threat to the host consists of cell activity, proteins, blood vessels and other elements that help in removing the problem and initiating the repair process [1, 77]. At its most basic level, the mechanism begins with cells that sense a problem exists and they respond by secreting molecules that are capable of regulating the inflammatory process [77, 119]. The process consists of an increased blood flow which can result in heat and redness, a build up of plasma fluid and proteins which can cause swelling or edema and white blood cells (also called leukocytes) that help remove the perceived threat [77, 119]. The inflammation process lasts until the offending source is removed and the repair process is completed [1, 77]. However, in the case of chronic inflammation, a problem associated with autoimmune diseases like RA, inflammation can continue and result in damage to healthy tissue [1, 77]. In the long term this translates to the immune system continually damaging healthy tissue in the host which can lead to joint damage, deformities and other complications depending upon where the disease spreads [76].

2.2.2 Goniometry

Goniometry is used by physiotherapists to measure an axis and range of motion to help determine the joint function of a patient [44]. This information can be used to document physical joint limitations relating to range of motion during a first visit, help in developing a therapeutic intervention and periodic monitoring of results to ensure effectiveness of treatment [44]. A goniometer is an instrument similar to a protractor that is able to measure a joint angle or assist in manipulating a joint to a specific angle (see Fig. 3). To measure range of motion and joint angles there are a few different possible methods, physically using a goniometer, visual estimation, high speed cameras, and manual estimation of still images to name a few [44]. The two problems that are common to all methods include reliability and validity [44].

Reliability in goniometry refers to the repeatability of a measurement and finding the

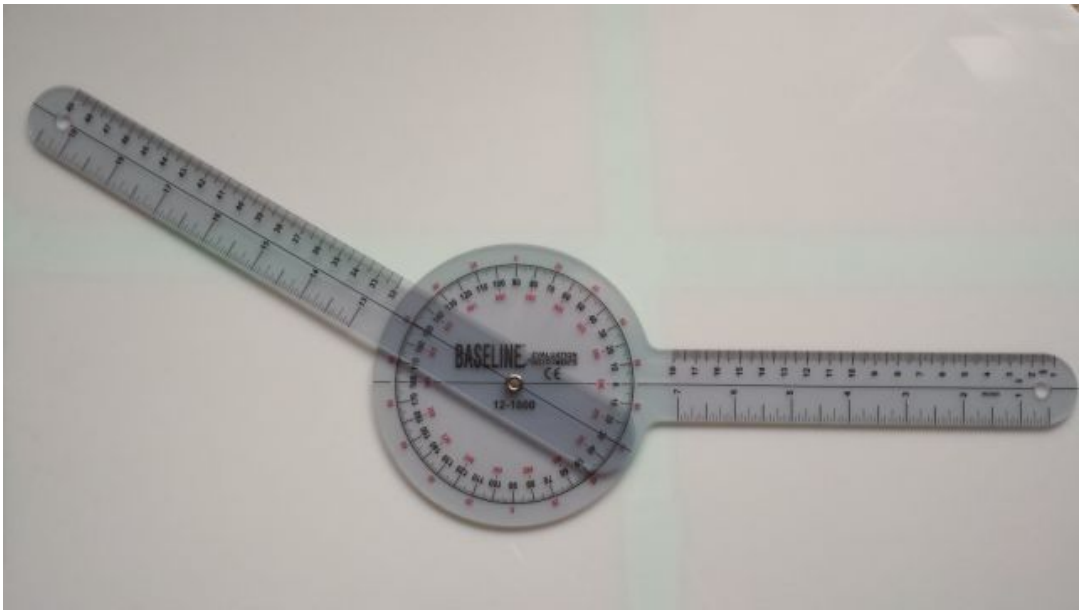

Figure 3: Goniometer

same result when the same conditions exist [44]. With manual measurements, this can make it difficult to achieve exactly the same results as there are a few potential sources of significant error [44]. Improper alignment of the instrument, misidentifying landmarks, and for active range of motion varied manual force applied are all potential sources of error [44]. Also, it is possible that the range of motion from one test to another can vary and in some cases it has been recommended to take an average measurement to reduce variability [22]. In addition, the more complicated joints are, the more difficult they are to measure reliably, for example a simple hinge joint like the elbow or knee typically have less variation in their measurements than a wrist [44]. One more problem with reliability relates to multiple individuals making the same measurements, the error between testers (inter-rater measurements) has been reported as less reliable for finger joint angles [52]. The amount of error reported in the literature varies from one study to the next, with common values of 5-10% or more in some cases [44].

Validity refers to how well the measurement describes the intended measure [44]. Goniometers have inherent limitations in themselves, in part their resolution limits degree of accuracy, although they are accepted clinical instruments as the error they introduce is

minimal [44]. Both reliability and validity are important aspects in goniometric measurements [44]. Some of the alternatives to traditional measurements cited in the literature include electromyography, electrogoniometry and cinematography [44]. Using still photography and cinematography comes with its own set of challenges including where to position cameras for optimal viewing of the subject and how to discover landmarks on the subject for making measurements [44]. The optimal means for discovering range of motion will likely always be radiography [44]. Using radiographic bone angles as a comparison for range of motion measures on healthy adults, one study reported that the first 15 degrees of knee flexion were unreliable with goniometers, likely due to joint rotation [35].

With the two main considerations as part of goniometry, reliability and validity, the goniometer is a clinically acceptable tool to satisfy range of motion measurements [44]. When it comes to which is more important out of the two, it is not a simple answer. One case reports that when a gold standard for measurement does not exist, it may be the reliability that is of greater importance compared to the validity [85]. More recent reviews in the literature report similar findings and still claim that inter-rater reliability is low [149] and a cause of potential error in range of motion measurements.

Relating goniometry to the telerehabilitation system described in this thesis, the range of motion for patients is considered using still imagery. Algorithms have been developed to extract the joint angle measurements and provide feedback for range of motion measures in several different hand poses. There are constraints for the image acquisition as hinted at in this section and also expanded on further in the upcoming chapter. However, the potential to reduce or eliminate inter-rater error is a possibility if the acquisition setup remains consistent from one session to the next.

2.3 Measuring movement performance

Having discussed the delivery medium (telerehabilitation) and the target demographic (RA patients), the next step is to examine some of the features associated with profiling finger-

hand function based on movement performance. Hand function is an integral part of daily life that many take for granted until impairment occurs. There are many tasks that require significant manual dexterity, grip strength and flexibility to perform (including getting dressed, opening containers, turning keys, driving, brushing teeth, getting washed, eating, etc.). Since a common manifestation of RA affects joints including the wrist, MCP and PIP joints in the hand [76, 136], examining hand function is a good target area to monitor in a treatment program. To provide a meaningful profile of finger-hand function, both movement ability and visual cues of the hand are measured. As part of the treatment plan for early onset of RA includes physical therapy to help strengthen and maintain joint function, the work for this proposal has been done in the context of supporting a physical rehabilitation program for delivery and monitoring of physical therapy for RA patients [84, 100, 136]. This section discusses features of movement performance that are used to describe ability.

Movement involving the hand is discussed as an extension of the telerehabilitation gaming system. To that end, the choice of input controller based on expert recommendation from a supporting physiotherapist will dictate the object physics, ergonomics and provide the end user with a tool to implement movements as part of their rehabilitation process (more details to follow in Sec. 3). Patient movement analysis is considered in the context of a custom built gaming platform that was designed to provide extensive reporting solely for that purpose, unlike commercially available alternatives. The resulting output yields information according to each in-game event that occurred during a session and provides the capability to generate an extensive movement profile for each of those events.

The study of goal-directed movement has been explored in depth, providing a solid foundation for models of examining voluntary movement. Woodworth [153] has one of the earlier reports that relates time and space in voluntary movements for precision aiming to demonstrate trade-offs between speed and accuracy. Fitts [39] later extended the work and helped form a relationship between speed, amplitude and tolerance in conjunction with information theory [129] to help categorize task difficulty. More recently there have been

a number of efforts that delve into precision aiming tasks as they are a common part of human computer interaction in what is commonly referred to as a WIMP interface (windows, icons, menu and pointing) [10, 95]. In an effort to study, improve and build better user interfaces, precision aiming tasks have come into the spotlight.

The type of movements employed in our telerehabilitation gaming system fall into the category of precision aiming tasks [10, 95]. Users are required to provide input control movements to achieve a goal in the game environment that requires precision aiming. This type of movement has been well documented and broken up into component phases (latency, initiation, ballistic, correction and verification phases) based on monitoring an individual movement [95]. When examining resulting data from a single movement, position versus time information is recorded, allowing reconstruction of the movement trajectory. Details of individual movements are then discovered through in depth analysis of the trajectories with some common measures including reaction time, rise time, total movement time, accuracy, gross scoring measures, velocity, acceleration and jerk [94, 95, 123, 146] (see Fig. 4 for example measures, note that in Fig. 45a, reaction time corresponds to the time between the start and the first dotted line and the rise time is the difference between the third dotted line and the second dotted line. Also, the accuracy measure in Fig. 45b demonstrates misses above or below the neutral plane corresponding to over or undershoot respectively when missing a target). In addition to these types of measures that provide insight into performance and movement quality, there are other possible avenues in measuring user ability. Skill measures will respond in a similar fashion to the performance metrics, fluctuating somewhat with task difficulty and user ability but are not always easy to discover from the aforementioned measures. There has been an extensive body of work to help in quantifying skill and predicting movement based on models that stem from the work of Fitts [39]. In developing models for predicting total movement time, kinematic patterns and characteristics for goal directed movement, several different graphical tools have been shown capable of rapidly assessing the quality of movement [10, 88, 155]. One

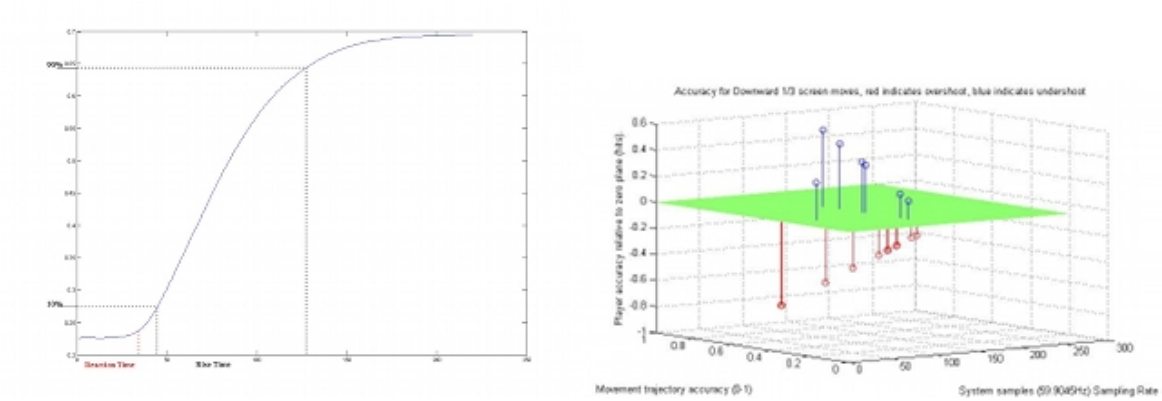

(a) Rise time and reaction time

(b) Accuracy measures

Figure 4: Example movement measures

of the more well known aspects of movement is the velocity profile [6,115]. Using velocity versus time plots, it is possible to see how well controlled user movement is at a glance. For a rhythmical aiming task (periodic), the velocity profile for a perfect movement will exhibit a symmetric bell shape profile [10]. For the case of a precision aiming task that is goal-based (non-periodic movement), the velocity versus position profile will exhibit half of the symmetric bell shape profile (which half depends on the direction of movement to achieve the goal). In addition, there are other supporting plots that have been shown in the same context, including phase plots (position versus velocity) and Hooke's plots (position versus acceleration) [10, 88]. Figure 5 shows an example of position versus velocity for a goal directed, non-periodic movement (half-circle). There is a definite skew to the left and also the outer edge of the circle has a jagged edge indicating a more difficult task than the ideal case of a perfect semi-circle. At a glance, it is easy to see that the performance is non-ideal.

Collectively there is a well understood body of research on precision aiming and/or goal-directed tasks. This provides both models for predicting movement and also an array of metrics for grading movement performance, efficiency and skill levels. Unlike commercial gaming platforms, our custom built gaming platform provides extensive reporting in support of establishing a range of metrics (discussed in this section and also in the upcom-

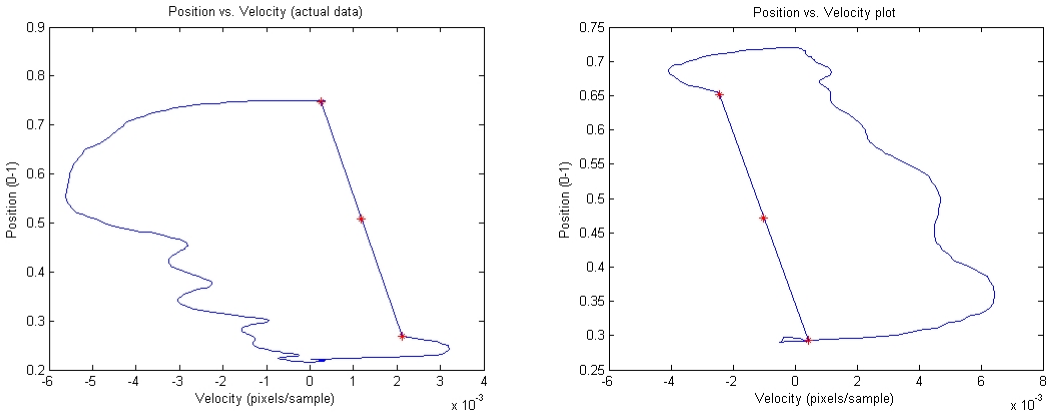

(a) Position vs. Velocity left move

(b) Position vs. Velocity right move

Figure 5: Phase plane plots

ing system architecture) to monitor user performance as opposed to the more traditional, coarse measures that are typically found elsewhere. For the case of gauging performance and condition of RA patients based on finger hand function, it is important to consider alternate avenues in addition to movement performance to obtain a broad view in support of a detailed status report. Next, we look at self-reported questions, referred to as clinical instruments.

2.4 Self-reported questions

To provide a well rounded approach to monitoring finger-hand function using telerehabilitation, alternate avenues in addition to movement analysis were considered. Clinical assessment instruments or questionnaires are a commonly used tool to rate patient condition as reported in the literature [60, 116]. There are therapist-rated and also self-rated instruments. For the context of our telerehabilitation system, self-rated questions/questionnaires are more suitable for a remote or home-based system where supervision may be limited.

Clinical instruments that are of interest for the research problem described in this document focus on the upper limb, specifically the hand and also disease-specific to RA. Narrowing the area of interest helps in reducing the number of possible instruments to consider,

yet there are still enough that standardization for comparison can be an issue [60]. Some of the more commonly employed instruments for upper-limb/hand injuries include the *disability of the arm, shoulder and hand questionnaire* (DASH) which contains 30 questions in a long form and 19 in a reduced QuickDASH version [41]. More specific to hand function is the *Michigan Hand outcomes Questionnaire* (MHQ) which contains 37 questions in a long form and 12 in a reduced form [131]. Narrowing the scope even further to ailment-specific is the *Arthritis Hand Function Test* (AHFT), this is more of a performance-based measurement system with specific equipment [116] and better suited to a clinical setting, as it requires more time to administer and specific equipment. There are a number of other hand function tests that measure ability in set tasks such as the *Grip Ability Test* (GAT), the *Jebsen Hand Function Test* (JHFT) and the *Cochin Hand Function Scale* [116]. Instruments that have set tasks become more challenging in the context of telerehabilitation where the patient is either remotely supervised or unsupervised during a session. In addition to the above mentioned instruments there are other more specific measures reported in the literature for RA including the *Health Assessment Questionnaire*(HAQ) [12]. There are both a full and shortened version of the HAQ that examine either 5 or 2 dimensions of patient health respectively [12]. There are also more clinical-based measures like the *disease activity score*(DAS), developed in the Netherlands [96]. There are several versions of the DAS, some based on aforementioned clinical measures in section 2.2 (i.e. erythrocyte sedimentation rate and c-reactive protein tests) [96]. In addition to the clinical measures these require clinician rated condition on a number of joints (The DAS28 includes hands, elbows, shoulders and knees).

Information provided from these types of clinical instruments have been proven to provide meaningful information in rating patient health status [76, 92, 100]. Unfortunately, without supervision, this eliminates some of the most commonly employed and most suited clinical instruments for measuring RA (i.e. the DAS and the full version of the HAQ). For self-reported questionnaires the shortened HAQ, the MHQ and the DASH are likely the bet-

ter choices for a standardized approach for assessing response to therapy for our purposes. One of the problems faced with any remote therapy delivery system is long term use. Maintaining motivation of patients to provide results over a lengthier time period is a difficult challenge as repetitive tasks often result in a loss of interest and ultimately they stop using the system completely. Studies have shown that even over what is considered a short period of time (6 months), the adoption rate for a home-based physical activity intervention will likely drop (for example, RA patient system adoption at six months dropped to 38% in this case [148]). With this in mind, retaining patient motivation is of vital importance for a telerehabilitation system targeting RA patients where treatment is ongoing. This rules out lengthy questionnaires that take up time and are repetitive. Self-rated questions would be a welcome addition to increase the reporting dimensions beyond movement performance. However, selecting appropriate questions and frequency of reporting are key choices that will either help retain or potentially lose long term client adoption of the telerehabilitation system.

2.5 Visual analysis

Although movement performance can be measured to provide insight into patient condition, part of an office or clinic visit will involve further examination using other senses. This includes both physical and visual analysis made by a qualified practitioner. Physical examination invokes an immediate interactivity level that necessitates both patient and care-giver be present simultaneously. However, visual inspection can be performed without direct supervision depending on the acquisition, target views and post processing of captured imagery that highlights local areas where problems can arise. This section covers background information relating to visual analysis of still imagery, paying particular attention to susceptible regions of the hands based on symptoms related to the target demographic.

A brief reminder of common symptoms for RA patients from a visual perspective re-

lates directly to inflammation in the immediate case and structural deformity for longer term damage. For immediate symptoms, the joint locations are of prime interest. Specifically both the MCP and PIP joints are most commonly affected, although all three joints in the fingers (and two in the thumb) are considered. The visual symptoms of the joints that we are interested in reporting on include swelling, redness and texture. In addition, symptoms that appear as the disease progresses can manifest as permanent joint damage that result in deformity. To capture and report on early warning signs of potential deformities, structural analysis of the hands is needed.

2.5.1 Image representation

Binary and greyscale digital images can be represented by two dimensional functions, $I(x, y)$ where the values of x and y correspond to cartesian coordinates or the location of a pixel [48, 111]. The value of I at a given location is referred to as the intensity, or for monochrome images, greyscale intensity [48, 111]. In the case of colour images, there are three separate channels of information for each pixel, one each for red, green and blue values [48, 111]. Each channel consists of a separate matrix containing the corresponding colour information. To display a colour pixel, the composite value for the three channels is required [48, 111]. This can be represented as $I(x, y, c)$ where c represents the colour channel, for example, 1 for red, 2 for green and 3 for blue. A single dimensional or greyscale image representation is shown in Fig. 6. Manipulation and analysis of the intensity values contained in the image matrices is the basis for all of the image analysis and computer vision related work that follows.

2.5.2 Segmentation

The segmentation problem is one of extracting meaningful information from an image and removing unnecessary detail, leaving only objects of interest [48]. For the application of still imagery of the hands, it is important to be able to extract the hands from their

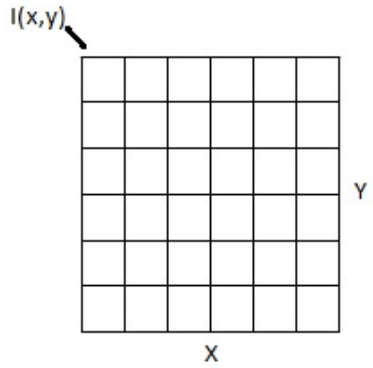

Figure 6: Matrix representation of a greyscale image

background. To avoid an unnecessarily complex problem, the setting for image capture was controlled and setup in a way to help segment our images. This was achieved through using a light, monochrome background, providing excellent contrast with a wide range of skin tones. This was specified as a requirement for all configurations of this system as a simple white backdrop (eg. towel, sheet, paper) sufficient to provide the necessary contrast for segmentation. An example using a light coloured foam-core posterboard is presented in Fig. 7. Examining these images leads to the problem of segmenting or how to separate the

(a) Hand image on high-contrast background (b) Hand image on high-contrast background

Figure 7: Hands in front of high contrast background

hands in the foreground from the monochrome background. Since the two (background and

hands) are significantly different in greyscale values (note images have been converted to greyscale although originals were captured in colour), it is reasonable to assume separation of those two groups of pixels is highly likely. The intention of segmenting the hands and background into two components is to extract the edges surrounding the hand.

One possible avenue of segmentation is through the use of clustering [111]. The aim of cluster analysis is to group similar objects together as separate entities within a composite space [48, 111]. This is well suited for the case of separating hands from a controlled monochromatic background as part of the segmentation process. The principal behind grouping similar objects together is achieved through measuring distances from mean values that represent the centroid of a cluster [27, 83]. For this case, an image g is represented as a matrix and input objects are considered on a pixel by pixel basis where each location in the image is addressed, $g(x_1, y_1), ..., g(x_n, y_m)$ (where n and m represent columns and rows of the input image, respectively). K-means takes the approach of looking for clusters of objects based on a number of k mean values. As the images in question have constrained environments, it is possible to select two well separated values and expect to segment foreground and background pixels based on intensity. This provides a result that groups skin tone pixels to a lower mean cluster value and all background pixels to the higher mean cluster value. The k-means algorithm follows a two-step process. The first step examines values in the image and compares them with the pre-selected mean values. When the difference is shorter between a pixel and mean value, it is considered part of a cluster around a centroid located at that mean value [27, 83]. The second step is to revise the centroid location based on all values in the cluster as elements are added or removed during the first step [27, 83]. As an iterative process, the cluster centroids will move to best fit the data and in some cases may require ending criteria if the stopping point is not obvious (i.e. when the mean values stop changing the process is finished) [27, 83]. To generate the distance measures, pixels are compared with each mean to discover which it is closer to (see Eq 1).

For this case, pixels will either belong to the background or skin-tone cluster.

$$S_i = min \sum_{i=1}^{k} \sum_{g(x,y)\epsilon S_i} \|g(x,y) - \mu_i\|^2, \tag{1}$$

where S_i refers to a set of observations (pixels) that fall within a shorter distance to the corresponding mean intensity, μ_i from the original image $g(x, y)$. Once all pixels in $g(x, y)$ have been compared to the mean values, the means are re-calculated and adjusted based on the cluster of data points surrounding the centroids to relocate them (see Eq 2).

$$m_i = \frac{1}{S_i} \sum_{x_j \epsilon S_i} x_j, \tag{2}$$

where the updated values of m_i are the newly revised means to better fit the centroid of the set of points in S_i which are represented by the x values. This process is then iterated until the mean values no longer move from one iteration to the next, providing the basis for discovering separate clusters of points for an input feature (or set of features).

Part of the segmentation problem often requires dealing with noise either before the process, after or on occasion both. Since we have a high degree of control over the image acquisition, only post processing was anticipated to eliminate unnecessary background noise arising from the clustering process. Some common problems discovered in segmentation included stray noise or fractures in the hand contour if light reflection off the hands was too bright (e.g. light reflecting off a fingernail). To clean up the images, morphological closure was applied to remove discontinuities and prepare the image for feature extraction. Mathematical morphology is rooted in set theory, so to provide an understanding of the techniques involved, a brief explanation of the underlying properties and process follows.

To help in smoothing out noisy edges and discontinuities in target images, a morphological $closing$ operator is used. Closing is a composite operation that consists of both fundamental operators, $dilation$ and $erosion$. These operators are built upon two set prop-

erties. The reflection of a set in an image consists of replacing coordinates (x, y) with $(-x, -y)$ [48]. This is formally represented in Eq 3

$$\hat{G} = \{p \mid p = -i, \ \ for \ \ i \epsilon G\}, \tag{3}$$

where i consists of any pixel located in image G, reflecting the values. Next, translation of a set is important when considering morphological operations. This shifts the pixel location in question by a set amount where the coordinates (x, y) become $(x + z, y + z)$ [48], (see Eq 4).

$$G_z = \{p \mid p = i + z, \ \ for \ \ i \epsilon G\}, \tag{4}$$

where i consists of any pixel from the image G, containing newly translated coordinates. Both of these set operations are employed in image morphology and are the basis for the fundamental operators (erosion and dilation).

Next, we look at the operators in morphological closing (see Eq 5)

$$A \bullet B = (A \oplus B) \ominus B, \tag{5}$$

considering that Eq 5 implies that it is a closing of A using the structuring element B. The structuring element B is a 2D set or shape selected usually based on prior knowledge of the target image and desired results [48]. There are a number of common shapes that are often used as structuring elements, for example Matlab provides a number of built-in options (ball, diamond, disk, line, octagon, pair rectangle, square) [62]. The two basic operators used in the closing are dilation and erosion. The process of applying an erosion operation is commonly referred to as an erosion of A by B where A corresponds to the set or image in question and B is the structuring element [48]. The operation is denoted as follows, $A \ominus B$ and is defined in (Eq 6) [48]

$$A \ominus B = \{z \mid (G)_z \subseteq A\}. \tag{6}$$

Thus erosion consists of the translation of a structuring element B by z, for which all values fall within A [48]. As the name implies, this results in an erosion around the extremities of A based on the shape of the structuring element B. The process of dilation is similarly considered between a set or image A and a structuring element B and is denoted by $A \oplus B$ [48]. The definition of dilation is presented in (Eq 7).

$$A \oplus B = \{z \mid (\hat{B})_z \cap A \neq \emptyset\}. \tag{7}$$

Dilation consists of both reflection and translation, with the structuring element reflected about its origin and then translated by z (the translation being similar to erosion) [48]. Besides the addition of reflecting the structuring element, the operation differs from erosion in that all elements are included when there is at least one element of overlap between A and B [48]. The outcome of dilation tends to enlarge the outer edge of the set/image in question (A) and erosion tends to prune the outer edge. These two operators form the foundation of morphology and allow for more complex operations.

The two techniques presented here are the basis for the image segmentation process used to prepare hand images for higher level computer vision problems. Once the desired information has been extracted, then it is a matter of deriving features of interest and representing them in a useful format for the TR system. More details can be found in the upcoming chapter on system architecture.

2.6 Developing patterns

Extracting digital features is the backbone of the research presented here. Being able to do something meaningful with those features leads to developing patterns. The corresponding goal of pattern development is to look for categories of similar objects based on input feature vectors [27, 111]. Considering the target demographic, pattern discovery can be used in a number of different ways. One possible avenue is to provide some degree of insight

into current condition compared to prior session data and whether they could potentially be at risk of damaging joints and/or exhibiting early warning signs/symptoms. There are three different types of features, movement performance, self-reported questions and visual features that are available to build patterns and establish similarities between session data. This section discusses a pattern development problem used to discover similarities in joint features and provides some background details on the chosen method.

Regarding patient condition, it can be difficult to compare from one subject to another. This is often the case because no two individuals are exactly alike. For each set of features there can be significant variability. For example, an individual who has good small movement dexterity based on either work or hobbies may consistently out-perform other people including both affected and normative cases. Similarly this applies to visual aspects as well considering that skin tones and hand shapes are not all identical. This requires comparing user data with average performance or a base-line comparison with a prior set of good results from that same individual.

For this case, the problem centres around patterns discovered in images of the hand and uses supporting information to reinforce similarity or nearness to build a refined joint location. The process of developing those patterns starts by establishing points or areas of interest. The next step is to look for similar points or areas of interest in other regions of the same sub-image of a joint. Through these comparisons, it is possible to extract information on the location of the focal area of the joint visual perspective. A discussion on patterns and how they are developed using set theory in preparation for comparison and building joint-representations via nearness measures follows.

Before expanding on picture set patterns, background details are provided on key concepts. Sets are considered to be collections of objects or members [4]. Members of a set have some relationship to one another [4]. When considering that relation, it is possible to describe similarity or nearness of a member, this gives rise to a distance function [111]. Distance functions or measures lead to metric spaces, introduced by Fréchet [42]. Metric

spaces can be represented as a pair (X, d) where X is a non-empty set and d is a distance function defined for measuring distance between members [111]. The distance function must satisfy the following criteria for all members of a set [111].

1. $0 \leq d(x, y) < \inf$ (non-negativity),

2. $d(x, y) = 0, if f x = y$ (identity of indiscernibles),

3. $d(x, y) = d(y, x)$ (symmetry criteria),

4. $d(x, y) \leq d(x, z) + d(y, z)$ (Δ-inequality).

To measure the distance between members or elements of a set, a measurable quantity or feature value is necessary. Feature values can be derived using probe functions [109], $\Phi(x)$. Depending on the application, there can be many feature values, resulting in feature vectors $\Phi_i(x)$. An example probe function for an image might be grey level intensity or gradient direction. Distance is measured between feature vectors for each member [111]. Two common distance measures that satisfy the above criteria are the taxicab (L_1 norm) and Euclidean (L_2 norm) distance [111].

$$d(x, y) = \sum_{i=1}^{n} \mid x_i - y_i \mid, \tag{8}$$

While simpler to implement, the taxicab distance (see Eq 8) also can incur more error depending on the subject matter, seemingly better suited for synthetic subjects with discernible straight edges. For subjects with a more natural form, it is likely that the Euclidean distance is a more accurate measure (see Eq 9).

$$d(x, y) = \sqrt{\sum_{i=1}^{n} (x_i - y_i)^2}. \tag{9}$$

Discussing distances leads to the concept of similarity or nearness of sets, this topic has been introduced and developed by Peters [109]. Our goal is to bring near sets techniques

into hand image analysis to discover patterns that can indicate joint location and potential disease activity. There are two types of near sets to consider, spatially near sets and descriptively near sets [111]. As the name implies, spatially near sets occur in close proximity to one another, limited by a chosen distance between pixels [111]. Descriptively near sets are not necessarily restricted by pixel distance from one another, they are sets that contain descriptively near feature values with one another [111]. For the purpose of this work, we are more interested in descriptively near sets when examining disease activity in the hand. To elaborate further on distance or proximity of sets, the concept of a metric topology and proximity spaces are necessary.

First, one has to consider neighbourhoods. The general case for a neighbourhood of a point in a non-empty set consists of a set of points that are near the original point [111]. For this case, nearness implies pixels within a certain amount of distance from the focal point [111]. Two different types of neighbourhoods are considered in images, spherical and descriptive [111]. Spherical neighbourhoods have a bounding parameter ϵ that restricts the size (where ϵ can take on any positive real value) [111], acting as a radius (represented in Eq 10)

$$N_x = \{y \in X : d(x, y) < r\}. \tag{10}$$

Descriptive neighbourhoods are not necessarily restricted to a set spatial distance from the target or focal point, instead they include pixels that match the feature descriptions [111]. When examining features, we need to revisit probe functions, $\Phi(x)$ that provide feature vectors,

$$\Phi = \{\phi_1, \phi_2, \phi_3, \ldots, \phi_n\}. \tag{11}$$

To establish descriptive nearness, comparison of feature vectors between the target and query pixel are necessary to build the neighbourhood [111],

$$N_{\Phi(x)} = \{y \in X : d(\Phi(x), \Phi(y)) < \epsilon\}. \tag{12}$$

Depending on the situation it might be favourable to focus on specific areas in an image and reduce the distance of the query to a bounded descriptive neighbourhood. This is enforced through a radius parameter r, similar to the spherical neighbourhood that limits distance of the query range [111],

$$N_{\Phi(x)} = \{y \in X : d(\Phi(x), \Phi(y)) < \epsilon \; and \; d(x, y) < r\}. \tag{13}$$

Up to this point, the neighbourhoods have been described as being less than a set bounding measure, either r or ϵ. This leads to the concept of open and closed sets. Open sets are considered sufficiently near the focal point, similar to what is shown in Eq 10 and 12 [111]. This implies that they do not contain the boundary points of the set [111]. Conversely, closed sets will contain the boundary points as well [111]. This relates directly to neighbourhoods, with the above expressions referring to open neighbourhoods and a closed neighbourhood can be represented as,

$$N_x = \{y \in X : d(x, y) \leq \epsilon\}. \tag{14}$$

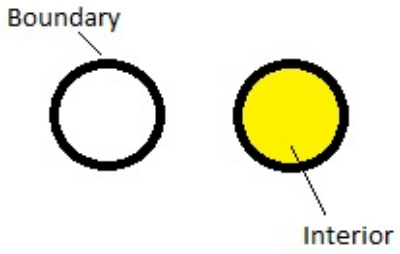

Figure 8: Boundary/interior visualization

The reason for mentioning this is that a family of open sets on a metric space can be considered a $metric\ topology$ or topological space, which is a more general case that satisfies the ensuing axioms for a metric space (X, d) [11, 111].

TS1. X and the empty set, $\{\emptyset\}$ are open.

TS2. All unions of open sets are open.

TS3. The intersections of open sets are also open.

Although there are other approaches to do so, these axioms are best suited to defining a topological space in the context of this work. As mentioned, a topological space is a more general case and there are variants with additional constraints for more specific purposes, such as proximity or tolerance spaces [56, 111, 113].

The previous discussion on sets, spaces and topology has been building towards providing a backdrop for a proximity space. This is a special case of a topological space that provides axioms for $nearness$ between sets instead of from a point-to-set perspective [111]. The proximity space was described by $Frigyes\ Riesz$ in 1908 [89] and later revisited and garnered greater attention by others, including Efremovič [31]. The axioms developed and published by Efremovič relate to a binary nearness measure between sets and define a proximity space. For example, consider subsets A, B and C of X where δ is a relationship between them [90, 111].

PS1. $A\ \delta\ B \Rightarrow B\ \delta\ A$.

PS2. $A\ \delta\ B$ implies $A \neq \emptyset$ and $B \neq \emptyset$.

PS3. $A \cap B \neq \emptyset \Rightarrow A\ \delta\ B$.

PS4. $A\ \delta\ (B \cup C) \Leftrightarrow A\ \delta\ C$ or $A\ \delta\ B$.

PS5. $(\forall E,\ A\ \delta\ E$ or $B\ \delta\ (X - E)) \Rightarrow A\ \delta\ B$.

The δ nearness measure, $A\delta B$ can be read as A $near$ B.

With a binary proximity relation δ defined for a proximity space, the concept is then extended into a more focused tool for our purposes in image analysis. Specifically, we are interested in descriptively near sets in a descriptive Efremovič proximity space. Descriptively near sets have been mentioned briefly already in Eq 13 above. They are concerned with a nearness measure based on feature values from a feature vector derived from probe functions [111]. The probe functions are real valued ($\phi : X \rightarrow \Re$) and provide individual features for pixel points in an image [111]. We are interested in a descriptive proximity

measure when examining images and it can be represented as δ_Φ where,

$$\delta_\Phi = \{(A, B) \in P(X)xP(X) : clA \underset{\Phi}{\cap} clB \neq \emptyset\}. \tag{15}$$

In Eq 15, clA and clB refer to the closure of a set [111]. The definition of a closure in a proximity space clA is the intersection of all closed sets that contain A [111].

Set patterns are examined in more detail to discover patterns in hand images, compare similarities throughout the hand and with base-line values. The proximity space described above gives rise to a *discrete uniform topology* when examining sets that have non-empty intersections with a given set [111]. This is what lays the foundation for studying visual patterns in images [111]. There are two types of set patterns to consider, spatial and descriptive [111]. A spatial set pattern consists of spatially near sets [111]. As we are more interested in descriptive features, the main focus is on descriptive set patterns which consist of descriptively near sets that are not necessarily spatially near [111].

There are different types of descriptive set patterns, including a descriptive point set pattern, a picture set pattern and a motif set pattern [111]. A descriptive point set pattern (denoted, $\mathfrak{P}_{\Phi(x)}$) is a set of points with a principal point $x \in X$ [111]. Elements in the descriptive point set pattern must adhere to the nearness property where a point in question must be descriptively near the principal or focal point [111]. The principal or focal points have also been referred to as *landmarks* by Grenander in his work [49]. Picture set patterns go one step further by examining descriptive properties of a collection of sets [111]. The elements of a picture set pattern must have common features to belong [111]. The last type of set patterns considered are motif set patterns, which are an extension of picture set patterns [111]. What distinguishes a motif set pattern from a picture pattern are axioms that the members of the set adhere to [111]. Although spatial motif set patterns exist, a discussion about them is not included (see [111] for a detailed discussion) as my focus is on descriptive motif set patterns. To elaborate on a descriptive motif set pattern, we are

given that $\mathcal{P}^2(X)$ is a set of collections of subsets in X and $M \in \mathcal{P}(X)$ corresponds to a motif [111]. Since we are dealing with a descriptive motif, a set of probe functions (Φ) that provide feature values for members of X are necessary along with a descriptive proximity relation, δ_Φ [111]. For $\mathfrak{P}_\Phi(M)$ (M is the motif set pattern) to be considered a descriptive motif set pattern, it must satisfy the following descriptive motif set pattern (DMSP) criteria,

DMSP1. Given A, $B \in \mathfrak{P}_\Phi(M)$ they can be spatially disjoint and also descriptively far from each other. Also, A and B can be descriptively near but spatially far from one another and finally, A and B can be descriptively near and spatially near each other,

DMSP2. $A\ \delta_\Phi\ M$ for every $A \in \mathfrak{P}_\Phi(M)$,

DMSP3. For pairs A, $B \in \mathfrak{P}_\Phi(M)$ that are descriptively near to the motif, M, a descriptive isometry exists that descriptively maps points in A into descriptions of points in B [111].

Up to this point, the description of set patterns has consisted of descriptions of the sets that are members of a collection of set patterns. Delving to a more granular level, it is possible to look at specific points within the collection of motif set patterns that match a specific focal point (or point of interest). These are described as $neighbourly$ or $salient$ points where the descriptive values of a focal point and query point are equal or very nearly equal (narrow tolerance) [111]. This can be represented as,

$$N_{\Phi(x,\epsilon,r)} = \{y \in X : d(\Phi(x), \Phi(y)) < \epsilon \; and \; d(x, y) < r\} \tag{16}$$

These are used to examine members of descriptive motif set patterns with a more constrained view, providing output that most closely resembles the focal point of the query. This concludes the background discussion on developing patterns for processing subject images in the context of extracting and refining meaningful information in support of visual hand assessment.

3 System Architecture

As a starting point, a global view of the telerehabilitation system is included to show the motivation and reasoning behind the inclusion of each element. As telerehabilitation has evolved over the years there are many different types of system builds for various purposes. For our case, the telerehabilitation system has been developed in response to the question of discovering a suitable interface technology that can support a clinician supervised rehabilitation program in either a clinical or home-based setting. To meet the requirement of remote rehabilitation, the interface must be flexible, easy to use, yet still effective and also maintain the interest of end users for the duration of their treatment program. The target demographic are rheumatoid arthritis (RA) patients, typically long-term or ongoing treatment plans are expected to help support them. This raises the stakes further to ensure that user motivation is taken into account to help provide the best possible interaction for the long term as part of their rehabilitation and maintenance process. To achieve this goal, gaming is used to more fully engage patients and provide a challenge. Although in the past, games have not been taken seriously, more recently there have been a number of publications on gamification at the workplace and using gaming strategies in the real world to improve productivity and work output [61]. There have been a number of recent studies reported and surveys of the literature that discuss gamification and its uses in more detail [26, 51, 61]. The distinction being gaming vs. play where serious gaming and tactics from gaming can be leveraged as motivational tools similar to competitions for example [51]. Although we are employing a game as part of the motivational tool, it is based on the idea of gamification of the interaction with the telerehabilitation system to increase the motivation with a challenge and hopefully retain client interest over a longer duration, with a more enjoyable experience.

Finger-hand function has been targeted over gross reaching or transport movements as a number of typical daily activities require a significant amount of manual dexterity (e.g. brushing teeth, getting dressed, eating). In addition, some of the most commonly affected

joints in early onset RA can be found in the hands [76], potentially manifesting changes that are readily measured. Hand function is also a good measure of quality of life considering how vital it is to actions that are often taken for granted until a problem arises [33]. The motion control problem associated with hand movements is customizable for the individual through choice of input control object. A given object has its own characteristics like size, shape, texture, centre of mass and kinematics. Bridging object movement with input control of a custom built rehabilitation gaming platform is our chosen means to motivate, study and quantify user movement performance in the context of precision, high-fidelity movements.

When surveying some of the common methods used for rehabilitation gaming in the literature the most popular methods usually fall into one of the following categories, a virtual reality (VR) setting [15, 25, 47, 57, 78], force feedback gaming [67, 86] and robotic assistance approaches [16, 72]. Each of these methods are suitable for solving a rehabilitation gaming motivation problem. However, the research presented in this report approaches the problem from a different angle, aiming for flexibility, ease-of-use and cost-effectiveness. Each of the methods mentioned above fails to meet at least one of our considerations. For the case of virtual reality systems, they are immersive and work well at keeping patient motivation high however the software and interface are a potential limiting factor due to cost and ease of use. Custom designed software and hardware are typically a requirement for VR systems. This will also limit the variety of games available and depending on the controller it can also limit who is able to use the system based on severity of the disability for the individual and also may limit the possible range of therapeutic movements. Force feedback gaming is similar in that the controller can limit the target demographic and/or range of therapeutic movements. Typical controllers include force feedback joysticks, mice and steering wheels). In addition, force feedback is not always supported in gaming platforms so the selection of alternatives can be limited. Finally, the robotic-assisted rehabilitation gaming approach has a few potential problems, a certain degree of flexibility/dexterity may be required for operation, also the other potential problem is cost. Robotic systems are bet-

ter suited for clinical or remote clinical environments as they are typically expensive and supervision during operation may be necessary to ensure safety. These different solutions for rehabilitation gaming platforms were considered when addressing the requirements for a telerehabilitation gaming system targeting RA patients.

Similar to others, our system design is built around a custom rehabilitation gaming platform. A common tactic is to have a self contained system where the gaming platform is a fixed component and there may be several modes of play or choices for environment to keep things fresh. Our approach is to use the custom gaming platform once or twice (at most) per session and restrict play time to a few minutes as a means to monitor movement performance and hand condition in a controlled setting. The reminder of the duration for a therapy session can be spent playing different games that suit a client's individual preference to help maintain their interest and motivation levels. Combined with various input control devices used to manipulate game sprites, this allows for similar activity in unmonitored settings to complement the time spent using the custom built gaming platform. This results in data logged only during the session when clients are using our game, the remainder of the session is intended to provide an opportunity for continued, unmonitored practice of the specified therapeutic exercises for the hand(s).

User performance is derived from data that is captured during the custom-built game sessions. Information from a given session is gathered, stored and can be uploaded to a server for post-processing. This process is used to determine patient performance and ability at a given instance in time. Given multiple sessions this presents a temporal sequence that can help show improvements, degradation or consistency in performance. This type of system is categorized as a $store\ and\ forward$ telerehabilitation design [152] as it is intended for partial or potentially unsupervised sessions occurring in a remote or home based setting. To help provide a visualization of the building blocks and how the components fit together for the telerehabilitation system design, Fig. 9 displays the system diagram (established in [80, 110]). This diagram includes a number of components from input control to

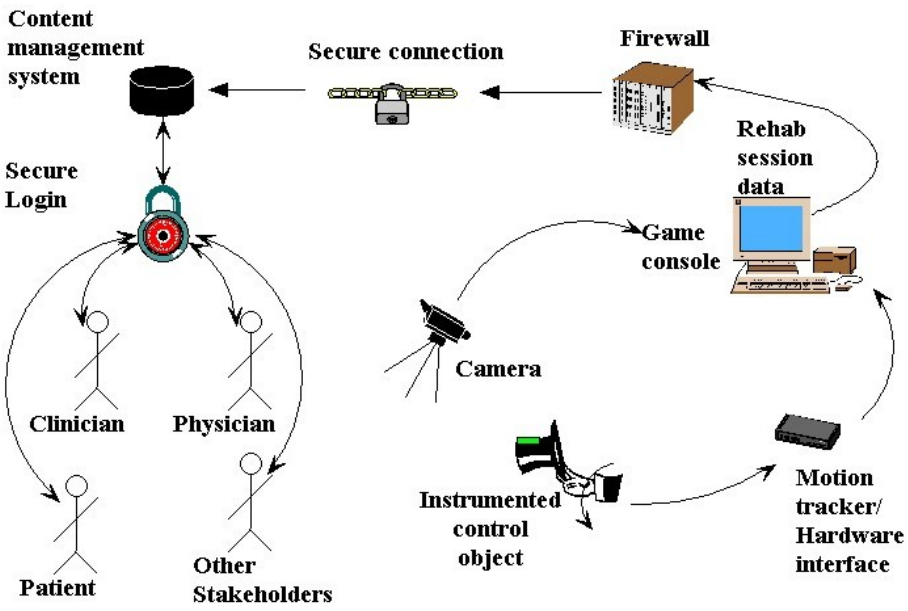

Figure 9: System diagram

data storage. The telerehabilitation gaming system consists of several main components including both commercially available and custom built items. The custom built components include a hardware interface between input control objects and a computer, the gaming platform and all of the data capture and processing software.

The remainder of this section discusses the components that make up the telerehabilitation gaming system. This includes the physical components of the system and their evolution, the custom gaming platform used to track user performance, the image acquisition setup for capturing still imagery of important hand poses, feature extraction on resulting movement performance data, hand pose image analysis and the content management system.

3.1 The physical system

The physical components that make up the telerehabilitation system are what bridges the system to the end users. This has evolved over the course of the project, starting with a setup found in Fig. 10b. From a high level perspective, the system consists of several com-

(a) Selection of control objects

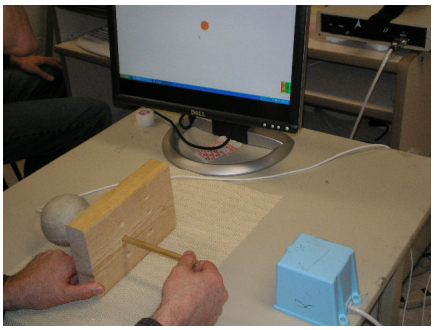

(b) Physical setup

Figure 10: Input control objects and example

ponents, input control objects, a motion tracker, an interface between the motion tracker and a computer that runs the gaming platform. As the work has evolved over time, the system has been refined but the main concepts still apply.

The first element addressed is the point of contact with a client, the input control element. Input control objects are specified by a clinician based on the therapeutic exercise value when translated into finger-hand control motion. The associated movement(s) are intended to be part of an exercise program to replicate common movements or situations encountered in daily life (e.g. turning a key, manipulating a cup, turning a screw cap). With that in mind, objects are selected to allow patients to perform willed, voluntary movements while our system tracks their performance during those events. With a myriad of objects available to harness as input control elements we are able to support varied end-user ability including severely limited movement ranges that can be scaled, filtered and mapped into full screen control. Our rehabilitation gaming platform supports either 1D or 2D planar movements. A selection of input control objects can be seen in Fig. 10, with an example showing a coffee cup being used to manipulate the game sprite. To provide a seamless experience with an instrumented control object, both fidelity and responsiveness of the interface need to be comparable with regular input control devices (e.g. mouse, keyboard) to avoid frustrating users and potentially losing long term system adoption. To that end, motion tracking with reasonable sampling rates for human motion was considered as a

potential solution to meet that requirement.

The individual motions or user actions need to be converted into control signals to interact with the telerehabilitation system. Commercially available devices have been used for that task, in both a more elaborate and expensive approach (suitable for a clinical environment) and also a less complicated, cheaper solution with less tracking features (suited for home use) yet still providing meaningful results. The more elaborate and expensive approach to motion tracking employs a magnetic motion tracker with six degrees of freedom (6-DOF). We used a miniBIRD® 500, available from Ascension Technologies [142]. This particular model is a pulsed-DC magnetic motion tracker that can track 6-DOF. A benefit associated with this device is the relatively small sensor size (5mm x 5mm x 10mm), making it easy to instrument a wide variety of input control objects and track them as a point source. The miniBIRD® samples at a fixed rate of 100Hz and has a short range magnetic field making it suitable for precise, contained movement such as finger-hand motion. There are drawbacks associated with the magnetic motion tracker. First, it has a wired sensor meaning that control objects are tied to the tracker and the wires must be accounted for and not obstruct user movement. Also, there is an obvious expense associated with using a magnetic motion tracker making it better suited for clinical settings with a budget for such a device and where trained staff can operate and assist patients in using the system. The output presented from the miniBIRD® is raw position and rotation data. A hardware interface was developed to provide seamless translation and rotation from the miniBIRD® sensor into on-screen computer control. The Szturm-Otto magnetic motion tracker-to-computer interface was developed to solve this problem by taking the input motion and translating it into computer control signals to replace common control devices such as a keyboard, mouse or joystick [102]. This supports instrumenting virtually any object as an input control device (an in depth discussion of the hardware interface is provided in [102]). In contrast, there have been several devices used as alternatives to magnetic motion tracking with an intent to support a less expensive approach for home use yet still providing a meaningful

experience and results. To replace the magnetic motion tracker with something less expensive and intuitive to use, commercially available devices provide the best alternative. Examples include a trackball and wireless gyro air mouse. The replacement items are self contained, not requiring specific hardware interfaces or motion tracking systems to provide feedback for movement performance. However, they are not able to track the full 6-DOF that the miniBIRD® system offers, instead they are limited to two degrees of freedom. This restricts the range of possible movement exercises yet still provides enough to support a feasible extension to the clinical-based alternative. There are recent advancements in technology that will likely lead to small wireless tracking units that are able to support more than two degrees of freedom yet still remaining cost effective for either the clinical or home domain. At the time of writing, there are wireless devices available but at a more expensive cost than would be suitable.

The elements of the physical system are described as having two configurations, a clinical and home based version. The distinction is cost and degrees of freedom available for motion tracking. For both cases, being able to slave any input control object to a computer, replacing the common input devices, allows use with almost any software package. This increases the range of game titles that can be used with our TR system to ensure that users can select what interests them to help create a more enjoyable experience for their therapy sessions. The potential downside to using commercially available software is lack of access to source code for customization and also limited reporting of outcome measures. In order to have a fully functional gaming platform that provides improved reporting over the more commonly found coarse scoring measures, a custom-built gaming platform with a detailed output reporting system built from in-game performance was developed to link movement with in-game events.

Comparing our physical system setup with the majority of builds reported in the literature there are a few important distinctions. First, the input control objects can take on virtually any shape or form as they are instrumented with a sensor (either through a magnetic

motion tracker, gyro mouse or an alternative). This means that the movements associated with system interaction can be tailored more closely to individual needs. Also, not all systems reported in the literature have low-cost options that support telerehabilitation for use in the home. Using something like a 2D wireless gyro mouse [50] which retails for less than $100 at the time of writing means that it is well within the means of most people to acquire the low cost device for home use. Some of the alternatives reported in the literature use data gloves [24, 150] or the more expensive motion tracker discussed above which can incur a significant cost, making it more prohibitively expensive for home users. There are other commercially available alternatives that are potentially already in the home in the form of video game consoles. Some examples are the Microsoft® Kinect being used for capturing user movement data for gait analysis [140], the Nintendo® Wii for post-stroke rehabilitation [74], and the Sony® Playstation 3 used in combination with a data glove and a virtual reality video game for telerehabilitation [47]. While the consoles do meet the needs of a low cost device that is also already potentially in the home, the potential problem or distinction between that approach and ours is the resolution of the movements being tracked and used for telerehabilitation. Fine movements of fingers require highly sensitive devices that can examine that level of fidelity. In our case, the input control objects can be specified to exhibit those fine movements and the quality of the movement is then tracked.

3.2 The rehabilitation gaming platform

The central feature of the telerehabilitation system is the gaming platform. This element of the system is responsible for solving the problem of providing in-game events that easily translate into 1D or 2D planar motions to support an array of input control objects. Also it must create a challenging and motivating experience for the end user, generate data from synchronizing user movement with in-game events and then transfer all resulting data for post processing and analysis. Although it is not without benefit to use commercially available games, our telerehabilitation system design requires a more

specific and verbose reporting system than is typically found. Adding this functionality directly to a gaming platform that is tailored to movements that suit a variety of input control objects and provide verbose feedback on what happened during game sessions is the challenge and what separates this approach from commercially available alternatives and builds on efforts by other groups which largely exhibit fewer in-game reported measures and/or rely on non-game related traditional performance measures acquired post-session [17, 20, 67, 70, 97, 108, 118, 132].

The premise of the game is built around sprite control of a rectangular paddle. Players are asked to destroy targets with a particular description by running into them with the paddle and avoid everything else that would be considered a distractor. This is similar in nature to some of the early paddle-based games such as Breakout from Atari®, Arkanoid by Taito®, etc. where targets can be destroyed or bounced off a paddle. Unlike the commercial alternatives, with complete control over the source code, the game has evolved over time, adding new game modes, improved settings for adjustment and refined output details for feature extraction and monitoring movement performance.

The goal of the game is simple in that users are required to destroy as many targets as they can using a paddle by running into them within a set period of time. The user controlled paddle appears at the bottom of the game screen for 1D movements and is free to maneuver around the screen for 2D movement. Paddle movements restricted to a single dimension can be rotated on screen to allow for East-West or North-South orientations depending on the control object and the optimal configuration. The paddle movements are slaved to either a rotational axis or translational movement of a specified input control object. For both cases, target movement is always from the perceived top to bottom of the screen and users have until the target leaves the bottom or edge of the screen to destroy it. An in-game parameter can allow both horizontal and vertical movement of targets if desired, allowing diagonal trajectories. Targets can have a total of up to five possible shapes including a triangle, circle, square, cylinder or sphere. Target descriptions are pro-

vided before a session begins so the player has a well defined task before they start a game. All shapes that are not considered targets are distractors (can be excluded if so desired). Depending on game settings, distractors can destroy the paddle when they contact each other to provide a penalty in the form of having an unusable paddle for a short period of time. A screenshot of gameplay is included in Fig. 11 to help demonstrate the components that make up game play. When considering movement in the game window, it is

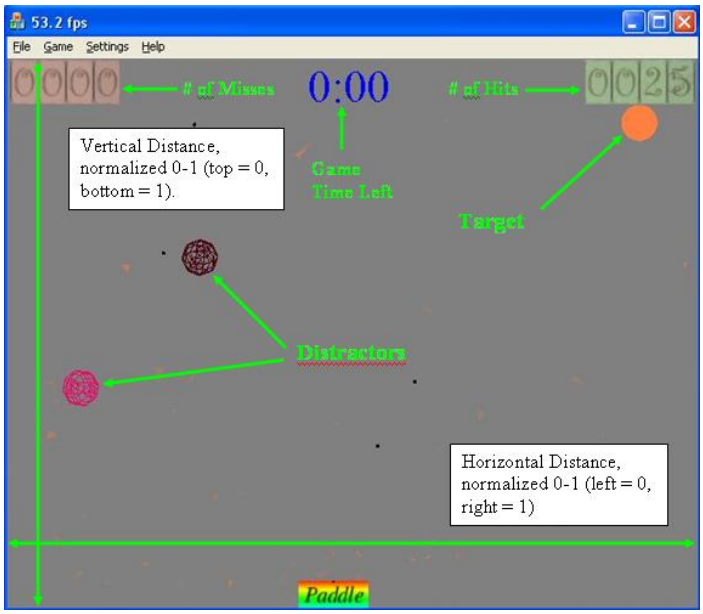

Figure 11: View of the game screen

important to note that the window has been scaled from 0 to 1 in both the horizontal and vertical directions with (0,0) representing the top left corner of the game screen and (1,1) representing the bottom right corner. This is important for establishing direction of travel and also provides a uniform range for measuring and reconstruction of movements during post-processing.

Self-reported questions were added to game sessions in the form of a pop-up window at both the beginning and the end of a session. Relating directly to symptoms of flare up conditions in RA, the pop-up windows allow users to specify their current joint pain and stiffness levels on a scale from 1 to 10. Users are asked to specify these values twice, once at the beginning of a session and once at the end to allow for comparison. An image of

the pop-up window is shown in Fig. 12. This allows subjective feedback from the user to accompany their movement performance output data to correlate any change in pain and stiffness with performance.

Figure 12: Pain and stiffness pop-up window

To ensure that the game is playable by virtually any skill level, there are a number of adjustable parameters available to help tune the experience and also match input control object movement to paddle movement. Table 1 contains a complete list of the parameters and a short description of what they offer to alter the game play experience. There are also parameters that allow the behaviour of each shape that appears in the game to be altered during setup. A separate table is included (see Table 2) as all shapes can be adjusted with these same parameters. The last set of adjustable parameters are set at the beginning of each game. They provide the ability to select the type of game and also specify a few more elements in reporting. The next table shows the final set of parameters for our game (see Table 3). Using various combinations of adjustable game parameters, it is possible to set the game up to provide a challenging experience for virtually any skill level or ability.

During the early stages of using the gaming platform, additional game modes were introduced as alternatives to the standard mode of play focused on non-deterministic user

Group name	Allows unique user name to identify output data
Data collection	Allow data to be saved locally or uploaded
Learning method	Learning method to alter difficulty during play
Lower threshold 1	# missed targets & destroyed paddles
Upper threshold 1	# missed targets & destroyed paddles
Lower threshold 2	Distance travelled by the target
Upper threshold 2	Distance travelled by the target
Background Color	Alter background colour
Framerate	Change fps rates or max setting
Collision detection	Allows CPU or a GPU to take on that task
Weapon selection	Paddle can be used as a gun
Weapon speed	Dictates how fast the paddle gun will fire
Weapon speed one-at-a-time	Weapon firess one bullet at a time
Weapon volume	Adjusts the speaker volume of weapon fire
Game volume	Adjust speaker volume for all game events
# of targets per second	Set maximum # targets on screen
Mouse sensitivity	Horizontal & vertical sensitivity adjust
Horizontal movement	Allow 2D target movement
Min distance between targets	Force a minimum movement
Paddle size	Range from 50% to 300% paddle size

Table 1: Adjustable game parameters

movements. First, a separate game mode that includes a single indestructible, oscillating target on-screen was developed. Users are asked to track the target as closely as possible with the game-paddle as it oscillates in a sinusoidal pattern. As outlined in the settings from the tables above, there are a few parameters that can adjust this game mode including time duration, frequency and amplitude of the sinusoid. The reason for including this type of game mode is that a number of other works have been reported using movement performance analysis on tasks similar to Fitts' work with rhythmical aiming (pendulum-motion) [10]. Inclusion of this mode allows easier comparison with existing work and provides an alternate mode for movement performance analysis. The next game mode added was a force-feedback teleoperated system. This game mode supports a game-session supervisor located in a different area (room, building, city, etc.) to monitor game progress in real time and deliver force feedback messages to an individual playing the game when specific events occur. The final game mode that was added supports a learning or adaptive

Show	Restrict or allow a given shape in current session
Rotate	Restrict or allow changed orientation
Change colour	Restrict or allow varied colours
One at a time	Restrict to one shape on screen
Distractor	Set shape as a distractor
Random size	Shape size is variable
Speed	Sets how fast target moves on screen
Size	Sets size of target to fixed value

Table 2: Adjustable game parameters for shapes

Difficulty level	Custom or auto (auto implies learning)
Vulnerable paddle	distractors will destroy paddles
Free paddle	Allows 2D movement of game paddle
Time limit	Select game length from preset times
Sinusoid tracking	Sinusoidal movement game mode
Time	Sets duration for sinusoid movement mode
Period	Sets the period of movement for sinusoid mode
Specify pain/stiffness	Pop-up window to describe pain/stiffness
Ask for selecting object	Record input control object

Table 3: New game parameters

mode of game play. The learning mode is able to alter the degree of difficulty of game settings during a session. This supports an optimal level of challenge approach where a set rate of desired success is applied and the difficulty settings will adjust to the point where the user is able to meet the optimal result criteria. A modular learning approach was used to support a variety of different learning algorithms, from a brute force approach that adjusts difficulty based on score to reinforcement learning modules like Q-learning that adjust game play based on temporal states, actions and rewards from episodic calculations [141]. Collectively the additional modules were completed with the intent to provide a multipurpose rehabilitation gaming platform that can log and provide in-depth reporting on user movement performance for a variety of conditions.

Typical gaming sessions are short, but the number of events provide a wealth of information from the movement tracked during that time. Throughout game play, all movement on the screen is captured and logged at a set sampling rate (minimum 50Hz). Human reaction times are typically no faster than about $200-250ms$ when considering visual tasks and

subsequent movement [144], meaning the Nyquist rate [114] for sampling would be two times the highest frequency of 5Hz. We are using five times that amount as our minimum sampling rate to ensure high quality sampled signals for user movement. The tracking includes both the user controlled paddle movement and also all on-screen object movement. For analysis, an in-game event is defined as the life of a target on the game screen. Implying that as soon as a target appears, the associated even begins and that event lasts until the target is destroyed by the paddle or leaves the screen if missed. Synchronizing user movement and the game events allows a more in-depth examination into movement strategy and performance analysis based on what happened during game play. The alternative being the more commonly found coarse scoring systems available in the majority of commercial platforms where only the number of target hits and misses would typically be provided.

For testing and validation purposes, we restricted the number of targets on screen to one at any given time. This provides a more meaningful analysis of user movement as they are not caught between multiple targets and having to make difficult decisions as to which target to destroy, potentially missing others as a result. Also, this ensures that gaming events are easily broken up into the life of a target and all associated paddle movement during that event can be seen as an attempt to destroy a single target, making it simpler to rebuild user strategy for analysis. All resulting data from a game session can be stored on a local machine or uploaded to our server for processing where movement performance features are extracted and examined in more detail. All game code was written in Microsoft® Visual C++.

3.3 Image acquisition for still hand poses

The next aspect to consider for capturing descriptive features of finger-hand function and condition relate to the visual domain. We are interested in examining several hand poses that were chosen specifically to look for common problems or conditions that can occur in rheumatoid arthritis either during disease activity or early signs of resulting damage from

disease activity. Three hand poses are considered, two from a top view and one from the lateral perspective. They are presented in more detail here along with the setup for image acquisition to get the best possible view and extract the desired features.

The first hand pose included is a top view of both hands in a relaxed posture (see Fig. 13). This pose is included to allow examination of the hand structure in more detail.

Figure 13: Hand pose 1: top view, relaxed posture

As mentioned in Sec. 2.2, one of the potential complications present in RA patients is when enough damage occurs to joints in the wrist that the fingers will begin to shift towards the ulna (ulnar deviation). To monitor the early signs of this type of deformity, structural analysis of the bone locations can provide us with a warning when changes are occurring in the joint angles. The traditional methods for examining this type of problem are through visual inspection, using goniometry or looking at x-ray images of the hands to determine or measure any changes. Part of the work presented here is to develop an algorithm to extract hand structure from the top view pose to elaborate on the progression of ulnar deviation should a problem exist or begin during a treatment program. In addition, the top view pose with both hands are examined for texture, area and discolouration of the joints, looking for signs of flare-up conditions manifesting as symptoms of inflammation in the hands.

The next hand pose uses the dominant hand and is intended to examine a lateral perspective, paying particular attention to the index finger. This pose has the subject position their hand at approximately 45° from the surface they are resting on (see Fig. 14). The rea-

Figure 14: Hand pose 2: side view, index finger, dominant hand

son for examining the index finger from this perspective is to capture a view-point of the hand that could lead to monitoring another complication that can occur with RA patients, the boutonierre or swan-neck deformities (see Sec. 2.2 for more details). These problems occur when damage occurs to the DIP and PIP joints that cause them to hyperextend or flex. When joint damage becomes significant enough, the result can be permanent fusion in those positions. Typically this would be measured using visual inspection and could also be tracked using goniometry or still imagery to monitor changes. The final element of structural information extracted from the still imagery involved development of an automated algorithm to extract joint angles from the side-view perspective of the dominant hand. Thus allowing us to monitor changes in the DIP and PIP joints as potential early warning signs related to the aforementioned deformities.

The final hand pose also involves the dominant hand and is included to discover active range of motion measurements. The subject is required to spread their fingers in flexion

and abducted from the centre of the hand for this pose (see Fig. 15). This pose is included

Figure 15: Hand pose 3: top view, spread fingers, dominant hand

to examine the typical range of motion (ROM) measures that would be used to assess the capability of hand-function for the patient on a given day. Also, it has the potential to discover subtle problems that could be masked by the first relaxed pose, specific to joint angles that could signal joint damage has occurred. Similar to the previous pose, range of motion is typically measured in a clinical setting using goniometry or still imagery with manual measurements taken from the image at a later point in time. Also as above, part of the work presented in this section is to develop an algorithm to establish the angles between the spread fingers to provide those same measures of joint angles in an automated fashion. In addition to useful ROM measures, this pose can also help spot and confirm potential early warning signs that manifest in other aspects of feature analysis from a given telerehabilitation session.

When considering how to capture digital images, there were several important things taken into account to ensure consistency and repeatability. Recalling that one of the problems with goniometry is repeatability from one subject to the next and also different people taking measurements, a simple setup to help minimize the chance for introducing error was

the goal. Different types of cameras were considered, how to position the camera, lighting and background were all parts of the image acquisition problem that were examined.

The starting point for the image acquisition system involved assessing digital cameras from a cost and performance perspective. The details we are interested in extracting from the hand poses are not considered difficult subjects to photograph and thus do not require very sophisticated camera equipment. At a minimum, resolution in the order of 1280 x 720 (1̃MP) pixels is required to have enough information to build hand structure, although greater resolutions are preferred to examine joint characteristics. This resolution lends itself well to virtually any digital camera including web cameras. Less expensive cameras and lenses come with their own set of limitations and some of them can be cause for concern, although our subjects are centred in the field of view and not intended to be compared between multiple cameras. This implies that minor distortion issues may not have a significant impact on the features of interest that are extracted from the various hand poses from one session to the next. For most of the example images, verification and experimental work, a Logitech® Quickcam 9000 webcam was used (see Fig. 16). All images taken of

Figure 16: Web cam used for capturing still imagery of hand poses

the hands were captured using a resolution of 1600 x 1200 pixels. Although web-cams are

not known for being the best cameras they have some distinct advantages. They are relatively inexpensive and often already found in most households. The best option are those that are not built into a device so they can be positioned easily and consistently for image acquisition during any given session. Although we used a web-cam for the verification and experimental work, any digital camera that can be positioned appropriately would fulfill the requirement.

Positioning the camera is an important aspect for proper image acquisition and repeatability. One of the potential problems with inexpensive cameras is that their field of view is narrow, standard lenses can have a $40 - 100^{\circ}$ field of view [151]. Our webcam has a 75° field of view, ensuring a mid-range value for testing and verification. To obtain the best possible view of the subject, it is important to position the camera close or directly above the target, with the field of view centred on the subject. A significant disparity in position can introduce excess error when establishing hand structure as the extremal fingers may be viewed from enough of an incident angle that the structural placement will be incorrect, potentially causing problems at the analysis stage.

The next element to consider in the image acquisition setup is appropriate lighting. To support consistent image capture and analysis, it is important to have similar lighting conditions for each session. One of the problems encountered during the testing and verification stages was excessive shading that caused localization problems when establishing joints in the hand. This was based on some of the assumptions made and how the image information was managed. To eliminate that problem and keep the lighting as uniform as possible while minimizing shadows and still providing a simple setup to promote repeatability, the best lighting was an artificial (incandescent), single source of illumination. This was achieved with a flexible desk lamp stand to allow for quick and easy positioning. Introduction of more light sources caused shadowing as it was not possible to have them all emitting from the same point. In addition to using a single illumination source, positioning the lighting for the best possible images again requires very close to directly above, sim-

ilar to the camera. This reduces the amount of shadows thrown by the fingers and hand, minimizing any potential error due to misplacement of bone structure or joint locations. A sketch of an example setup for image acquisition is included to visualize how images were captured.

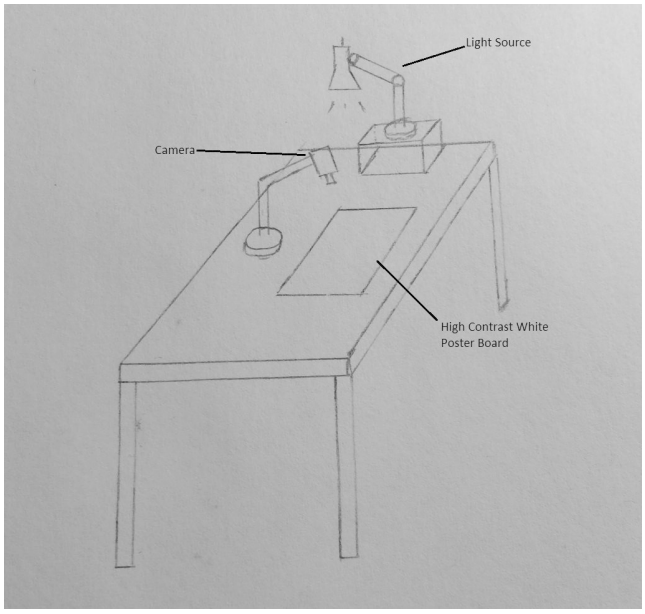

Figure 17: Sketch of image acquisition setup

The last ingredient for the image acquisition problem is the background. The environment for capturing hand images is easy to control and the best possible background for a segmentation problem would be monochrome and high contrast compared to the subject. The possible range of skin tones is varied meaning that for a general high-contrast background, a light, uniform colour would work best. Several iterations were experimented with before settling on a matte-white foam-core poster board cut down to a manageable size for a desktop. The contrast it provides and overall resilience to shadows simplifies segmentation of the hands from the background when preparing each of the hand poses for feature extraction.

3.4 Movement performance features

Once a telerehabilitation gaming session is complete, the first stage in analysis of resulting data is to examine movement performance features. The challenge is to bridge our data analysis with movement performance measures from goal-directed or precision aiming tasks (see Sec. 2.3) and provide a suite of features that can categorize movement performance in an automated fashion from a game session. A number of features are extracted from the raw data to provide a picture of how the user performed during a given session. The measured aspects include accuracy, reaction time, rise time, path length, total score, and the number of times the game paddle was destroyed during play. The movement performance measures operate under the basis that the number of events are $N > 0$, or they will not be included in post analysis (e.g. if there are no missed events, the accuracy measures are not generated). All measurements are taken as a function of normalized screen distance from 0 to 1 and are thus considered unit-less and provided as percentages. In addition there are self-reported questions for levels of pain and stiffness at both the beginning and end of a gaming session, allowing users to specify how they feel at the start and if there is a change after they finish a session. Collectively these measurements build the basis for a set of digital features that are able to classify user performance.

The resulting data from a game session is compiled into one long sequential file that has a protocol for timestamp and movement delimiters, allowing it to be parsed into events (see Fig. 18). Game events are determined by target lifecycle and all movement that occurs during the life of a target is considered part of the corresponding event. During each game event, all objects on-screen are tracked, allowing re-construction of paddle, target and distractor movement. The movement strategy and performance are derived from this information. During verification and testing, we restricted the movements to single-dimensional, using a fixed-axis for paddle movement (either North-South or East-West depending on the input control object).

One common measurement for goal directed aiming tasks is accuracy. We have sev-

$TimeStamp$	$PVis$	$PaddleX$	$PaddleY$	$Object$	$ObjectX$	$ObjectY$	$BRadius$
11871	1.00	0.00000	0.95000	c0000	0.78362	0.20415	0.02888
11882	1.00	0.00000	0.95000	c0000	0.78362	0.21105	0.02888
11893	1.00	0.00218	0.95000	c0000	0.78362	0.21795	0.02888
11903	1.00	0.00416	0.95000	c0000	0.78362	0.22421	0.02888
11914	1.00	0.00852	0.95000	c0000	0.78362	0.23111	0.02888
11925	1.00	0.03250	0.95000	c0000	0.78362	0.23801	0.02888
11935	1.00	0.05627	0.95000	c0000	0.78362	0.24428	0.02888
11945	1.00	0.08402	0.95000	c0000	0.78362	0.25056	0.02888
11955	1.00	0.11570	0.95000	c0000	0.78362	0.25682	0.02888
11966	1.00	0.21382	0.95000	c0000	0.78362	0.26372	0.02888

Figure 18: Cross section of example data from a game session

eral accuracy measures that help demonstrate and explain user movement performance and strategy to monitor for potential changes in movement quality, either improvement or degradation. First, we examine overall accuracy at the end of a movement, where the paddle ends up in relation to the target at the end of the event if it was not successfully destroyed. The accuracy is an absolute measure of normalized screen distance (see Eq. 9). Reporting on a complete session takes the average value of the accuracy measure over all missed targets during a game session, providing a general accuracy performance metric (see Eq. 17).

$$Accuracy = \frac{1}{N}\sum_{i=1}^{N}\sqrt{(x_{i2}-x_{i1})^2(y_{i2}-y_{i1})}, \tag{17}$$

where i corresponds to events where the target was missed and the distances measured are from the centroid of the paddle (x_1, y_1) to the centroid of the target (x_2, y_2) and N represents the number of missed events. The average accuracy measure provides a general indication of user performance in the sense that over time if changes occur it is possible to quantify how much movement accuracy has been affected in an overall capacity indicating whether the client is demonstrating improvement or degrading performance.

The second accuracy measure is the average overshoot for all missed events. Overshoot occurs when the paddle has moved beyond a target during the event. This distance measure makes use of prior knowledge for starting location of the paddle and the target to decide if

a missed target has incurred overshoot error in a given event (represented in Eq. 18).

$$Overshoot = \frac{1}{N}\sum_{i=1}^{N}\sqrt{(x_{i2}-x_{i1})^2(y_{i2}-y_{i1})}\; iff\; d(x_f,y_f) > d(x_e,y_e), \qquad (18)$$

where i is the count for N missed events and the conditional statement requires that the final distance $d(x_f, y_f)$ be greater than the exact distance of the target from the paddle at the start of the event $d(x_e, y_e)$. The overshoot error represents a specific type of game strategy where the user is generally moving too quickly or applying too much force on the input control object to closely adjust during the correction phase of movement when meeting the target. This can indicate potential problems developing as a result of stiffness or any other underlying condition that can be a result of disease activity in the hands that may cause the user to make faster or more sweeping movements when fine dexterity is reduced compared to normal.

The third accuracy measure is average undershoot for all missed events. Undershoot error occurs when the paddle is not moved far enough to reach a target during an event movement phase. Similar to the case of overshoot, the distance measure makes use of prior knowledge for starting location of the paddle and the target to decide if a missed target has incurred undershoot error in a given event (represented in Eq. 19).

$$Undershoot = \frac{1}{N}\sum_{i=1}^{N}\sqrt{(x_{i2}-x_{i1})^2(y_{i2}-y_{i1})}\; iff\; d(x_f,y_f) < d(x_e,y_e), \qquad (19)$$

where i is the count for N missed events and the conditional statement requires that the final distance of the paddle from where it began be less than the distance of the target compared to the paddle starting location. Undershoot error can occur based on a more cautious game playing strategy where the user is not applying enough force during the ballistic phase of movement. This can result in missing the target during the correction/verification phase of movement. Similar to the previous measure, this can indicate an underlying cause if the undershoot measure is greater than expected values from past performance. Pain, stiffness

or weakness could all be contributing factors that slow user movement and indicate that the input control object is difficult to manage for a given task.

The fourth and fifth accuracy measures are the residual and RMS residual error for the movement trajectories. The residual error represents the difference between the average of a group of movement trajectories made by the user compared with an average movement trajectory made by a group of healthy individuals. Since movement in the game was broken down into three categories based on distance traveled, three average movements were required when making comparisons in each direction. A more detailed discussion on how the movements were captured and verified can be found in the following chapter on system verification. The average movements from healthy individuals were stored and recalled as separate movement signals when measuring the distance between a user movement and the average to generate the residual error. One potential problem when comparing movement signals is that lengths are not always identical. There are three possible cases, the patient can have an average trajectory that is longer, shorter or equal to the number of samples contained in the healthy average movement trajectory. This requires taking steps to synchronize lengths before making comparisons. For the case when the two are equal, a simple distance measure can be used (see Eq. 20),

$$Residual\ error = \frac{1}{N}\sum_{i=1}^{N}\sqrt{(y_a - y_{cm})^2 + (x_a - x_{cm})^2}, \tag{20}$$

where N is the length of the current movement (cm) and also the average (a) movement trajectory. For the case when the current movement trajectory is larger or smaller in length than the average movement trajectory, interpolation is required. Interpolating by some factor I will interpolate or add new samples between current values of the signal in question [117]. The interpolated movement trajectory will have a greater number of samples to match the average trajectory through estimating the values in between the existing samples using the factor I, which is a fraction of the number of samples in the current trajectory

divided by the number of samples contained in the larger, average trajectory and then subtracting that ratio from 1. A number of possible avenues for interpolation exist, the method I chose was to use a cubic spline as it is well suited for approximating the movement signals. The movement trajectories are typically representative of the average with some deviation. An example average movement trajectory is shown in Fig. 19. Spline functions

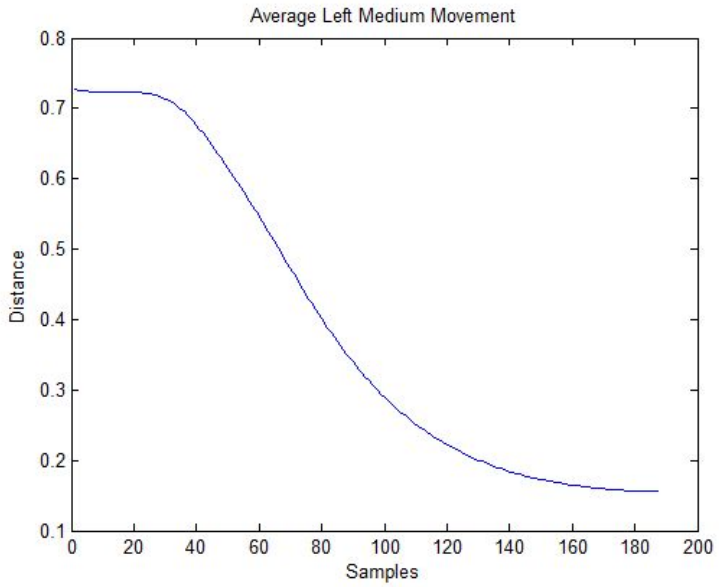

Figure 19: Average movement trajectory example

are lower order polynomials that can be used for interpolation to connect data points [21]. The spline functions perform well at interpolation when there are abrupt changes in the data [21]. This suits the movement data as typically the paddle is at rest and once a target appears and is recognized then movement suddenly occurs as is evidenced in Fig. 19. Once interpolated and the trajectory signals are matching in length then the residual error can be generated from Eq. 20. The fifth accuracy measure is the RMS value of the residual error. This consists of taking the square root of the mean squared residual error (see Eq. 21).

$$Residual\ error_{RMS} = \sqrt{\frac{1}{N}\sum_{i=1}^{N} Residual\ error_i}, \tag{21}$$

where i is the count for the number of movement trajectories being addressed.

The next movement performance measures are temporal in nature, including average reaction and rise time. The reaction time has already been briefly mentioned (see Sec. 2.3) as part of the discussion about movement performance, and also relating to sampling rate within the gaming platform to ensure high quality movement trajectories are captured. The reaction time is defined as the period of time between when a stimulus is provided and a corresponding reaction is made [71]. The reaction time is not a fixed value for a given individual, it will vary depending on the complexity of the stimulus, noise or distractions [71]. For the telerehabilitation gaming sessions, we restricted the number of targets to one at a time and limited any background noise to provide a clean stimulus as part of the experimental work. Typical human reaction times for these types of events range from 200-450mS [71]. The reaction time of an individual is similarly generated as an average value over an entire gaming session. The value is generated by examining a given movement trajectory and locating the first instance of intentional movement once a target has appeared on screen. More details with regards to the rise time can be found in Fig. 4. This measure consists of the time it takes for the user to move from 10% of the total distance to 90% on their way to the target. This is similar conceptually to electronics or control theory but the intent is to monitor the amount of time it takes an individual to make the bulk of the movement during the ballistic phase [95].

$$Rise\ time = 90\% \cdot (\#samples) * (\frac{1}{F_s}) - 10\% \cdot (\#samples) * (\frac{1}{F_s}), \tag{22}$$

in this case, samples refers to one complete movement trajectory, the multiplication provides the 90 and 10 percent values and F_s is the sampling frequency. This measure provides some insight into the game-play strategy and also the average type of movements made. The bulk of the movement or time spent moving should fall into the rise time category without limited movement occuring before or after. For the case when the other phases of movement contain a larger quantity than expected, it implies that the movements are un-

usual, potentially erratic or slower and it is likely that more time is spent in the correction phase, trying to reach the target.

Path length is the next movement performance feature intended to examine the variation between successive samples contained in the movement signals. This indicates if movements are clean and smooth or if they are broken up with a stop and start or stuttering alternative. The path length measurement corresponds to the average value of the distance between two samples in sequence throughout the movement (shown in Eq. 23).

$$Path\ length = \sum_{i=2}^{n} \frac{\mid s(i) - s(i-1) \mid}{\mid i - 1 \mid}, \tag{23}$$

the count starts at the second sample as it requires a previous sample to measure from and the range is up to the n^{th} sample where $s(i)$ represents the current sample and the total path length will contain the average value of the difference between each sample pair in a movement trajectory. Larger path length values indicate more erratic movement and smaller values correspond to more efficient and smooth movements.

To complement the performance measures, we next turn our attention to the self-reported pain and stiffness values. The idea was first mentioned in Sec. 2.4, including how self-reported questions fit into the rehabilitation gaming platform in Sec. 3.2 along with the visual representation in Fig. 12. There are two separate popup windows that appear at both the beginning and end of a gaming session. Each allows the user to select a numerical value to represent their current level of self-rated pain and stiffness. Although these are self-reported measures, they support the movement performance data and provide some valuable insight into how the individual perceived their current condition relating to pain and stiffness during a session. Both are common symptoms relating to RA and can be present during disease activity [76]. The numerical scale ranges from 1 to 10 and comes with descriptions to assist in selecting appropriate values. Higher values for either are likely to have a direct correlation with impaired movement.

The final performance metrics are categorized as coarse measures, comparable to traditional scoring in games. This includes the total score, the number of targets hit by the paddle and the number of times a distractor hit and destroyed the user controlled paddle. These three measures are useful and provide some insight into the degree of success in destroying targets that was achieved during a game. However, they can be seen as a supporting group of features that provide a more general measure of either good, consistent or degrading performance during a game session. The movement performance parameters and their measured value are listed in table 4 for convenience. As a group, these features

Number	Feature	Measured Value
1	Accuracy	[0,1]
2	Overshoot	[0,1]
3	Undershoot	[0,1]
4	Residual Error	[0,1]
5	RMS Residual Error	[0,1]
6	Reaction Time	mS
7	Rise Time	mS
8	Path Length	[0,1]
9	Pain Measure	[1,10]
10	Stiffness Measure	[1,10]
11	Total Score	Positive Integer
12	Missed Targets	Positive Integer
13	Distractor Hits	Positive Integer

Table 4: Movement performance features

represent movement performance characteristics extracted from a telerehabilitation gaming session for episodic, random movements.

3.5 Computer vision applied to hand images

Examining what transpires during office or clinical visits for rehabilitation, not only is movement performance tested and rated but also a visual inspection is done to assess any outward signs that could indicate developing problems. Expanding into the visual domain involves establishing the problem of what to examine, how to achieve the necessary views

and then extract meaningful features that allow classification or the ability to comment on condition of an individual from their visual data via telerehabilitation.

As discussed in Sec. 3.3, there are three separate hand poses to examine structure and monitor potential problems. In addition, we are interested in descriptive features relating to joints and their manifestations as part of the symptoms of RA. Potential symptoms that can be viewed at the joint level include swelling, redness and changes in skin surface texture. The challenge is to develop a means to establish reliable hand structure and extract meaningful features relating to the joints and to do so in an automated fashion, eliminating the need for human involvement during analysis. This implies being able to manage various hand shapes, sizes, varied skin-tones, different focal distances and resolutions.

3.5.1 Image preparation

The first step in a computer vision problem after acquisition is image preparation for more sensitive or complex operations. The image acquisition setup being used is strict in the sense of limiting background noise, positioning the camera and also limiting light to a single source to eliminate or significantly reduce the effect of shadows (see Sec. 3.3). These are straight forward requirements that are inexpensive and relatively simple for anyone to setup and tear down in a short period of time. Images captured using this type of setup help improve the segmentation process dramatically, providing excellent separation of foreground and background (see Sec. 2.5.2 for a detailed discussion on the segmentation process). In addition to these considerations, there are a few common problems in image acquisition that need to be addressed, these include variations in scale, rotation and translation.

The variation in scale (different focal distances) are an important consideration for home based equipment as it is not always guaranteed that an individual will have space to leave equipment setup at all times. Each session could see small or large variation in focal distance. This has been addressed by having an initial setup phase when a patient

first employs the telerehabilitation gaming system. When the first session takes place, an account needs to be generated for the user on the server side content management system. This takes place when the first session is completed and the data is uploaded. The process has two stages, manual location of landmarks on the top view of both hands and generation of an identity number and corresponding directory for storing all subsequent session data. Once set up, clients are able to send session data at regular prescribed intervals.

Establishing location of specific landmarks on the hands has two functions. First, it aids in repeatability and second it eliminates the problem of a variable focal distance from the camera to the subject. The process involves having an expert establish a set of landmark locations on the hands for each finger tip, DIP, PIP and MCP joint. The inflection point between the fingers is also included as a landmark for establishing length of the digits in a finger or thumb. These lengths are measured in pixels, and converted to percentage distances of the finger, between joints. Since the measures are based on pixel distance, it is preferable to have the first session completed with a higher resolution camera if possible to ensure a more accurate set of measurements. Prior knowledge in the form of a table of distances between joints allows for quick reconstruction using key landmarks that can be found as part of an automated process (example of landmark selection shown in Fig. 20). The process of placing landmarks is done through the use of a separate graphical user interface(GUI) that was written specifically for the task. The expert user responsible for placing the landmarks will load the top view image of both hands into the GUI and then receives prompts to click on each of the locations in turn. Once complete, a table of data corresponding to the percentage lengths of each digit in the hand is generated. This establishes a record of the condition at the beginning of all telerehabilitation sessions for that individual. The percentages corresponding to digit length are stored in a table in a unique directory on our server for use when processing new sets of images. An example of how the data is stored can be found in Table 5, showing information for the right hand. Data for the left hand is mirrored and stored in the same table, below. To elaborate further an example of

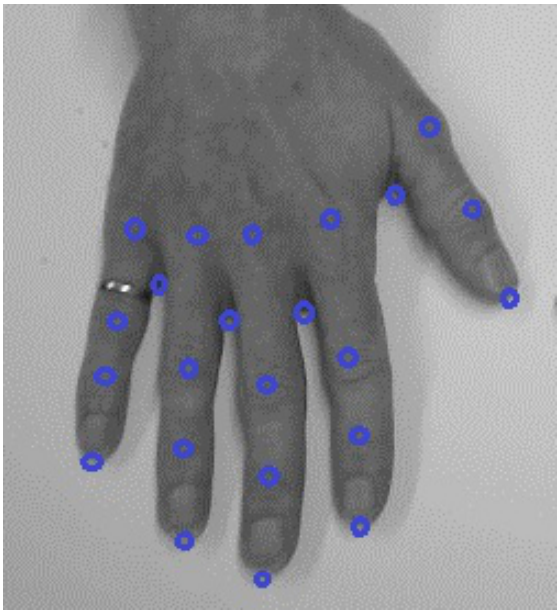

Figure 20: Landmarks displayed on the right hand

Right Hand

Pinky	Ring	Middle	Index	Thumb
Distal Phalanx	Distal Phalanx	Distal Phalanx	Distal Phalanx	Distal Phalanx
Int. Phalanx	Int. Phalanx	Int. Phalanx	Int. Phalanx	Prox. Phalanx
Prox. Phalanx	Prox. Phalanx	Prox. Phalanx	Prox. Phalanx	0
Inflection Point	Inflection Point	Inflection Point	Inflection Point	Inflection Point

Table 5: Storage of digit length percentages

actual digit percentages is included to provide an idea of what was discovered and used in the preparation process (see Table 6). All measurements in Table 6 are percentages that correspond to a given digit, the distal, intermediate or proximal phalanx. The final row for the inflection point refers to the percentage distance from the inflection point between fingers to the tip (the landmarks are placed as circles in Fig. 20).

The final element of preparation before extracting visual features requires segmentation of the hands from the background (discussed in Sec. 2.5.2). The first stage in segmentation employed k-means clustering to segment groups of pixels. The conditions for image acquisition provide strict environmental control to help improve both speed and reliability of the segmentation process. With the assumption made that the hand image background will be a light, matte, monochrome shade of white and anything darker in the image will

33.306279	28.136299	25.887046	30.143550	48.728670
25.144262	27.719536	30.451696	24.678556	51.271330
41.549459	44.144165	43.661259	45.177894	0.000000
70.890818	72.666760	76.871642	71.338377	66.253987
49.000008	28.136870	26.853054	28.611742	33.165446
50.999992	25.957372	27.889456	26.870621	22.796004
0.000000	45.905758	45.257490	44.517637	44.038551
69.657935	73.078652	76.943072	74.272319	72.514013

Table 6: Example digit length percentages

be considered skin tone for the hands, wrist and fore-arms. I used two clusters to separate foreground (hands) from the background. The contrast between the two is significant, reducing the number of iterations required by the k-means algorithm. On average over 10 sets of input images, 3 passes were required before the mean values were discovered and the segmentation was largely successful. This resulted in separation of the hands from the background into two separate clusters (see Fig. 21). Problems encountered during the

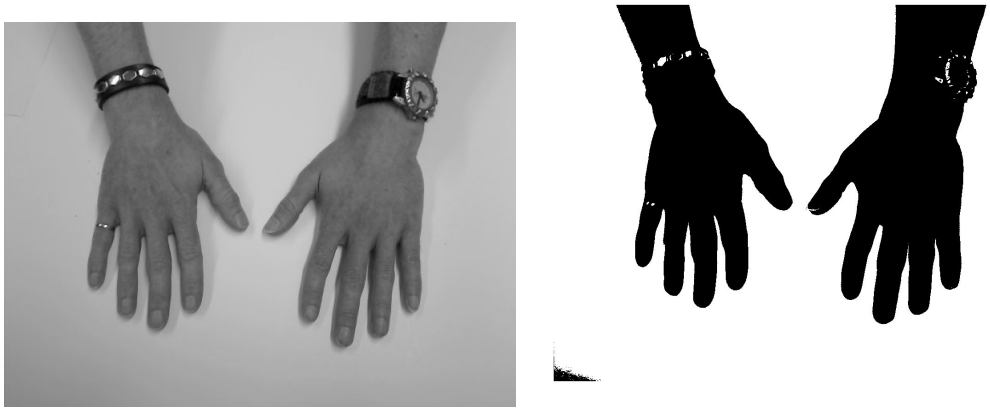

(a) Original image of hands

(b) Binary, segmented image

Figure 21: Example results from k-means segmentation

segmentation process related mainly to images where an individual was wearing a watch, bracelet, rings or exhibited long finger-nails. Each of those can potentially reflect light and cause mis-classification, leaving a discontinuity along edges in the hand/wrist/fingers. To manage this problem, post-processing of the hand images is performed to smooth over the edges and remove any unwanted discontinuities without introducing too much noise

or other potential problems. To smooth and close up the edges of the segmented image, a morphological closing operator was used. This operator was selected as it is typically used to fill gaps in contours and smooth edges [48]. Both of these problems occurred in early experiments during the segmentation process of hand images. Morphological closing builds from the background discussion found in Sec. 2.5.2. The structuring element selected was a small disk with a radius of 3 pixels, this is to ensure that it will fit into narrow spaces (in between fingers) and reform the boundary of the fingers and fore-arm that exhibited problems. Compared to other possible shapes, the rounded edge was better suited for the task as hand shapes do not typically exhibit hard, straight edges. The closing operator also helps to remove spurious pixels that can potentially present problems during feature extraction. An example of a morphological closing result is shown in Fig. 22. Once the images are

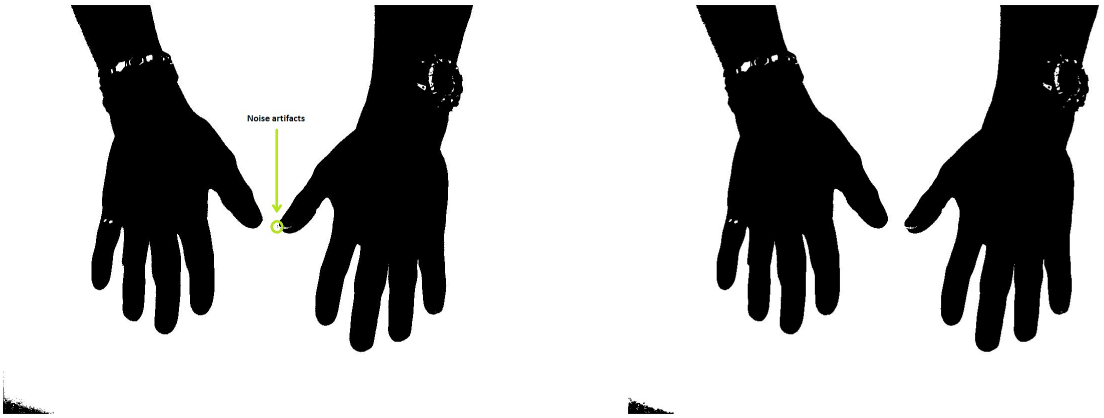

(a) Segmented image with artifacts

(b) After morphological closing

Figure 22: Removal of artifacts from segmentation via morphological closing

prepared and ready for further analysis, the next step is feature extraction from the various poses to discover more about the current condition of the telerehabilitation gaming system user.

3.5.2 Hand structure: Pose 1, top view, both hands included

The various hand poses are assessed in turn, looking for structural and feature-based information. The first hand pose discussed is the top view, focused on the back of the hands. The goal of monitoring structural information from this perspective is to watch for potential changes that can indicate the presence of joint damage leading to impairment and a more severe condition [76]. There are well established methods for discovering internal object structure in image processing, including morphological skeletonization [48] and also a thinning algorithm that looks for a skeleton of a region (the medial axis transformation (MAT) [9]). After considering both possibilities, the results were not well suited for skeletonization of the hands, incurring excessive error and requiring extensive post processing to provide a reasonable approximation to hand structure. The alternative and method of choice in this case was to create a novel algorithm to develop the hand structure to provide similar information that can be found from an x-ray image. Each of the methods are briefly discussed to weigh the pros and cons and demonstrate why I developed a new approach for the problem of extracting structure from hand geometry.

Morphological skeletonization was the logical starting point for discovering structural information in hand images. Building on the details discussed in Sec. 2.5.2 on morphology, the process of skeletonization uses erosions and openings to discover structure [48]. The opening operator in morphology is similar to closing, but the operator order changes.

$$A \circ B = (A \ominus B) \oplus B, \tag{24}$$

where A represents the image and B is once again the structuring element. Opening consists of an erosion and a dilation of the image with the structuring element, which generally smooths contours and eliminates noisy edges [48]. To elaborate further on the skeletoniza-

tion process, it is considered a union of $skeleton\ subsets$ represented as follows [48].

$$S(A) = \bigcup_{k=0}^{K} S_k(A), \tag{25}$$

where the skeleton subsets, S_k are described in Eq. 26,

$$S_k(A) = (A \ominus kB) \circ B. \tag{26}$$

The skeleton subsets consist of multiple erosions and an opening operator, k represents the number of times the erosion operator has been used and ranges from zero to the point where A erodes into the empty set (no longer containing any detail) [48]. The union of these skeleton subsets provides structural detail for the set in question, A, the original image. The main problem encountered when using morphological skeletonization was discontinuities in the remaining structure and the amount of work needed to extract useful detail for the hands. An example of the results using morphological skeletonization is shown in Fig. 23. The details that are recovered from using this technique include much non-essential struc-

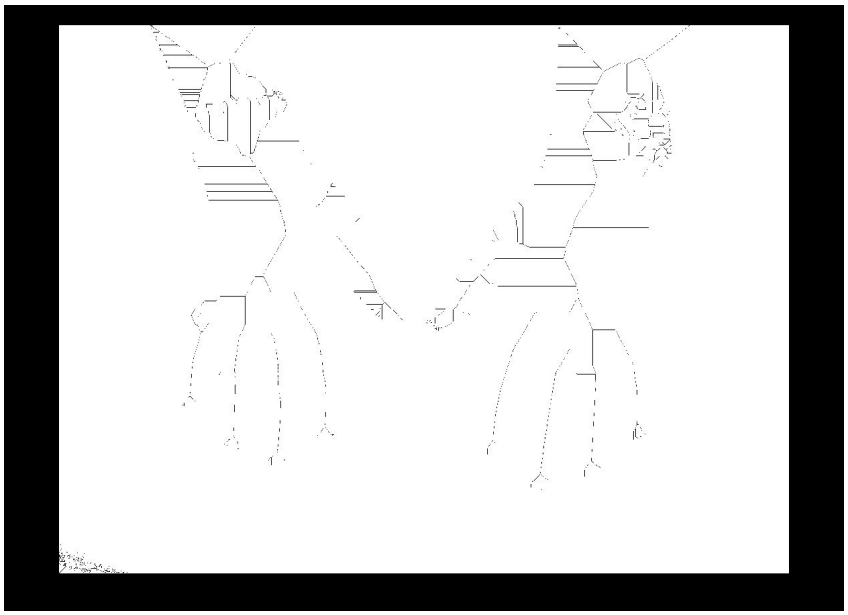

Figure 23: Morphological skeletonization of a pair of hands

tural information that will not be of use for my work. In addition, with discontinuities and required pruning, the amount of post processing required was prohibitively expensive and thus eliminating it as a possible solution.

The issues with discontinuity from morphological skeletonization is well known and extensive work has been done to eliminate the problem and provide a meaningful skeleton structure. The medial axis transformation (MAT) developed by Blum has been used to address this problem [9, 48]. Finding the medial axis is based on a thinning process that uses an approach commonly referred to as a $prairie\ fire$, where thinning is applied from each edge, in towards the centre, yielding a final connected structure [9, 48]. A connected structure is more in tune with the goal of finding the skeletal structure in the hand (similar to an x-ray) when determining joint angles. However, the results from using the MAT results in areas that would still need to be cleaned up with pruning, similar to what can be seen in Fig. 23 in the finger tips where the structure splits. Although these skeletonization techniques have their uses, the goal of establishing bone structure in the hands and determining joint angles does not lend itself well to discontinuities or extensive pruning requirements, especially considering the underlying goal is to have the telerehabilitation system operate in an automated fashion without input on a case by case basis. Along with developing an algorithm to look for structure, consideration was also given to establishing joint locations, angles and storing that information for further feature extraction.

The algorithm developed for establishing the structure of both hands from a top view is presented here (see Algorithm 1). Although this method avoids the common pitfalls associated with the other methods, it is not free from problems of its own. A consistent image acquisition setup (see Sec. 3.3) is the key to success with this method, employing a high contrast background, even lighting and a similar camera setup from one session to the next.

There are some necessary assumptions made when processing the hands using Algorithm 1. The first assumption is that bone structure in the fingers are located approximately

Algorithm 1: Establish joint locations, build skeleton structure, calculate joint angles

Input: Hand image (top view), land mark location data
Output: Joint angles, right hand: DIP,PIP x 4 fingers, DIP x 1 thumb; left hand: DIP,PIP x 4 fingers, DIP x 1 thumb

```
foreach Hand (RH then LH) do
    find first instance of associated arm pixel from top corner of image (either R or L);
    foreach Finger do
        find tip;
        find inflection point;
        generate remaining land marks using location data (for DIP, PIP and MCP joints);
    foreach Thumb do
        find tip;
        generate remaining land marks using location data (for DIP and MCP joints);
Connect joints via centred, directed vectors;
Establish angle of deflection between vectors to generate joint angles;
```

in the centre of the external 2D structure. This assumption is based off examination of x-ray databases of the hand/forearm. Making this assumption aids in placing land marks for the joints as they will be centred along the digits located at the specified lengths from the prior data recorded in a first session account setup table. The second assumption is that all images will have an unobstructed view of the hands, wrist and part of the forearm for processing. This is essential to have a good view of the wrist when building a baseline to establish the metacarpal bone locations in the back of the hand. The final assumption relates to orientation of hand placement. Users of the telerehabilitation gaming system will be advised how to pose for the camera to ensure a certain degree of consistency. The requirement is not overly strict, only requiring that the hands face the same direction, if they are skewed at an angle somewhat from one session to the next it will not have any significant impact on structure and feature extraction.

The next part of this discussion involves how to employ computer vision techniques to extract bone structure in the hands, minimize the estimated error and be able to derive joint angles for the DIP, PIP and MCP joints. The first step is to locate landmarks in the hand,

specifically finger and thumb tips and also the corresponding inflection points. This task begins by discovering the first instance of skin tone pixels from the k-means segmented image of the hands shown in Fig. 21b in the first row of the matrix representation (see Fig. 6) for the image. With the prior assumption made of general orientation for the hands during image capture, the first row and first instance of skin tone pixels in that row will correspond to part of the forearm. Once a starting point on the forearm is located, the next

Figure 24: First skin tone pixel in row 1

step is to find the first finger tip. Since orientation of all images will be the same, the right hand will be addressed first and the pinky finger will be the first digit encountered.

Finger tip discovery takes advantage of prior knowledge from locating edges of the hand and fingers during segmentation. This process involves examining the derivative of the external edges or outline of the hand (see Eq. 27) [145]

$$\frac{dy}{dx} = \frac{(y_2 - y_1)}{(x_2 - x_1)}. \tag{27}$$

The key to locating a finger tip is to look for derivate values of zero or changing signs (positive to negative or vice-versa) along with a change in the direction of the $y - value$ along the edge of the hand. Those changes signify that a local maximum or minimum point has been reached in the edge of the hand indicating a corresponding finger-tip or inflection

point. Care needs to be taken as there are potential pitfalls that can occur. First, when digitizing an image of hands and extracting an edge to follow, it is conceivable to have a condition where the quantized values $x1 = x2$. For this case, the derivative is undefined so steps must be taken in software to prevent this from causing a problem. In practice, the simplest solution is to increment the location being tested by one sample value. Most often this will avoid the issue for cases such as where the wrist joins the hand and forearm and in close proximity to the finger tips and edge points where the values are more likely to be problematic. Also, cases where there are groups of points where the same x-values occur pose the same problem, then it becomes a matter of adding a small amount to the denominator to avoid divide by zero errors. Undefined values aside, the key element is to monitor for sign changes of the derivative along with the numerator or y-values. Anytime sign changes are discovered corresponds to tip or inflection point locations when they occur together. Once the landmark discovery phase is complete, refinement of the positions takes place. A brief example of pinky finger tip location consists of starting at the first instance of skin tone pixel and proceeding along the edge of the forearm. Upon reaching the wrist, the slope will change signs (see Fig. 24), however the change in y-values will remain positive. At the finger tip, the derivative will reach zero before changing sign and also the y-values (from the numerator in Eq. 27 will change sign indicating that the tip has been discovered. This procedure continues until another value of zero occurs at the inflection point and then the y-values return to negative, indicating that the inflection point was found. This process continues for all tips and inflection points, establishing landmarks in the right hand. Upon completion the process repeats in reverse for the left hand resulting in the discovery of all finger and thumb tips and corresponding inflection points.

The hand orientation is likely to be such that the fingers are not exactly straight along the $y - axis$ in an image, this implies that the centre of the finger tips may not necessarily coincide with the landmark discovered. To address this problem, a fine-tuning adjustment of the position takes place before establishing joint locations to refine finger tip locations.

This consists of moving a small percentage of distance in the $-y$ direction from the estimated tip (towards the palm). Through experimental work with a number of test subjects, a value of 10% of the distance from the top of the image to the furthest finger-tip provides ample distance for the alignment procedure. Next, the edges of the finger are located by looking for the border between background and skin-tone pixels, $(x + \delta x)$ and $(x - \delta x)$. Once the external values are acquired, line segments are built along the exterior of the finger on either side and then joined together with a normal line to locate the centre of the finger. The refined position of the finger tip is then discovered through extending the centre point toward the tip, iterating the edge detection and centre placement at each step. This continues for approximately half the distance to the finger tip, at which point an equation for the line is derived and used to discover where the edge between skin-tone and background occurs at the finger tip. This location provides a best estimate to the actual location of a finger tip.

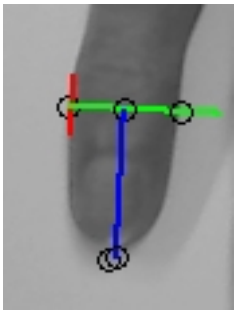

Figure 25: Re-positioning finger tip

Once landmarks for the finger tips were adjusted, the next steps include addition of intermediate landmarks for the DIP, PIP and MCP joints and refinement of those positions. Following that, joints are connected with line segments to represent the underlying bone structure in the fingers. These correspond to the distal, intermediate and proximal phalanges in the fingers and the distal and proximal phalanx in the thumbs. The line segments were centred in a similar fashion to the method discussed regarding the finger tip position, see Fig. 26 for the result. This is a significant improvement compared to the other skeletonization methods discussed as it only includes approximations for the bone and refined joint locations. The remaining problem was to discover the location of the metacarpal bones as they are required to monitor MCP joint angles. The challenge is to discover hidden bone locations as they are seated in the back of the hand and even if tendons are in

Figure 26: Custom skeletonization of a pair of hands

view, they are not necessarily representative of bone locations (one can palpate the hand to verify this easily). To avoid using x-ray images, which are more invasive and prohibit home use, a means to estimate metacarpal bone location is described next.

There are a number of resources available online that contain publicly available x-ray image databases of various body parts. These include the hands and some examples can be found in [14, 34, 79]. Examining a collection of various x-rays of healthy hands in relaxed poses and paying particular attention to separation between the metacarpal bones, demonstrates that there is a reasonable similarity from one individual to the next. This pertains to the angle between metacarpal bones with respect to the wrist as a baseline. An overlay on top of a hand image shows the desired bone representation (see Fig. 27). To establish an approximation of the separation between the metacarpal bones, a group of 30 x-ray images of the hands in a relaxed pose were examined. The angular separation between the second and third, third and fourth, and fourth and fifth metacarpal bones were measured. Measurements were taken using a protractor with 0.5° resolution. The results are shown in Table 7. The cross section of images included both male, female, large and small subjects to see if any significant differences were present. The variance was larger than

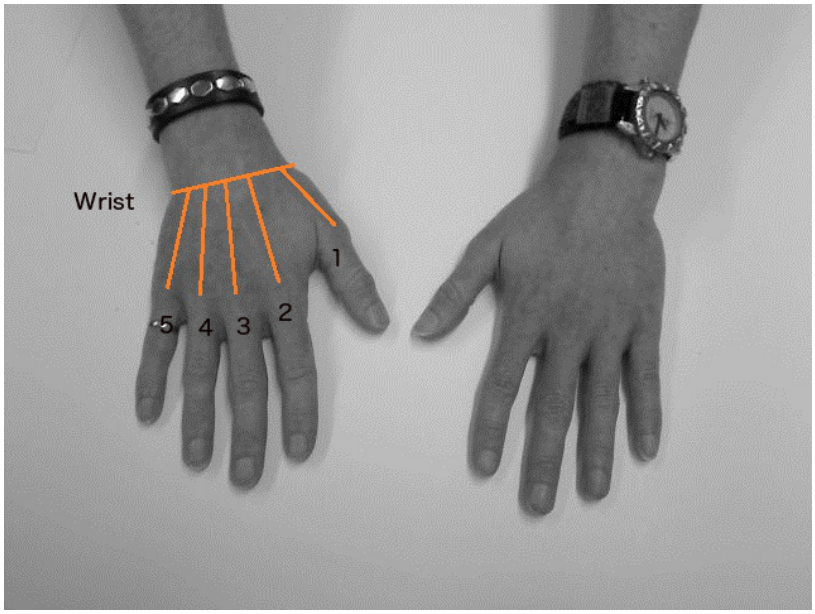

Figure 27: Metacarpal bones and wrist highlighted on hand image

Metacarpal 5-4	Metacarpal 4-3	Metacarpal 3-2
Mean Values		
10.25°	8.75°	8.75°
Variance		
3.0°	3.25°	2.25°

Table 7: Angle of separation between relaxed metacarpal bones

anticipated, but in part due to several poses not being fully relaxed. The result of stretching the fingers shifts the metacarpal bones slightly, introducing a greater degree of variance. For our application, discovering the first and fifth metacarpal bone locations are reliable as they correspond to edges of the thumb and palm respectively, aiding in discovery. However, the second, third and fourth metacarpals are problematic to locate and require knowledge of the angle of separation and wrist location to establish their placement.

The general procedure for building a representation of the metacarpal bones to accompany the rest of the hand structure is as follows. First, the wrist location needs to be approximated for a baseline to measure metacarpal bone separation angles. Then the fifth metacarpal bone is established from the wrist baseline to the fifth MCP joint. The following steps involve using the mean angle of separation to approximate locations of the second,

third and fourth metacarpal bones in between the wrist and their corresponding MCP joint. Finally, the first metacarpal bone is established separately (thumb), completing the hand structure.

Localizing the wrist required developing a model of the outer edge of the forearm and using that to establish the base of the wrist. Starting with the total length of the hand/forearm in a given image, the maximum length of the skin-tone pixels were calculated (from forearm to tip of the middle finger). To get a useful amount of data for generating a linear model, 15% of the total length of the skin-tone pixels were taken starting at the first instance to approximate the forearm. The following representation was used to develop a linear model of the external edge for the forearm from the hand images,

$$m = \frac{(\sum(y_i) - \mu_y)}{(\sum(x_i) - \mu_x)}, \tag{28}$$

$$b = \mu_y - m * \mu_x. \tag{29}$$

The linear regression model provides the slope, m and intercept b to build a representation of the forearm.

Next, using the linear model from the first 15% of the forearm is extended from one end of the image to the other. The method for locating the wrist stems from examining how closely the linear model approximates the forearm and looking for incremental error. Beginning at the top of an image and working towards the wrist, the average approximation error remains low. Passing through the wrist will find a point where error starts increasing steadily and once it reaches a given threshold (e.g. 10% was used in this case), rolling back to the first local minima before the threshold was reached is proposed as being a reasonable representation for wrist localization (see Fig. 28). It is important to note that wrist localization is being used to establish an approximate location for the wrist which is a base for comparing the metacarpal bone separation angle. Thus the required accuracy

is significantly lower than that of systems that are specifically looking for the wrist when examining detailed hand gestures (e.g. [91]).

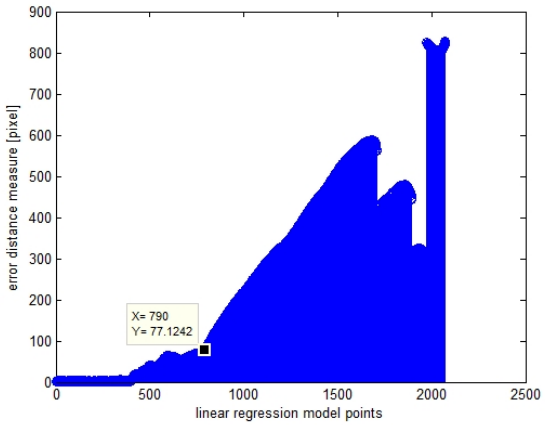

Figure 28: Stem plot of error measure from linear model and wrist localization data point shown on plot

Using the estimated wrist location from the linear model, a normal line was generated to provide an approximate representation of the wrist. The following step requires locating and placement of the metacarpal bones as an overlay onto the back of the hand from the top view. This began by examining the 5th metacarpal bone located at the right edge of the right hand. Based on prior information gathered from the X-ray images, the 5th metacarpal runs approximately parallel to the external straight edge on the back of the hand. Beginning at the fifth MCP joint an initial naive, or straight approximation of the metacarpal bone was overlaid, extending the geometry for the proximal phalanx. Revision of the metacarpal position was then achieved through establishing a linear approximation (as in Eq. 28 and 29) of the exterior of the back of the hand that runs in parallel and adjusting the geometry accordingly. This results in revised placement of the 5th metacarpal bone.

The remaining 4th through 2nd metacarpal bones were similarly extended from the proximal phalanx geometry (MCP joints) down to the wrist baseline. From there, angular separation based on the measured values from the X-ray images in Table 7 are employed. The arctangent of the angles provides the required information when reconstructing the

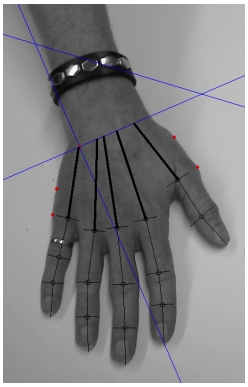

Figure 29: Hand image with complete structural information overlaid on top

metacarpal bone representations. The first metacarpal bone was located similarly to the fifth as the external edge of the thumb closely parallels the bone according to empirical evidence from the X-ray images. Placing the final metacarpal bone completed discovery of the proposed hand structure for top view images. Figure 29 shows the final structure with the wrist location lines and points left on the image to demonstrate the approximate wrist location and the metacarpal bones have thicker lines, emphasizing their locations. With structure established, the final step is to extract joint angles. The procedure consists of measuring the angle between two lines,

$$\theta = atan\frac{\mid m_1 - m_2 \mid}{\mid 1 + m_1 \cdot m_2 \mid}. \tag{30}$$

For this case, the lines represent bones in the hand (metacarpal and phalanx).

3.5.3 Hand structure: Pose 2, lateral view, dominant hand only

The second hand pose examines the lateral or side view of the index finger to look for potential changes in structure relating to joint damage. There are two well known deformities often associated with rheumatoid arthritis, the swan-neck and boutonniere deformities [38]. In both cases, damage to the joints result in deformities that can manifest as abnormal hyperextension or flexion, most commonly affecting the DIP and PIP joints. As a result, we

are interested in monitoring the corresponding joint angles from this perspective to keep an eye on fluctuations in joint angles that may signify damage to the hand structure.

The procedure to discover joint angles from the lateral pose followed a similar method to that of the top view with a few minor differences. The first step was deciding on how to position the hand to get the best view of the index finger side profile. After experimenting with various poses, it was determined that placing the hand at an angle of 45 degrees with the surface plane was best. The main reason for selecting that angle, was to afford the best view while minimizing issues with shading/lighting during image acquisition and also to be able to extract distinct edges of the index finger, separating it from the middle finger. During the verification stages, it was discovered that one hand at a time was optimal for this pose. Introducing the other hand presented problems with shading as the light source position would only be able to focus well on one hand, leaving shadows surrounding the other, introducing errors into the segmentation process. This is demonstrated via the two images in Fig. 30. Attempts to manage both hands simultaneously were made through the

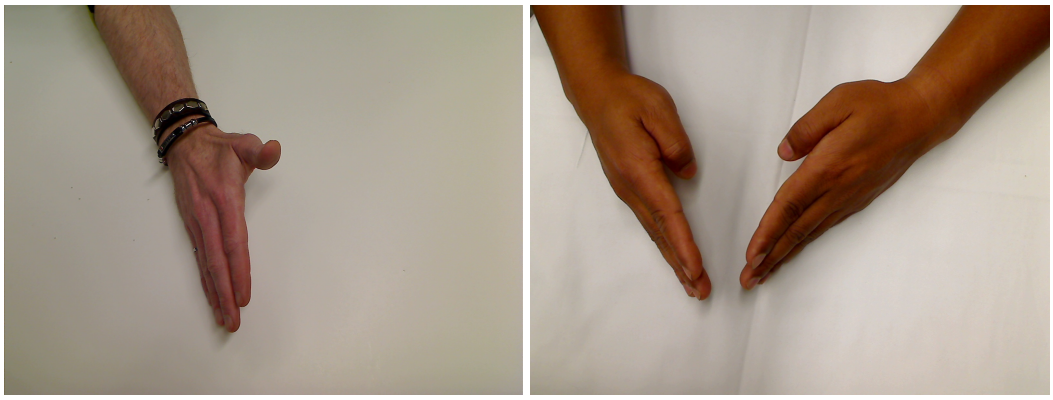

Figure 30: Side view hand pose demonstrating increased shading

use of multiple light sources and referring to photography and film experts on the subject. However, adding multiple light sources exaggerated the shadow-forming problem, which led to the eventual decision to go with one hand at a time for this hand pose.

The procedure for analysis of the lateral pose images of the hand followed a similar approach to top view imagery. The first step was to extract edges, revisiting the k-means clus-

tering technique for segmentation. Since the environment and the subject had not changed, we found equally good results in separating two clusters, one for the background and foreground.

Figure 31: Side view hand poses demonstrating k-means clustering segmentation

Several steps are required to extract the joint information for index finger joint angles. The first step is discovery of the index finger tip, followed by pinpointing the DIP and PIP joint locations and estimating the MCP joint location as it is not as necessary to know the exact location for this pose. Once joint locations are established and using geometric properties, extraction of the angles from this hand pose are taken for the DIP and PIP joints. Similar to the top view hand pose, the subject is asked to keep their hand straight but without extra effort to do so (i.e. a relaxed pose to provide the best view of the joints at rest). The algorithm used to extract joint angles for the lateral view of the index finger is similar to that of the top view (see Algorithm 2). To help in feature extraction, morphological closing was used again to smooth out the edges and reduce any potential problematic noise without affecting the segmented image significantly.

From the lateral view perspective, locating the DIP, PIP and MCP joints allows us to take advantage of some distinct features of the finger. After examining our dataset which includes a group of hand images from both a top and lateral view perspective, paying particular attention to the palm-side of the fingers, there is a crease or indentation at the approximate joint-centres for the DIP and PIP joints in all cases in between the finger pulp.

Algorithm 2: Extract DIP,PIP Joint Angles

Input: Hand image (side view)
Output: Joint angles, index finger: DIP,PIP
foreach *Hand (RH then LH)* **do**
    find first instance of associated arm pixel from top corner of image (origin);
    foreach *Index Finger* **do**
        find tip;
        find land marks for DIP, PIP and MCP;
Connect joints via centred, directed vectors;
Establish angle of deflection between vectors to generate joint angles;

For this case, we are not as concerned with the MCP joint location accuracy as it is used to establish a partial bone segment representation instead of the full segment and joint location needed in the top view. This is due to the joint angles and their requirement to find the angle between bone segments. This implies that the proximal, intermediate and distal phalanges must be represented to discover the angle between the segments using the slope-tangent approach (Eq. 31)

$$tan(\theta) = \frac{m1 - m2}{1 + m1 \cdot m2}, \tag{31}$$

where θ is the angle between the two bone-segments and $m1$ and $m2$ are the corresponding slopes.

Locating joint centres in this hand pose uses distinct land marks on the palmar side of the hand. The palmar creases in the skin that allow joint flexion corresponds closely to joint centre locations. This is the case for the DIP and PIP joints, although not for the MCP joint as it resides further into the palm of the hand. An assumption that is made for this pose is that the actual location of the MCP joint is not required as the focus is on the DIP and PIP joint angles. Instead, the crease that corresponds to the MCP joint, which does not correspond to the joint centre, actually serves as a landmark in forming a partial bone segment approximation that represents the proximal phalanx.

The process of finding joint centres via the palmar crease in the skin provides a location along the palmar edge of the index finger representing each joint. From this information,

locating the corresponding point on the opposite edge of the index finger allows us to locate the joint centre. Using traditional edge detection techniques was insufficient to extract the opposite edge reliably. Instead, a decreased average intensity was used as a marker to locate the opposite edge considering it will be resting on the middle finger and be separable via shading or darker intensity values. Locating the opposite edge was achieved using a moving average (Eq. 32) over a set number of columns, where the average of n columns are used to discover the first significant change or drop in intensity that signifies the opposite edge of the index finger has been found. This location corresponds to the distinct edge between the index and middle finger. At this point the joint locations are centred between the edges and placed in the overlay on the index finger along with the linear representations of the bone segments between joints. The results are shown in Fig 32.

$$MovingAverage = \frac{1}{n}\sum_{j=1}^{n} I(i,j) \tag{32}$$

The DIP and PIP joint angles are extracted from the bone segment construction overlay,

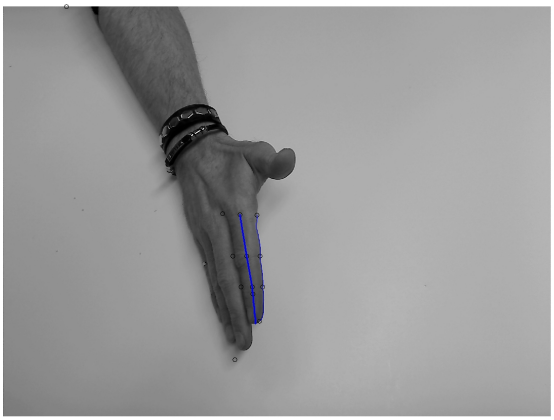

Figure 32: Hand image with index finger joints and bone segments overlaid

providing insight into possible changes that can occur as a result of damage from the conditions associated with rheumatoid arthritis.

3.5.4 Hand structure: Pose 3, top view, dominant hand only

The third and final hand pose revisits the top view but includes only the dominant hand. This pose also requires the fingers to be extended and abducted from the centre of the hand [93]. The information we are interested in extracting from this pose are the angles between the centre of the hand and each digit when they are extended and stretched out. This provides an active range of motion (ROM) measure where the fingers are spread intentionally by the subject [44].

The same image acquisition setup from the previous two hand poses is used to capture the third pose. We revisit the dominant hand again in part because it will be most likely used more often and susceptible to potential damage and likely manifest early warning signs first. The dominant hand is placed in the centre of the monochrome background and field of view of the camera to provide the best possible view and contrast. An example of the third hand pose is shown in Fig. 33. Separation of the background from the foreground followed

Figure 33: Third pose, top view, dominant hand, fingers extended and abducted

the same procedure as the previous two poses, using k-means clustering to segment the images into two clusters. The result of segmentation for Fig. 33 can be seen in Fig. 34. Once segmented, a similar approach to the first hand pose was used to establish the preliminary landmarks, finger tips and inflection points, expanded on in Algorithm 3.

Figure 34: Segmentation of third hand pose

Algorithm 3: Locate tip and inflection point, build skeleton and establish angle of deflection

Input: Hand image (top view), dominant hand only
Output: Angle of separation between extended, abducted fingers/thumb
Segment hand from background;
foreach *Finger/Thumb* **do**
    Locate finger tip;
    Locate inflection point;
    Build skeleton estimate for the finger/thumb;
Locate mid-line of the hand; Build linear approximation for each of the fingers/thumb;
Measure angle between each finger/thumb and the mid-line;

Some refinement was necessary in building linear approximations for the fingers to discover the ROM measures. The further out a digit from the mid-line, the greater the angle and the greater chance of a finger tip misplacement. This can be evidenced when looking at the automatic landmarks that are placed on the hand in the second pass (see Fig. 35). At this point, the preliminary skeleton structure has been built throughout the fingers and thumb, the inflection points and finger tips have been placed and the mid-line has been located and established. The final step is to approximate finger locations and

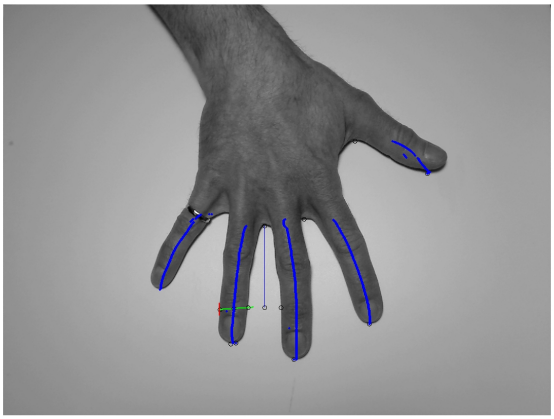

Figure 35: Landmarks placed on third hand pose

measure the angle of deflection between the mid-line and the fingers and thumb, providing us with the range of motion angular measurement. Linear approximations were constructed for each of the fingers and thumb and overlaid on a separate image along with the mid line (the darker/thicker line in Fig. 36). Using Eq. 31, the angles of separation from the mid-line are generated providing measurements for the ROM. The corresponding measurements for Fig. 36 are provided in Table. 8 as an example set of results.

3.5.5 Joint features

Using the classical definition from Celsus [127] and constraints associated from image analysis, two of the four symptoms associated with inflammation are considered from a

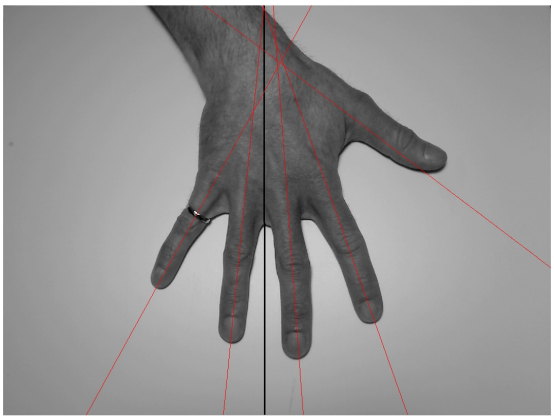

Figure 36: Hand geometry from third pose for measuring ROM

Finger	Angle of separation
Pinky finger	28.85°
Ring finger	5.7°
Middle finger	4.13°
Index finger	19.38°
Thumb	52.78°

Table 8: Pose 3 example results

visual perspective, swelling and redness. This pair of symptoms are well suited for visual analysis via still imagery. They provide an extra degree of insight into potential symptoms/signs of disease activity to accompany the hand structure features discussed in the previous sections.

The first visual joint-related symptom addressed is swelling. During analysis of the top-view hand structure including both hands, all joint centres are discovered. As a result, to focus on swelling, we start by finding the maximum axis surrounding each joint centre. This value is used to construct a square area surrounding the joint. As swelling occurs, the length of this axis can potentially fluctuate, so it is important to normalize the measure so it is comparable from one session to the next, should the focal distance fluctuate. Prior knowledge of digit lengths are stored upon establishing an account from a first telerehabilitation session. Since they are recorded as percentages of total distance and are

unlikely to change dramatically unless significant deformity occurs, the length of the finger is used as a normalization factor. As the joint width changes, the length of the finger will remain constant, providing an indicator of changes in joint area indicating variations in size, potentially related to swelling as a function of inflammation.

Joint swelling alone may not be enough to detect early warning symptoms associated with disease activity. The possibility also exists that it can be difficult to detect very mild amounts of swelling and also fluid build-up in the hand can settle around or underneath joints, increasing the difficulty of detection from a visual perspective. Extending visual inspection of the joints for signs of inflammation to include discolouration or redness, associated with the inflammation process [127], surrounding the joint areas is also included.

Any increase in redness can be a potential indicator of disease activity. For the case of fingers, increased redness in inflammation is a result of heat transported with extra blood-flow from the core to the affected area [19]. Under normal conditions the skin would be cooler and less likely to exhibit discolouration that can imply disease activity [19].

To quantify the change in discolouration associated with increased redness, there are two steps involved. The joint area examined for swelling provides a square area surrounding each joint. These sub-images are extracted from the top view of the hands. There are corresponding sub-images for each joint in the fingers and thumbs (DIP, PIP, MCP). As a result, there will be a total of 14 sub images per hand or 28 per pair. Examining redness content in each sub-image consists of establishing histograms and obtaining an average value for the individual colour channels (red, green, blue). This technique has been used in previous work for filtering out specific types of imagery containing larger amounts of skin tone pixels and it was found that higher redness content typically indicated skin tone appearing in images [73]. The surrounding area for the joints is shown in Fig. 37, demonstrating a case where three joints from the middle finger on the left hand have been extracted. Once sub-images have been established, the next step is to examine their colour content, paying particular attention to redness values to determine if they contain an un-

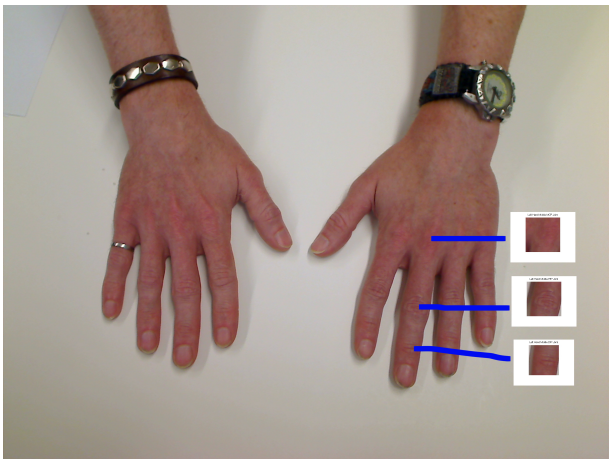

Figure 37: Hand image with joint sub-images extracted

usual amount compared to the baseline value collected during the primary session or an average. An example set of histograms are shown in Fig 61, where it clearly shows the colour content of the joint for each of the three channels and the red channel as expected, exhibits a higher concentration than the other two.

$$av = \frac{1}{n}\sum_{i=1}^{n} r_i \tag{33}$$

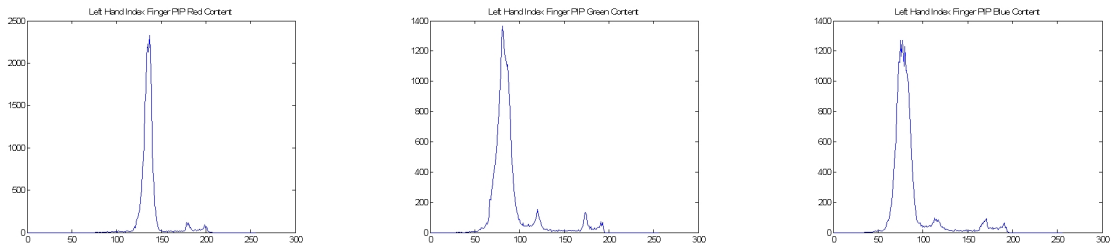

Figure 38: Red, green and blue channel histograms

Swelling and redness are both elements of the inflammation process, although they may not always be readily visible. This was discussed during development of the project when addressing features and the result was inclusion of joint texture. This was added as a means to monitor changes in texture of the skin surface as a function of inflammation. The com-

mon approaches used to extract textural features from visual imagery include structural, statistical and spectral analysis [48]. Structural analysis is often better suited to synthetic shapes (edges, man-made structures, etc.), a statistical approach is better suited to naturally occurring textures as it examines the characteristics of the occurrence of grey levels [130] and spectral analysis is best suited for describing the presence of periodicity or periodic patterns in images [48]. As we are dealing with natural subjects, a statistical approach was selected.

Statistical texture analysis builds off work from the previous section in examining histograms of the colour channels. In addition, it is possible to look at the statistical moments for the histograms to discover more information about a specific colour, or using grayscale conversions, to look at the properties of the image as a whole [48]. The statistical moments of the histograms provide information with respect to the entire image, including the average value, variance, skewness, etc. [48]. Although this is useful information in image description, we are interested in also examining location or proximity when describing texture as a feature.

Use of the co-occurrence matrix was introduced by Haralick [54], providing a statistical means to examine texture in images based on grey level, pixel location and proximity to one another [48]. The procedure to generate a grey level co-occurrence matrix (GLCM) starts by scaling down the range of intensities, keeping the size of the GLCM more manageable as its dimensions correspond directly to the range of intensities. Establishing the GLCM consists of checking for pixel pair intensity levels based on a distance and angle. For example, using a distance of 1 pixel, Fig. 39 shows a neighbourhood representation where the point of interest corresponds to the X and the pixel pairs can either be at 0° (1,5), 45° (8,4), 90° (7,3) or 135° (6,2). This enables us to select a specific orientation of expected texture when generating the GLCM. Alternately, and as is the case for natural texture, it is not always possible to predict which angle might provide the best representation so all four are calculated and averaged to provide an overall picture of the texture.

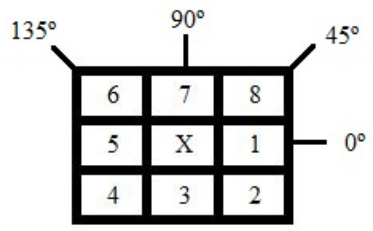

Figure 39: Representation of distance-1 neighbourhood to establish the GLCM

From the GLCM, features are extracted that help describe texture contained within the original image based on the probability of occurrence for gray levels [54]. Haralick [54] described 14 possible texture features extracted from the GLCM. For our purposes, we are interested in four of them, including contrast, energy, homogeneity and correlation. These textural features are weighted sums of varying order which dictates how they respond to the probabilities found in the co-occurrence matrix [54], allowing them to provide insight on various aspects of the GLCM and the corresponding image texture. A brief discussion, including how to represent each texture feature is included for completeness. Note that N_g refers to the number of grey levels in the GLCM, i and j are the row and column variables, and $p(i, j)$ refers to the GLCM at location (i, j).

$$Contrast = \sum_{i=0}^{N_g-1} \sum_{j=0}^{N_g-1} |i - j|^2 \cdot p(i, j) \tag{34}$$

Contrast (shown in Eq. 34 is used to discover if an image contains high concentrations of grey level values outside of the principal diagonal of the GLCM, which indicates that there are varied intensity levels in the specified neighbourhood [124].

$$Energy = \sum_{i=0}^{N_g-1} \sum_{j=0}^{N_g-1} p(i, j)^2 \tag{35}$$

Energy (shown in Eq. 35 demonstrates if the GLCM content is consistent throughout, for the case when it is constant (smooth texture), the value of energy will be at its highest [124].

$$Homogeneity = \sum_{i=0}^{N_g-1} \sum_{j=0}^{N_g-1} \frac{p(i,j)}{1+|i-j|} \tag{36}$$

Homogeneity (shown in Eq. 36) demonstrates if the distribution of elements in the GLCM is close to the principal diagonal. Less dispersed values from the diagonal, will exhibit higher homogeneity [124].

$$Correlation = \sum_{i=0}^{N_g-1} \sum_{j=0}^{N_g-1} \frac{(i-\mu_i)(j-\mu_j)p(i,j)}{\sigma_i \sigma_j} \tag{37}$$

Correlation (shown in Eq. 37) measures how close a pixel is to its neighbour throughout the image [54]. A perfectly correlated GLCM will result in a high value and a negatively correlated GLCM will result in a low value [54]. Note that μ refers to the mean value of the GLCM and σ refers to the standard deviation.

These four features are extracted from the information provided by the GLCM for a joint sub-image to yield more information about skin surface condition from a textural perspective.

3.6 Content management system

Once a telerehabilitation gaming session is finished, a complete data set is available to upload to our content management system (CMS) (appearing in Fig. 9). The CMS is a hub that links together all stakeholders in the system. At present we have included only registered user access intended for care providers who are able to login and examine data and perform queries on patient performance. Although moving forward, adding user access for patients to examine their own records in a read only capacity along with other care providers in their health network are projected expansions. Collectively, the CMS consists of a server for connecting with game clients to transfer session information, a front-end user interface, a database containing performance metrics and system processing routines that perform feature extraction on the raw data uploaded from individual clients.

The CMS employs a Java secure socket server that listens for game clients and receives completed raw game data files. This implementation has been considered in the context of feasibility, assuming low traffic conditions. Raw data is collected and filed based on unique user identification numbers (anonymous). The core of the CMS is built around the $Joomla!^{®}$, open-source software package [75]. This provides a complete front end user interface where individuals are able to login, request an account with access to query the system and examine reports on their client performance. $Joomla!^{®}$ is well suited for smaller, rapid-prototype work, where the most significant customization comes in the form of user registration, access control and modularity of the system. To support user friendly reporting, web forms were developed using scripting languages (JavaScript and JQuery) and all processing takes place on the server side before updating forms via PHP code, linking queries from the MySQL database that is built in and supported as part of the $Joomla!^{®}$ open-source platform.

Once active, the CMS awaits resulting data from telerehabilitation gaming sessions, which are automatically uploaded upon completion (via game settings). Data is separated into user directories corresponding to identification numbers. Ensuring anonymity, names are excluded and would be housed separately from the data for security purposes. Feature extraction of movement performance takes place once a user account has been added and also anytime subsequent data for that individual is provided. Movement performance features are extracted using code written in Java, which interfaces with and is executed via calls from the PHP code. All data is stored in a MySQL database and readily available for insertion and queries. The visual features have been extracted through the use of Matlab® and have been converted into executable files that can run from automated calls as a result of queries from the web forms. This provides a complete set of session features that are stored in a database.

The front end of the CMS is intended to provide a user friendly web interface allowing login via any device and interaction with the system to the degree their security access

provides. There are help files detailing the use of the system, the analysis tools available and how to access data. A separate form was built as part of the CMS that houses the scripted interface, allowing queries by user ID, and date ranges as parameters. The interactive web forms were left at a preliminary stage of development to demonstrate plausible functionality and complete the feedback loop for the telerehabilitation system. Example images of the front page and a remote query for a test account stored in the database are shown in Fig. 40. The example screen capture demonstrates results from three sessions for a test case over a

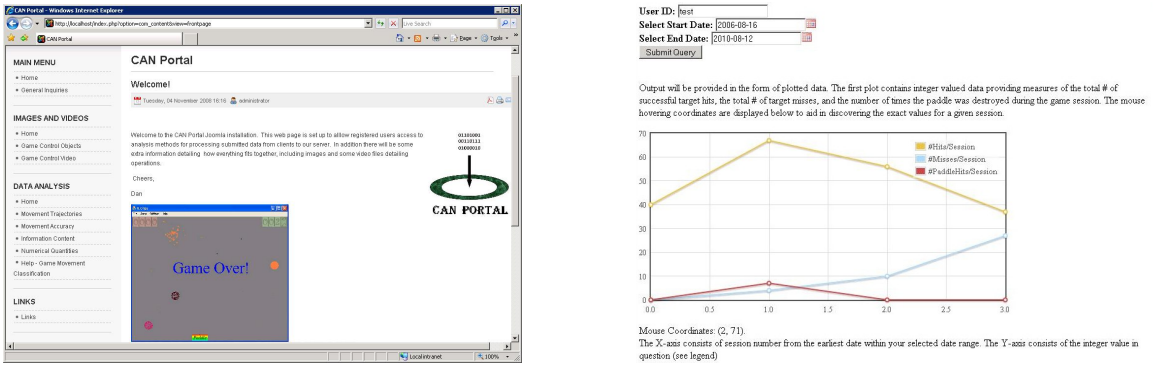

Figure 40: Content management system home page and query form

specified date range. To keep the plot manageable, only three elements were displayed at a time, however all performance parameters can be plotted together or separate as desired, allowing registered users to track performance of their clients over time.

4 System Verification and Experimental Work

This section of my thesis provides a brief system overview and discusses verification tasks that occurred throughout the development cycle.

4.1 System overview

The system overview presented in this section is written from the perspective of component verification. Referring back to the block diagram in Sec. 3, the main components of

the system that need to be addressed are as follows. The rehabilitation gaming platform provides verbose output in the form of position data of all objects on-screen at any time during game play. Addressing the validity of outcome measures is essential when it comes to being able to provide meaningful and reliable feedback. In addition, the images captured during each session are processed and have a number of different features extracted, examining the validity and utility of those in greater depth is essential for inclusion in the final suite of digital features for profiling finger hand function. For a quick visual inspection, block diagrams are included to visualize how the elements fit together and are addressed in this section.

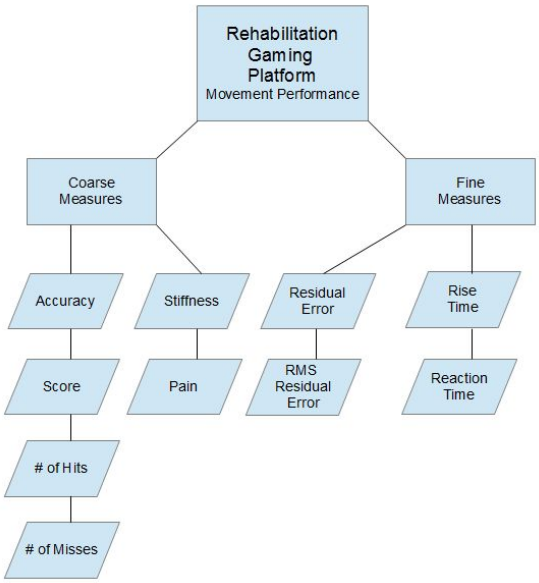

Figure 41: Block diagram of verification for movement performance features

In addition, another important consideration is ease of use, this applies to setting up a game session, playing the game, constructing a simple image acquisition setup and being able to readily repeat the process at a later point in time.

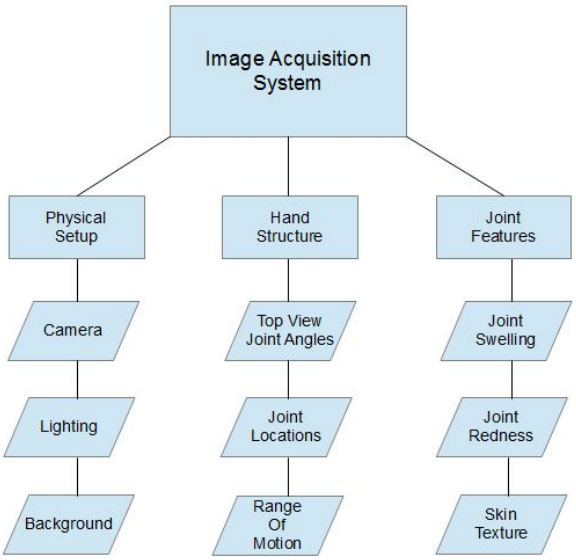

Figure 42: Block diagram of verification for image features

4.2 The rehabilitation gaming platform and outcome measures

The rehabilitation gaming platform has already been discussed at length in Sec. 3.2. Over the course of a project lifetime, there is a tendency to change and grow. This occurred in conjunction with feedback and suggestions from my collaborators at the College of Rehabilitation Sciences at the University of Manitoba. The evolution of both the game and analysis tools have been extensive as part of the adjustment to meet the needs of both a clinical and home-based scenario through various experimentations.

Modifications to the gaming platform spawned a variety of changes to in-game adjustments, settings, output, etc. User actions in the game translate into movements in real life that are slaved to input control objects. Through these movements of a specific control object, players are able to successfully take part in the game with non-standard input control devices that provide therapeutic exercise with the motivation of a challenge in the form of playing a game or group of games. Game durations are kept short, restricted to 3 minutes maximum. The intention behind short durations of game play are to use the rehabilitation gaming platform at the beginning and end of a session to provide two sets of data.

In between the rehab game play sessions, alternative platforms can be selected to allow customization of a session to better suit the client and their preferences.

During the experimental and testing phase of the gaming platform, development of different game modes, settings, and performance metrics were added. The first alternative game mode introduced included learning methods where the difficulty of the game could adapt automatically during a session. Thus allowing for ramping up/down difficulty levels by changing speed, size and amount of targets visible on screen. Although this did change difficulty levels based on desired optimal results, post processing of data became more difficult to compare with fixed difficulty settings as performance would rise and fall with the parameter adjustments so this mode was abandoned. Next, a force feedback, teleoperated mode was implemented to provide haptic feedback to a client for cases when targets appear on the screen in specific areas. This was intended to target clients with visual impairment on one side, known as hemispheral blindness or blindsight [18]. This game mode was implemented but later abandoned as it was prone to network delays and not well suited for our target demographic (RA patients). The episodic, non-deterministic game mode was decided upon as the most suitable. There are a wealth of settings available to alter the game as needed, before a session begins. These range from adding or removing the number of targets/distractors on screen at a given moment to adjusting shape, size, sensitivity of the paddle or input control, etc. The episodic, non-deterministic game play provides a rich set of outcome measures that are able to report on a number of important aspects of user movement. Our goal is to monitor those performance parameters and provide a composite report for each individual that employs the telerehabilitation gaming system. A significant amount of effort has gone into refining both the gaming platform and performance analysis metrics.

Once data capture began, the next step was to evaluate the resulting processed output. Verification of some features were straight forward, such as the coarse measures from Fig. 41. These include absolute accuracy, overshoot, undershoot, the scoring metrics for

targets hit and missed along with the number of times the game paddle was destroyed. The values that required more in depth verification included the temporal measurements, starting with reaction time and rise time and also including the residual error accuracy measure.

The initial reaction time measurements demonstrated problems in the form of false triggering at the start of an event. This was typically categorized as movement in the order of less than 100mS from event onset, which is atypical of human performance. The cause of this problem was due to left over movement from a prior event or from user introduced noise, unrelated to the current movement. To help visualize this problem, an example plot of movement trajectories that demonstrate this concept is highlighted in Fig. 43. To

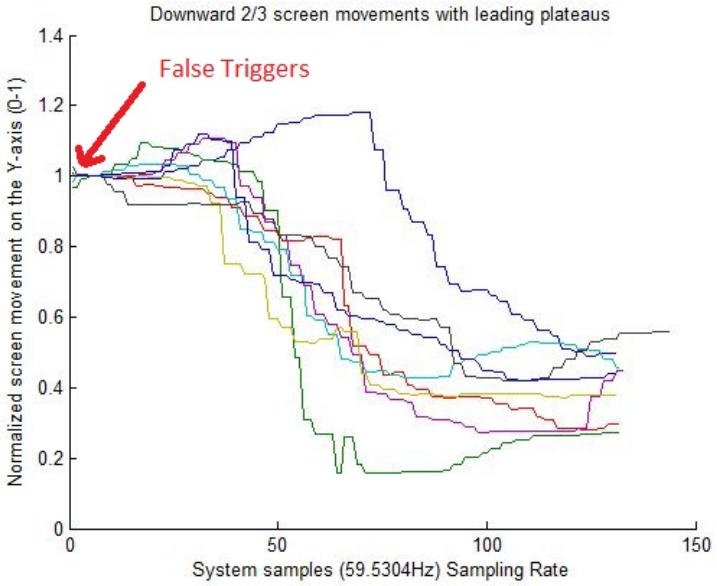

Figure 43: False movement triggers

remove false triggers, it is necessary to discover typical reaction times for what can be expected of human performance. There will always be some degree of variability for lapses in attention but on average, few people will reach speeds faster than 250mS [71]. During testing and verification users were presented with a single target on the screen at any given instant in time. This eliminated additional time required to process multiple targets, which would slow down reaction time. This is discussed and modelled in Hick's work which demonstrates that reaction time slows proportionally with additional choices as it requires

more time for visual processing [58].

To prevent false triggers when measuring reaction times, a plan was developed to distinguish between actual and false movement onset times. A minimum reaction time of 250mS was set as a baseline for commonly accepted human performance when faced with some degree of visual processing before issuing motor control commands to manipulate the input control object [58]. This was considered reasonable because at a minimum, users are required to make a decision on which direction to move the paddle to reach a single target [58]. The addition of multiple targets or distractors will slow down reaction times even further [58]. When looking for movement onset during analysis the first 400mS of a given movement are examined, paying attention to the mean and standard deviation of the amplitude. Those values are compiled during that period and used to help determine movement onset. To establish the actual beginning of movement onset, trajectories are examined beginning at 250mS and then looking for the first instance where the amplitude reaches one standard deviation above the mean value. There are still potential problems encountered with this approach. One example is for those individuals that employ movement strategies where they wait until the last possible moment to move quickly towards a target. Little or no movement may occur in the first 400mS. To combat this problem, an extremely small or zero value is replaced with a minimum of 10% of the total movement amplitude (as opposed to one standard deviation above the very small mean value) to be considered crossing the movement onset threshold. This can potentially introduce some error but as these types of movements employ a strategy where little or no movement occurs early in the event and then a great deal of movement happens all at once, the movement onset threshold will be reached quickly, limiting the measurement error. Tests were done on 300 movements for comparison and the only trajectories that failed corresponded with invalid data where the individual did not perform as expected (e.g. when the game timer runs out, an event in progress will end immediately, truncating the movement trajectory and preventing the user from completing the task).

Rise time was addressed in a similar manner because the temporal measures relating to movement amplitude onset or ending are susceptible to false positives or noise when measuring either the start, end or both elements of movement trajectories. Rise time requires both the beginning and the end of the movement be discoverable quantities before being able to provide an output measure. This performance parameter measures the time it takes to go from 10% to 90% of the total distance to the target from the starting position. Movement onset has the same concerns as reaction time and the solution discussed is also applicable to rise time measurements. The end of a movement trajectory still needs to be addressed. This was discovered by looking for short duration plateaus towards the end of a movement trajectory when the paddle has either reached and destroyed a target or missed and has stopped in between events (a visual representation is shown in Fig. 44). To locate

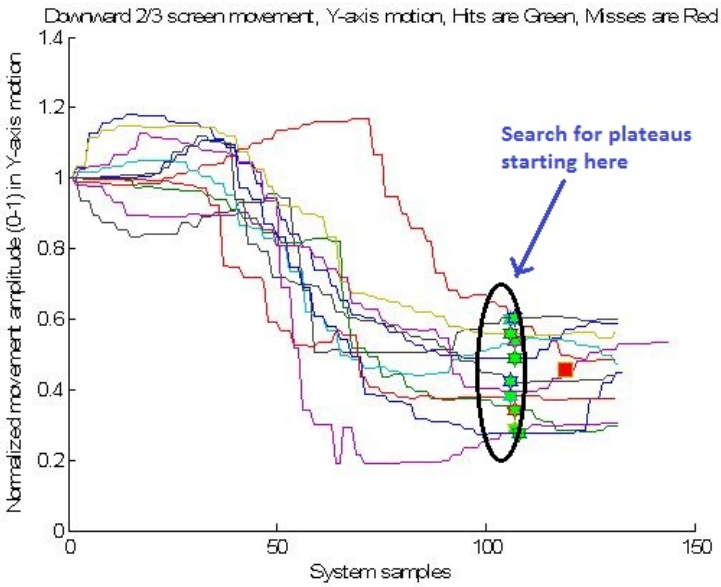

Figure 44: Finding the end of a movement trajectory

the end of a movement, trajectories are polled, starting from the end of an event and working backwards (event endings are marked on Fig. 44 with a star for success or a square for a missed event). A short duration plateau of 100mS was considered enough time elapsed that the user is deemed to be waiting at the end of an event for the next task to begin. User strategy again has the possibility to affect this measure, but in general paddle movement

dwindles toward the end of an event when users are in or at the end of a correction phase of the movement process with fine-tuned movements of the paddle position to reach and destroy the target. After a plateau at the end of a movement has been discovered, it is marked as the movement ending. Movement onset is already a known quantity, the two amplitudes are then marked as 0% and 100% and locating the 10 and 90% values provides the rise time performance metric. Due to similarities with the reaction time, verification using the same data containing the 300 movements exhibited similar results with few cases providing bad measures. In all cases, these corresponded to invalid data.

As briefly mentioned already, both reaction and rise time were verified and tested using a set of 300 movements. To ensure the results were expected and are reliable, manual comparison with the actual movements was done to ensure that the outcome measures provide the results they are intended to. After the updates in handling discovery of movement onset and ending, the results coincide exactly with the manual measurements. The exception being for incomplete events or data that corresponds to a bad/failed event (e.g. if a user is temporarily distracted and misses an event entirely then there is no movement to process).

The next movement performance feature that required validation for the gaming platform outcome measures is the residual movement error. This measure consists of the difference between any given movement and an average expected movement for that particular task. The first attempt at establishing residual error began with looking at what an ideal movement would be like, essentially going from one place to the next at exactly the optimal rate to reach the target in the time allowed without straying from the path or having large or small movement segments linked together. As this is not the case with human movement which exhibits several different phases [95] (discussed in more detail in Sec. 2.3), an alternative verification process is used.

At this stage in the verification, smaller movements had been abandoned as they provide little usable information. The residual error focused instead on the medium and large movements associated with game play. The movement sizes relate to normalized distance

covered on the screen by the paddle during a game event (the screen size is divided into thirds, $\frac{1}{3} - \frac{2}{3}$ is medium and $\frac{2}{3}$ or more are large movements). Instead of using the ideal movement, I set about generating an average movement trajectory from healthy individuals. This involved having 10 healthy subjects play the game for a short duration of 2 minutes, twice a day over a period of five days. In addition, they were asked to use a mouse for the input control object (or whatever device they normally use and are comfortable with). Data collected over that period of time for the group provided over a thousand movements for each of the movement categories considered. The categories are as follows, large and medium movements in the four possible directions using single-axis movement (up, down, left and right). The game settings were fixed at a medium difficulty with a single target appearing on screen at a time and no distractors. Targets were forced to appear no closer than 40% of the screen distance from the paddle starting position to ensure a significant amount of movement was required in each event. This provided optimal conditions for moving toward a target to yield a successful movement trajectory. After compiling the average movement trajectories for the healthy individuals, the results were excellent, the output exhibits smoothness and demonstrates a typical healthy human movement (see Fig. 45).

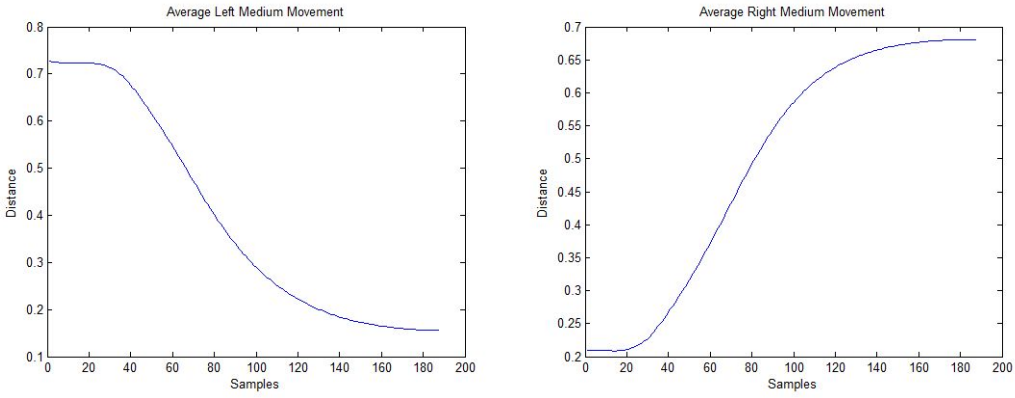

(a) Average left medium move

(b) Average right medium move

Figure 45: Average medium movements from healthy individuals

The residual error was introduced in Sec. 3.4 and discussed along with sampling rates

and compatibility between various platforms or hardware. Since not all systems sample at the same rate and not all events are the same time duration, it was necessary to interpolate signal lengths to match sampling rates for a proper comparison between the two. The resulting error measure for each trajectory is shown in Eq. 38,

$$AR_e = \frac{1}{n} \sum_{1}^{n} \mid t - a \mid . \tag{38}$$

The quantity provided is the summation of the absolute value of the average movement samples contained in a, subtracted from the actual movement trajectory values in t, divided by the number of samples to provide an average. Using the average movement trajectory compared to an ideal movement trajectory provided a more reasonable and realistic error measure as it is virtually impossible to make ideal movements from start to finish of an event.

4.3 Image acquisition setup verification

As part of the system involves being able to capture reliable images, both in a clinical or home based setting, the next important aspect is to ensure reliability in image quality. The alternative will result in poor or bad data that may yield either incorrect or invalid outcome measures, rendering that element of the system inoperative. This reinforces the idea that the image acquisition setup is not only important, it needs to be as efficient and simple to set up as possible to ensure repeatability for both varied locations and users. There are three main elements that make up the image acquisition setup, a background, a light source and a camera. There were several stages of evolution in each of these three components throughout the verification stage.

One of the key elements in any image or photograph is the backdrop or background. This will either make or break the quality and utility of an image and the subject within. As is often the case, an interesting background is desired for the photography enthusiast.

However, in our case, removal of the background is essential as only the foreground is of interest. Selection of an appropriate background went through several iterations, beginning with more texture and clutter in the field of view. This quickly became troublesome as a wide variety of image analysis techniques were needed and not always the same ones to deal with each set of problems, ramping up the difficulty for a planned automatic segmentation process. As an alternative, several different types of monochromatic, uncluttered backgrounds were experimented with before settling on a matte white foam core poster board. Several of the different choices tested are shown in Fig. 46 and 47. The best

(a) Textured background (b) Dark background

Figure 46: Example background mediums

selection for the greatest range of contrast and separability was the smooth light coloured background, favouring the matte white foam core poster board. This turned out to be optimal for the segmentation process, as it is easy to keep clean, uncluttered and introduced the least amount of noise. The other alternatives present interesting possibilities from the perspective of contrast but often exhibit problems with shading or noise, either in the form of texture, discontinuities when using a paper background and light coloured dust/dirt particles showing up easier on dark backgrounds.

Lighting is the next important consideration in image acquisition. The discussion in Sec. 3.3 highlights the choice made and how to position the light source. There were

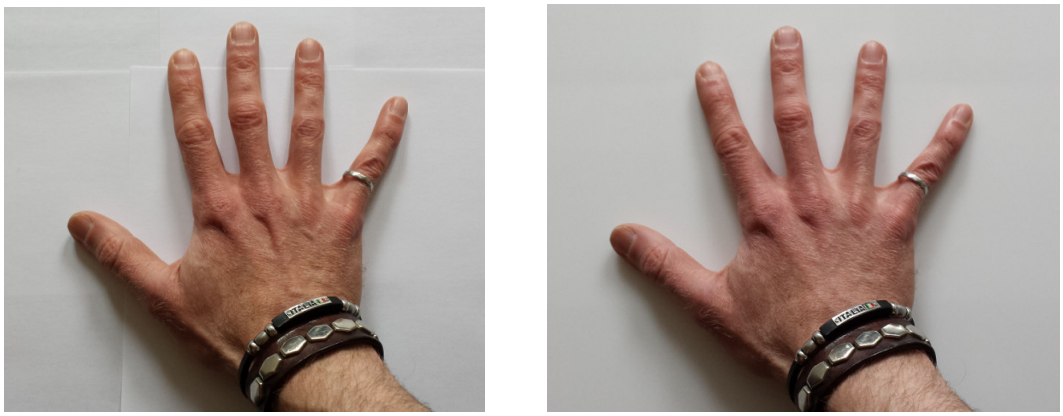

(a) Light discontinuity (b) Light smooth

Figure 47: Example background mediums - 2

several other lighting systems experimented with before arriving at this decision. The preliminary images were captured in a lab environment with standard building illumination in the form of fluorescent bulbs at regularly spaced intervals overhead. These tend to light up rooms reasonably well, but will cast uneven shadows if you are not directly underneath one source or well surrounded by several. An example that demonstrates this problem can be seen in Fig. 48. Although there are shadows, hand images with this type of lighting can

Figure 48: Shadows from fluorescent lighting

still be used, however the extra error incurred during segmentation from improper lighting is undesirable and easily avoidable. With some exploratory research into how film sets and professional photographers apply light to their subjects, a 3-point lighting system was experimented with. Typically photography applications employ background, fill and subject lighting, together providing a setting for capturing portrait quality images [107]. Experience with the fluorescent lab lighting made it difficult to expect much improvement with multiple light sources and this was what I discovered (see Fig. 49). Although there are a

(a) Light in NW,NE,SE corners

(b) Light in NW,NE,SW corners

Figure 49: Three point lighting setup

number of different types of light sources, (e.g. LED, halogen, fluorescent, incandescent, natural) the type of light is not as important as the consistency of using the same source from one session to the next, ensure accuracy in comparison over time. A single point light source centred directly overhead casts the least amount of shadows and provides the best view of the subject concerning visual features of interest. The recommendation for a light source is a garden variety desk lamp with a simple four-bar linkage that allows for easy adjustment. Most inexpensive models come with locking screws that allow retention of the position once a desirable setup has been discovered. My preference is incandescent lighting as I prefer the colour and the light that it casts compared to the alternatives, although any

light source will do as long as it adheres to the positioning requirement. When considering placement in the physical setup, positioning the light above the camera but in such a way that it does not cast a shadow from the camera is the preferred location. This provides the best view of the hands without introducing shading effects.

The final element of the image acquisition setup that went through verification was selection of an appropriate camera and establishing a guideline for how to set up. The technology in some of the most inexpensive cameras today is satisfactory enough to capture the information that we need. The resolution and true colour saturation or any other specific element that drives prices up and improves picture quality is unnecessary for our use case. We are able to employ a simple web-cam to capture 2-megapixel images that provide us with all the detail needed. Smaller cameras or web-cameras are preferred due to their portability or ease of mounting on a stand that allows for simple, rapid positioning to capture images of the hands. Along those lines, the best possible view of the hands would be directly above. This avoids skewed views of the subject which in turn distort the hands and add error potentially resulting in unusable data. To avoid placing many restrictions, making it prohibitive for home use, the goal is to have the hands in view with a light, matte-white background and set the camera up directly over where the hands are placed. An example to help demonstrate how to position the image acquisition setup is provided in Fig. 50. The view in the image on the right has been purposefully exaggerated to demonstrate perspective error in Fig. 50. Fluctuations in focal distance is not a strict requirement. As already discussed, digit lengths are stored as a function of percentage to allow repeatability at varying focal lengths. That way if the image acquisition setup needs to be moved or put away, fluctuations in equipment set up are more forgiving. There are other elements of cameras that were considered including lens widths relating to sensor sizes, although it was found that a normal or standard camera is well suited to our needs. To avoid over-complicating things or incurring extra cost in the camera equipment, there was no need to explore alternatives.

(a) Good perspective (b) Bad perspective

Figure 50: Demonstrating perspective

4.4 Joint feature verification

The joint features are intended to complement the other metrics used to describe the current condition of a client using the telerehabilitation gaming system. To ensure that the visual metrics are reliable and able to provide a means to measure the proposed features, verification and testing of each was incorporated into the development. The three joint features of interest include swelling, redness and texture. Each of these relating to specific symptoms for the target demographic, RA patients.

4.4.1 Joint swelling

The first feature addressed is joint swelling. The process of locating joints takes place during the structural analysis. Once joint centres have been established, extracting the surrounding area that would be considered part of the joint, takes place. As it is difficult to monitor swelling in two-dimensional images, the best possible approach is to examine surface area of the joint. This is done through looking for a maximum axis or greatest width of the joint in question and establishing a square region surrounding the joint centre with the dimensions equal to the maximum axis. Keeping track of joint area over time presents

a possibility of varied focal lengths due to camera positioning between sessions. To help reduce this problem, normalization of the area is taken by using the length of the finger (in pixels) corresponding to the joint being measured. This ensures that the surface area will always be reduced by the same factor and make for more consistent comparisons on a smaller scale. The other favourable factor for error relating to focal distance is that all joints will exhibit greater or less surface area if that is the cause. While that is a major concern if it is legitimate, it also poses the possibility of being non-symptomatic as per the discussion on RA and early onset symptoms that do not always manifest symmetrically [76].

When examining joint area, one of the first realizations met was that the MCP joints will not provide reliable information. They are difficult to see using a 2D image from a camera as they are contained in part of the palm and thus changes due to swelling in those joints can be masked by the surrounding area to some extent. The MCP joints are still included as part of the analysis, but for verification and greater sensitivity, looking to the DIP and PIP joints is the better choice for this feature. An example set of joints extracted from the top view are shown in Fig. 51. For the example cases, joint areas are 31,684 for the PIP joint and 21,316

(a) DIP joint

(b) PIP joint

Figure 51: DIP and PIP joints

for the DIP joint. Normalizing those numbers with the finger length yields values of 52 and 35 respectively. This results in a loss of sensitivity to some degree but it helps minimize

the effect of changes in focal length while still being able to monitor changes in joint area. To test this hypothesis, I took the same joint sub-images and added a group of dark pixels around the outside, leaving everything else constant to see if the system would recognize the change and indicate larger joint area was discovered. To help stress test the swelling metric, I decided to place extra dark pixels along the right border instead of on both sides of the joint. That way the maximum axis will still increase the set amount but the centre location will change. Problems were encountered as soon as the updated joints were processed. As expected, the assumption of swelling being a symmetrical process had been taken into account with the original code and at this point it was revised to accommodate both uniform and non-uniform swelling should that case ever occur. Three levels of increased joint size were included, a 1%, 5% and 10% increment. These were selected as they are a reasonable representation of potential problems occurring, where from 1-5% may be equipment error or very minor disease activity, from 5-10% represents a warning level where something has likely changed and anything greater than 10% would be significant enough to warrant action.

To test the joint swelling measure, three versions of the PIP joint were generated, one each with 1, 5 and 10% increased maximum axis length through the addition of extra skin-tone pixels in a band next to the joint along the right edge of the hand image. The three versions are presented in Fig. 52, 53 and 54. The next step involved processing

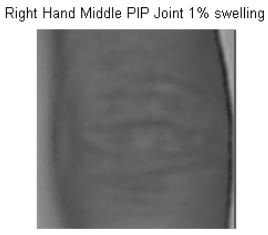

Figure 52: 1% increase

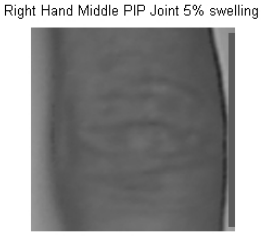

Figure 53: 5% increase

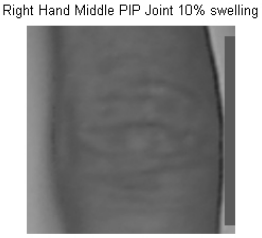

Figure 54: 10% increase

the modified versions of the hand image and generating the joint swelling feature to find

out if the artificially increased joint size would have the desired effect. The results for the joint swelling verification tests are shown in Table. 9. Since the joints belong to the same

Joint Description	Area	Normalized measure	% change	Adjusted %change
PIP - unaffected	31,684	52	0%	0%
PIP - 1% swelling	32,400	52.94	1.8%	0.9%
PIP - 5% swelling	35,344	57.75	11%	5.5%
PIP - 10% swelling	38,809	63.4	22%	11%

Table 9: Joint swelling area

hand/image as the default or unaffected PIP joint, the normalization factor is the same. The normalized results are shown in the third column of Table. 9. The percentage change shows twice the expected value as the affected area will have increased twofold based on using a maximum axis to change the size/shape. As a result, reducing the effect of dimensionality will halve the error, providing the true change in joint size, appearing in the final column. The final values of change are representative of the amount of area that was artificially added to the joints. The slight discrepancy is due to the values that were chosen for the additional joint area, at 1, 5 and 10%, the number of extra columns of pixels required were 1.8, 8.9 and 17.8 respectively. With pixels being a fixed, base unit, this provides a minor source of error. Even with the error after normalization, the joint swelling errors are close enough to be meaningful indicators of change in the size/shape of a joint at fairly low increments (1%) that could potentially indicate signs of day-to-day fluctuations that may result from inflammation before they are readily visible.

4.4.2 Joint redness

The next joint feature addressed in the system verification process is redness. As the name implies, this involves examining joints for signs of increased redness, one of the key symptoms of inflammation first reported by Celsus [127]. Visually, monitoring redness may be of limited value depending on the subject as not all skin tones readily display changes in redness unless there is a significant amount. However, symptoms relating to inflammation

are worth investigating as they are strong indicators of disease activity in RA. One benefit that we have relates to the use of digital cameras and their sensitivity to the visual spectrum and beyond into infra-red wavelengths, potentially working in our favour as heat is better represented in the lower frequencies [23].

Spending time looking at joints in the fingers reveals interesting patterns and shapes. There are typically a collection of lines or wrinkles in the skin surface that allow the fingers to flex at the joints. When in a relaxed, extended position, similar to the images that have been shown of the hands up to this point, the skin surface is slack and the wrinkles are more pronounced.

There is a vast network of arteries, veins and capillaries in the hands and fingers as part of the circulatory system [93]. With an increase in blood flow to the joint capsule areas during inflammation, my assumption is that the increased warmth will begin surrounding the joint capsule and the first visible signs will appear central to the joint, in between the wrinkles of the skin as they are fractionally closer to the joint surface than the exterior sections of skin.

Figure 55: Wrinkles in extended PIP joint

Preliminary experimental work examined average redness (see Sec. 3.5.5) as a function of the entire joint surface area to see if it provided a reasonable measure for comparison to measure fluctuations. This turned out to be more of a coarse measure that provides useful information but the decision was made to follow up on exploring further, anticipating a potential need for finer measurements of change with potential to improve the capability for monitoring skin tones that might not show changes in redness at a more coarse level that the average histogram values present.

The starting point when refining the joint locale we are interested in is looking to sur-

rounding edges of the wrinkles or skin-folds. To locate the area of interest, the gradient of a joint sub-image is generated (see Fig. 56). The gradient of a sub-image is represented as

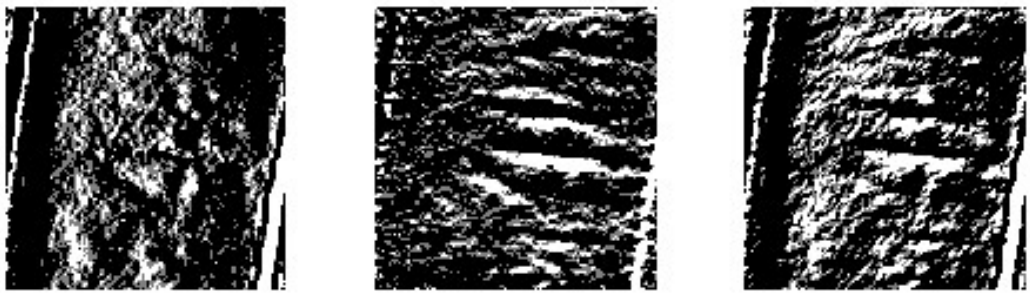

Figure 56: Gradient of a joint sub-image

follows,

$$\nabla f = [\frac{g_x}{g_y}], \tag{39}$$

where g_x is the gradient in the $x-direction$ and g_y is the gradient in the $y-direction$ [48]. The magnitude of the gradient consists of the sum of the squares for the gradient components (Eq. 40),

$$magnitude(\nabla f) = \sqrt{g_x^2 + g_y^2}. \tag{40}$$

In Fig. 56, the first two sub-images are plotted values for g_x and g_y respectively. The third sub-plot is the gradient magnitude, according to Eq. 40. The values reported by the gradient magnitude represent the rate of change in pixel intensities for each point. The result is that anywhere edges exist, there are greater magnitudes for the gradient and this is evidenced in the magnitude plot [48].

After examining the gradient corresponding to edges surrounding the joint, the next step was to locate a point of interest where likelihood of symptoms appearing might be present during inflammation. The joint centre in a sub-image is the best candidate for monitoring the key area for feature fluctuations and based on the edges can be found using

the following process. Converting the image into a logical representation is done first, this simplifies the matter of looking for connected regions in the image [48]. The following step is to locate the centroid for each of the regions. The centroid of a region in an image consists of the arithmetic mean for the x and y coordinates [48, 121]. Centroids in an image are represented as 2D moments (see Eq. 41).

$$m_{pq} = \sum_{x=0}^{M-1} \sum_{y=0}^{N-1} x^p y^q g(x, y), \tag{41}$$

where m_{pq} represents the raw 2D moment order of a greyscale image $g(x, y)$ of size MxN [48]. For the centroid of an image (or sub-image), equation 42 and 43 represent the x and y components respectively.

$$C_x = \{\frac{m_{10}}{m_{00}}\}, \tag{42}$$

$$C_y = \{\frac{m_{01}}{m_{00}}\}. \tag{43}$$

For the case of m_{00}, this corresponds to area of a binary image or the sum of grey level values for greyscale images as the general form of the raw 2D moment reduces to equation 44.

$$m_{00} = \sum_{x=0}^{M-1} \sum_{y=0}^{N-1} g(x, y). \tag{44}$$

Once the centroid of each region has been established, the $centroid - of - the - centroids$ is the desired focal point and it consists of the weighted average of all centroids (see Eq. 45).

$$(C_x, C_y) = \sum_{i=1}^{n} ((C_{xi}, C_{yi}) \cdot Area_i)/total\ area, \tag{45}$$

where the centroid locations are weighted by the area that they contribute and then divided by the total amount of area to discover the centroid of all regions, which coincides with our point of interest. An example joint with connected regions, centroids of each and the

centroid of all regions is shown in Fig. 57. Starting with the centroid of the connected

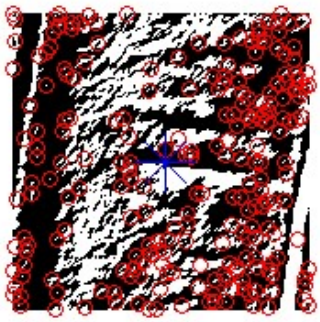

Figure 57: Centroid of connected regions

regions, we develop a seed value (point of interest) and subsequently the corresponding neighbourhood of interest or $motif$. The surrounding region is examined at a distance of a set radius value (see Fig. 58). This limits the area of interest to near the centroid of the

Figure 58: Radius limited neighbourhood

wrinkled or skin fold details in the finger joint. As such, going one step further, we include feature values from the probe functions, Φ_i for the motif pattern [111]. For this case, we are interested in two features, redness content and the gradient. These two features will help focus on edges between skin folds along the wrinkles, paying particular attention to signs of increased redness similar to the joint centre. The feature vector is represented in

Eq. 46,

$$\Phi = \{\phi_1(red), \phi_2(gradient)\} \tag{46}$$

The next step is to examine nearness in the context of neighbourhoods. This involves comparing probe function values with the motif pattern within the sub-image of the finger joint. As the motif was chosen to demonstrate key aspects of the joint, any other areas in the joint that demonstrate similar aspects will be considered near to the pattern motif and provide insight into similar regions. The nearness measure in this case is based on both a distance and an epsilon value, or tolerance factor. This is represented in Eq. 47 when considering a given point and the query point, x,

$$N_{\Phi_{(x,\epsilon,r)}} = \{y \in X : d(\Phi(x), \Phi(y)) < \epsilon \; and \; d(x, y) < r\}. \tag{47}$$

The distance between the vector of probe functions can be represented as,

$$d(\Phi(x), \Phi(y)) = \sum_{i=1}^{n} \mid \phi_i(x) - \phi_i(y) \mid, \tag{48}$$

where the individual features are compared within a tolerance value of ϵ apart to be considered near to one another descriptively. The spatial distance relates to the established neighbourhoods when comparing a given neighbourhood to the motif. All points included in a neighbourhood must be within a set distance from the query point to be considered near, in this case I use the $Euclidean$ distance. The radius was set to a value of 16 pixels in length for this case. This provided enough regions of interest (with overlap) to highlight points that have matching or near-matching descriptions to the unique query point (the centroid). An example of the resulting points that are near to the motif are shown in Fig. 59. Various parameter values were experimented with during the verification process and it was discovered that larger values of radius had little benefit, but increasing the value of ϵ, rapidly included a great deal more pixels as the values of redness were closer in value

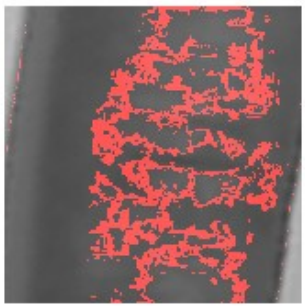

Figure 59: Nearness of points, $\epsilon = 0.01$, r = 16

Figure 60: Nearness of points, $\epsilon = 0.05$, r = 16

(see Fig. 60. Adhering to neighbourly or nearly identical points with a small $\epsilon = 0.01$ value provided excellent results.

The original motivation behind establishing pixels that relate to the wrinkles of the skin and that exhibit a certain degree of redness is to refine the focus of redness values on areas more likely to exhibit fluctuations in redness first during inflammation and see how much change needs to happen before the redness probe function will register a difference. Starting with the points displayed in Fig. 59, redness values are incremented by fixed amounts to see how the redness measure responds. The probe function consists of taking the average red channel intensity of the histogram over the entire joint. To test the ability to measure

change, altering values of pixels that are near to the motif will change the average intensity of the histogram by a set amount (1, 5 and 10%). Several example values of increased red intensity have been included in Table 10. The percentage change provided by the average

Intensity Increase	Normal Avg.	New Avg.	Diff.	% change
70	129.4915	143.2760	13.7845	10.65%
35	129.4915	136.3837	6.8922	5.32%
10	129.4915	131.4607	1.9692	1.52%
5	129.4915	130.4761	0.9846	0.76%

Table 10: Joint redness histogram average measure

histogram measure required a signifiant amount of increased redness surrounding the joint in the points near the motif. This was partially expected, although if my assumption is right and the first signs of warmth in the joints appear surrounding those points, a substantial improvement for monitoring changes in redness can be detected by examining only the points near to the motif for the joint (see Table 11). As expected, the sensitivity is far greater,

Intensity Increase	Normal Avg.	New Avg.	Diff.	% change
70	0.5174	0.7919	0.2745	53.1%
35	0.5174	0.6547	0.1373	26.53%
10	0.5174	0.557	0.039	7.6%
5	0.5174	0.5370	0.0196	3.79%

Table 11: Joint redness nearness measure

in the order of 5 times more than the average red intensity measure of the entire joint. In addition, examination of the joint image being tested demonstrates the effects of increasing the red channel values. The interesting element noted was that the lower values are not easy to detect with the naked eye, similar to performance of the histogram measure. Using the nearness measure provides a potential means to monitor far smaller changes due to a more selective view. The results from verification of joint redness provided two plausible feature values. A more general overall redness measure and then a fine, nearness measure. The amount of redness present in inflammation from one individual to another will not always be the same or necessarily easily detectable, making it even more appropriate to have the

Figure 61: Artificially added redness, 35, 10 and 5 per pixel

secondary measure. For our purposes, it is important to be able to detect slight changes and also more significant changes that could indicate anywhere from the early stages of developing problems to more serious situations with the intent of reporting on and providing a greater degree of accuracy in the visual condition description of the individual.

4.4.3 Joint texture

The final feature considered when examining joint sub-images was that of texture. This is a statistical measure based on grey levels and their proximity to one another in various angles [54]. There are four individual measures that are being addressed for texture, correlation, contrast, energy, and homogeneity [54]. These measures were discussed briefly in Sec. 3.5.5 and are now discussed in more detail in the context of verification.

The first consideration with the statistical texture measure with a grey-level co-occurrence matrix (GLCM) are the details specific to the GLCM. The purpose of using the GLCM approach is to examine textural features of a pixel compared with other pixels in the image. The first decision is the quantization level or the size of the GLCM. The joint images are typically small, as they contain only a small portion of the hand image. For preliminary work and verification, a GLCM size of 128 was selected ($m\ x\ n = 128\ x\ 128$). The choice was set at 128 to provide enough detail to test the measures without sacrificing too much dynamic range of the original image [0-255]. Once the size was selected, the next element in using a GLCM is to select the orientation of the texture that you are interested in examining. The joint wrinkles are likely to exhibit a predominantly horizontal orientation when

it comes to the texture of creases in the skin, although depending on the orientation of the hands during image acquisition this may not always be the case. There are four possible orientations and rather than restricting our selection to just one, the average of all four was selected to provide the best chance of discovering changes in textural features. The offset for measuring texture was left at a distance of 1 pixel for all features.

The first textural feature examined was contrast, a representation of how similar the texture is throughout the image, for smooth images or those without much texture, the contrast measure will typically be low. This feature value ranges from $[0, 127^2]$ for this case. Verification began with the example joint sub-image used from the previous verification experiments (left hand, middle finger, DIP joint) as it provides a good view of the joint area. The contrast measure for this joint is shown in a table format (see Table 12). Based on the

Angle	Radius	Contrast
0°	1	2.3404
45°	1	1.9719
90°	1	0.4329
135°	1	3.2307
Average	1	1.994

Table 12: Joint texture, contrast measure

range of values, contrast of the joint image varies very little. This was not unexpected but the small amount of variance makes it potentially a less suitable metric for commenting on changes in texture of a joint. Although the entire joint surface area is important to consider, it is less important for the redness and texture measures compared to swelling. Similar to the joint redness, a refined view for our region of interest can be generated as the area most likely to exhibit change in texture will be near and surrounding the joint centre. This can be achieved through the use of the nearness measure mentioned in the previous sub-section. Employing the redness and gradient features, the wrinkles around the joint were highlighted in Fig. 59. Capturing the surrounding region provided by the $nearness - selection$, the revised area of interest when looking for changes in texture (including contrast) is shown in

Figure 62: Selection of region of interest via nearness measure

Fig. 62. This was decided upon as the joint centre locations are good, but on occasion with varied lighting conditions or changes in orientation there are instances where the maximum axis generated area will capture background details as part of the joint sub-image (as can be seen in the example DIP joint image). To combat this problem it was decided that a refined selection of the region of interest directs focus to the desired area surrounding the joint centre, providing consistent improvements.

The remaining textural features, correlation, energy and homogeneity were all addressed together in the verification process. These measures tend to fluctuate similarly while describing unique information as they all relate to one another through the GLCM. To briefly revisit the three additional measures, correlation is the measure of similarity from a pixel to neighbours specified by proximity/angle, energy represents the variation in a neighbourhood and homogeneity represents the distribution of elements in the GLCM measured as distance from the diagonal. The following table (see Table 13) shows the results of all four texture measure for Fig. 62.

To discover how these metrics respond to changes in texture, a select amount of area in the target joint sub-image was artificially smoothed. Five separate test cases with varied degrees of texture were generated. These included constant and random control images along with three copies of Fig. 62 with percentages of area smoothed out. The three modified

Angle	Radius	Contrast	Correlation	Energy	Homogeneity
0°	1	0.2481	0.9874	0.0558	0.8766
45°	1	0.5417	0.9723	0.04	0.7873
90°	1	0.4163	0.9788	0.0465	0.8268
135°	1	0.4881	0.9751	0.0416	0.7974
Average	1	0.424	0.9784	0.046	0.822

Table 13: Joint texture, contrast, correlation, energy and homogeneity

versions of Fig. 62 were altered as follows. The centre of the region was located, then three quantities of total area were selected, 1, 5 and 10% surrounding the centre. The average intensity in those regions were then generated and all pixels within that region were set to the average value. The results are displayed in Table 14, each row corresponds to one of the five input images. The GLCM parameter values selected included a radius of one and the average of all four angles (of 0°, 45°, 90° and 135°) based on potential fluctuations in finger orientation. The constant image used for the first experiment contained all pixels with an

Experiment	Contrast	Correlation	Energy	Homogeneity
Constant	0	1	1	1
Random	2,700.43	0.01	0.00014	0.062
1% Smoother	0.45	0.977	0.0475	0.825
5% Smoother	0.401	0.978	0.0543	0.835
10% Smoother	0.377	0.979	0.067	0.848

Table 14: Joint texture verification, contrast, correlation, energy and homogeneity

intensity of one and the random image pixel values were uniformly distributed over the full range of 8-bit intensities [0,255] (all images had the same dimensions).

The average results presented in Table 14 help demonstrate what can be expected from the statistical texture measures relating to changes in joint texture. The constant and random images were included to demonstrate the extreme cases, in practice neither case is likely to occur. However, it was helpful in understanding how the metrics respond when they have images that are at the extremes of texture values. Following from the two extremes, it is expected that as a joint image smooths out in texture, the values for contrast will drop as there will be more similarity. Conversely, the values for correlation, energy

and homogeneity are expected to increase when this occurs. This is evidenced for both the energy and homogeneity although the correlation measure was less sensitive. The original joint sub-image (Fig. 62) yielded almost the same correlation value as the modified images, this suggests that even if swelling is present, causing smoothing of the skin surface texture, correlation will not exhibit a significant change in value. Moving forward, the contrast, energy and homogeneity texture features will be used to monitor fluctuations in joint texture.

4.5 Hand structure - top view

The first step in the process of extracting hand structure is to look for landmarks. We are interested in discovering the finger and thumb tips along with the inflection points of the hands. The desired locations are shown in Fig. 20 with circles indicating the points of interest. Joint centre locations are derived from the location of finger tips and inflection points in conjunction with information stored in Table 5. A detailed discussion of the method to locate finger tips and inflection points has been covered in Sec. 3.5.2. To verify joint locations, comparison with manually located values are included to determine accuracy of the method.

The procedure for gathering manually selected values of the correct locations of the finger tips and inflection points is through a separate, scripted user interface that was developed for the first session data when a user account is created. During the setup process, the operator must select the top view image and manually locate all finger/thumb tips, inflection points and joint centres. This information is stored in a tabular format and converted into percentages to avoid problems with fluctuations in focal lengths if the camera position is not fixed for all sessions. Next, the same image was provided to the analysis software to extract landmark locations and compare values with the manual measures.

The user provided data appears in Table 15, and the corresponding automatic software gathered data for landmark locations appears in Table 16. The error between the user and

Hand/Finger	Tip(Coord)	Inflection(Coord)
R/Pinky	(569,1697)	(728,1298)
R/Ring	(779,1880)	(890,1364)
R/Middle	(971,1958)	(1061,1346)
R/Index	(1187,1850)	(1271,1061)
R/Thumb	(1544,1313)	
L/Pinky	(2610,1844)	(2510,1421)
L/Ring	(2390,2012)	(2340,1472)
L/Middle	(2170,2066)	(2150,1424)
L/Index	(1940,1913)	(1988,1112)
L/Thumb	(1664,1337)	

Table 15: Manual location of tip and inflection points

Hand/Finger	Tip(Coord)	Inflection(Coord)
R/Pinky	(587,1707)	(711,1331)
R/Ring	(792,1895)	(878,1414)
R/Middle	(992,1968)	(1046,1372)
R/Index	(1201,1855)	(1245,1100)
R/Thumb	(1545,1314)	
L/Pinky	(2586,1854)	(2492,1520)
L/Ring	(2395,2013)	(2315,1563)
L/Middle	(2177,2072)	(2130,1433)
L/Index	(1962,1914)	(1948,1152)
L/Thumb	(1722,1329)	

Table 16: Software-based location of tip and inflection points

software gathered values is measured via the Euclidean distance and presented in Table 17. As a function of pixels, some of the error measures are significant. The corresponding mean error values for the landmarks across all fingers/thumb are (18.3,6.7) for finger tip(X,Y) placement and (17.3,38.7) for inflection point (X,Y) placement. Plausible reasons for the error are twofold, the most significant contributor is the angle of view from the camera and second relates to shading surrounding the hand, making it difficult to automatically extract the inflection points. The finger tip error measure is generally smaller as you move in towards the centre of the image. Confirming an original suspicion that the optimal location to situate a subject is important and directly beneath the lens of the camera centred in the field of view. Images were captured at full resolution from our web cam (8MP, $2448x3264$

Hand/Finger	Tip(X,Y)(Euclidean Error)	Inflection(X,Y)(Euclidean Error)
R/Pinky	(18,10) (21)	(17,33) (37)
R/Ring	(13,15) (20)	(12,50) (51)
R/Middle	(21,10) (23)	(15,26) (30)
R/Index	(14,5) (15)	(26,39) (47)
R/Thumb	(1,1) (1)	
L/Pinky	(24,10) (26)	(18,99) (100)
L/Ring	(5,1) (5)	(25,91) (94)
L/Middle	(7,6) (9)	(20,9) (22)
L/Index	(22,1) (22)	(40,40) (57)
L/Thumb	(58,8) (59)	

Table 17: Finger tip/inflection point location error (pixels)

Figure 63: Automatic placement of landmarks for top view hand image

pixels), placing the distances represented in context with respect to the error in pixels. To help visualize the error in placement, the software placed landmarks are shown in Fig. 63. The joint locations are also represented in Fig. 63 and the corresponding measures of distance are presented in Table 18, the first set of parentheses contains the error in the X and Y directions and the second set of parentheses is the Euclidean distance/error. Scaling the error measures based on image resolution (2448x3264) implies the largest error in either the X or Y direction is 6%. The mean error values for joint placement are (28.5,60.4) for the MCP joint, (16.9,32.5) for the PIP joint and (18.8,23.1) for the DIP joint. The main sources of error are related to shading and perspective for the camera field of view. This can be seen in the results, where the joint placement exhibits greater error at the outer edges and less

Hand/Finger	MCP	PIP	DIP
R/Pinky	(27,38) (47)	(17,16) (23)	(9,13) (16)
R/Ring	(15,71) (73)	(2,36) (36)	(1,25) (25)
R/Middle	(15,57) (59)	(1,19) (19)	(10,13) (16)
R/Index	(9,23) (25)	(2,4) (4)	(7,4) (8)
R/Thumb	(42,45) (62)		(33,41) (53)
L/Pinky	(40,145) (150)	(35,68) (76)	(37,44) (57)
L/Ring	(52,130) (140)	(32,85) (91)	(23,41) (47)
L/Middle	(36,3) (36)	(29,26) (39)	(26,11) (28)
L/Index	(29,2) (29)	(17,6) (18)	(22,4) (22)
L/Thumb	(20,90) (92)	(20,35) (40)	

Table 18: Joint placement error (pixels)

toward the centre. Error in the X-direction is typically lower as it relies on perceived width of the finger, implying that it would be affected more by shading and width mismatches. The Y-direction error is typically greater at the edges as it is reliant upon landmark location which is skewed by camera perspective. Centred digits in the field of view exhibit less error making it clear that centring the subject is important and can introduce a significant source of error. Noisy data is not unexpected in establishing landmarks and joint positions. Next, we look at how significantly it affects hand structure shedding insight into how much error propagates through the algorithm, affecting extracted features. Joint angle will likely be the most heavily influenced feature as the landmark locations affect construction of the digit segments. The joint features are less likely to be affected as they are discovered via the surrounding area of interest using alternate techniques that refine joint location before processing.

Next, we look at building hand structure from the landmarks and joint locations. The outcome measures derived from the hand structure are joint angles. These are commonly measured for range of motion or to detect the first sign of problems that can occur in deformities that are a result of damage to joints [76]. Locating landmarks for the hand has already pointed out potential pitfalls with image acquisition and the structure will likely be affected accordingly. A comparison with manual goniometer measures was made with the

structure in Fig. 64. The manual measurements were taken from the same image in print, using a goniometer. The structural error measures are presented in three separate charts,

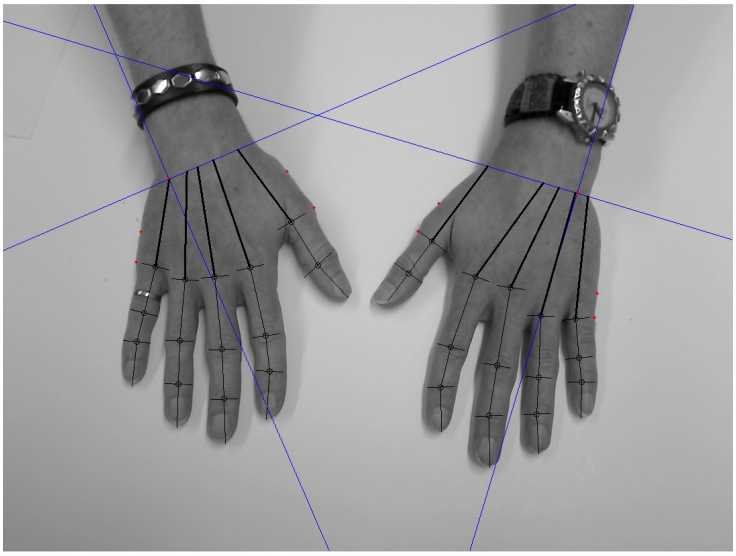

Figure 64: Complete structure for top view hand image

one for each joint, MCP, PIP and DIP (see Fig. 65, 66 and 67). A quick visual inspection confirms that the right hand exhibits less measurement error compared to the goniometer measures. The camera perspective error along with the presence of shading in between fingers causes problems for the landmark location procedure and the error cascades into the joint angle measures. The mean error at the joint angles was 6.3° for the MCP joint, 1.54° for the PIP joint and 3.06° for the DIP joint. The presence of greater error in the MCP joint angle presented concern initially that assumptions about bone angle separation might be a significant contributor but separating the error values from right hand (MCP - 1.81°, PIP - 1.66°, DIP - 1.85°) to the left hand (MCP - 10.74°, PIP - 1.43°, DIP - 4.27°) indicates that perspective is the greatest contributor of error. Both perspective and shading are tractable problems with the appropriate image acquisition setup constraints, such as eliminating all but one light source and placing the camera with an optimal perspective where the field of view is centred over the subject. All goniometer measurements were taken with the $Baseline$ goniometer shown in Fig. 3 and used to measure a printed copy

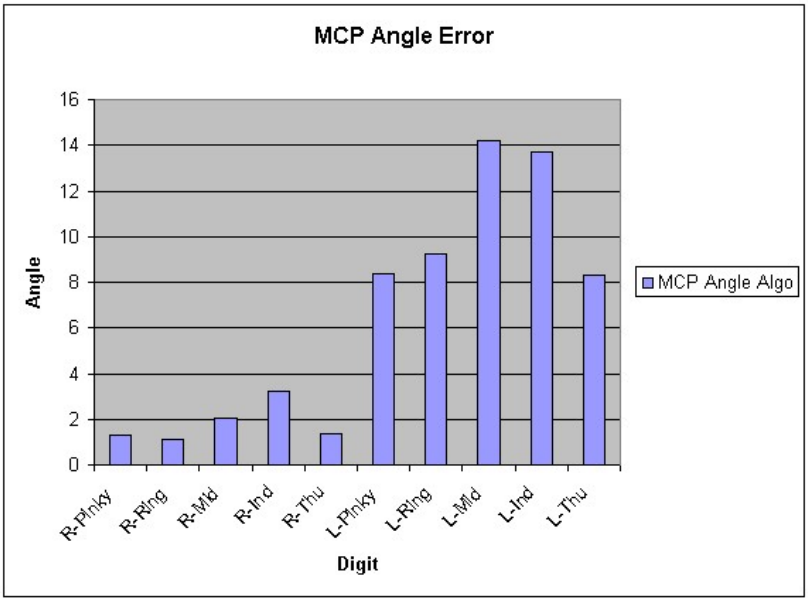

Figure 65: Error measure between algorithm joint angles and manual goniometry, MCP

of the original image.

The reasoning behind including two hands in one image was to simplify the process of image acquisition for the end user, limiting the amount of hand poses captured and the amount of data transferred from the client after a session. Furthermore, telerehabilitation targets remote or rural communities that may have limited access to broadband thus presenting an annoyance after each session of long upload times. After going through the verification experiments and results, this pose requires further consideration and begins by examining the remaining hand poses.

4.6 Hand structure - lateral view

The next visual perspective considered was the lateral hand pose. This is intended to provide an improved view over the index finger of the dominant hand paying particular attention to the DIP and PIP joints which are commonly affected in RA patients. We are interested in the joint locations and angles. For verification purposes, this process does not require prior knowledge of landmarks as seen in the first pose. Instead, the structural

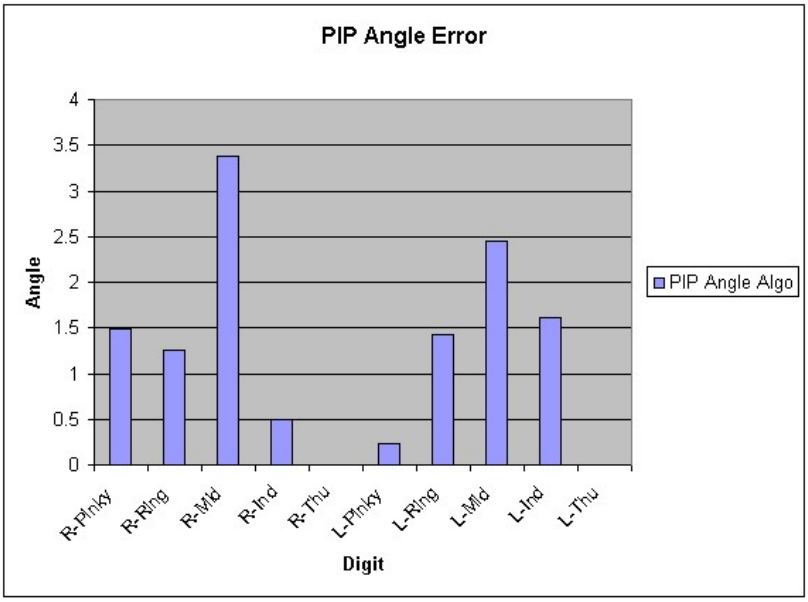

Figure 66: Error measure between algorithm joint angles and manual goniometry, PIP

information required can be extracted from the images.

Several variations of the lateral view pose were investigated to obtain the best possible view and ability to extract the desired information. First, the angle of incline from the surface plane was addressed. To maintain a useful view of the index finger, a range of 45 to 70° was tested for shadows, finger separation and perspective. The view from this range of the angle of incline are sufficient to extract the desired information and still provide a reasonable tolerance for variation from one individual or session to another. The next variation in pose was whether to extend the thumb or have it partially hidden in flexion. Depending upon the individual and disease activity, the pose in flexion may not be possible, although both are suitable and only have minimal effects on the view of the index finger (e.g. minimal change in position and shading).

For verification experiments, both the flexed thumb and straight thumb poses were tested to ensure expected results. The manual $Baseline$ goniometer measurements are used for comparison. The hand geometry problem differs for this case, requiring only location of the finger tip at the extremity of the image. Once located, the remaining points of interest are determined through landmark features common to fingers. Building on re-

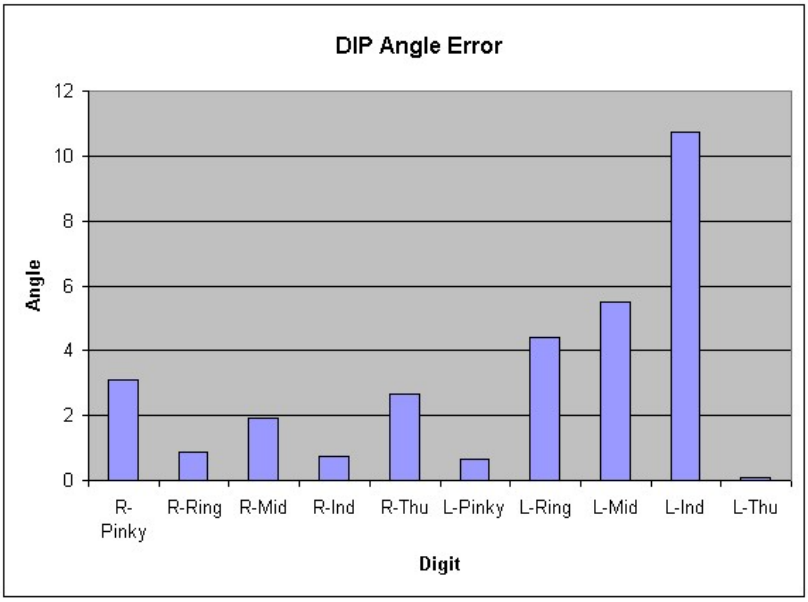

Figure 67: Error measure between algorithm joint angles and manual goniometry, DIP

sults from the first pose, proper lighting and maintaining the hand close to the centre of the camera field of view were taken into account. Focal distance to the subject was considered but is less of a concern due to the algorithm using geographical landmarks on the hand to extract features of interest relating to structure. With sufficient resolution and size of the subject, changes in focal distance will not affect the structural measures (joint angles).

The outcome metrics are both angular measures, corresponding to the angle for the DIP and PIP joints. To extract these joint angles, the structure of the finger, or estimated bone segments need to be established to measure the angles between them. The gold standard for these type of measurements is radiographic images and although it would be nice to compare with, we settle for the safer and less invasive visual spectrum and address the still imagery.

Two subject images were used, one with the thumb extended and the other flexed. The lighting was kept uniform and the angle of deflection for the first subject was 45° and the second was captured at 70°. The resulting measurements are extracted from Fig. 68a and 68b. The figures have been cropped to highlight the subject in the viewing area. A third image was added to experiment with greater finger flexion displayed by the subject,

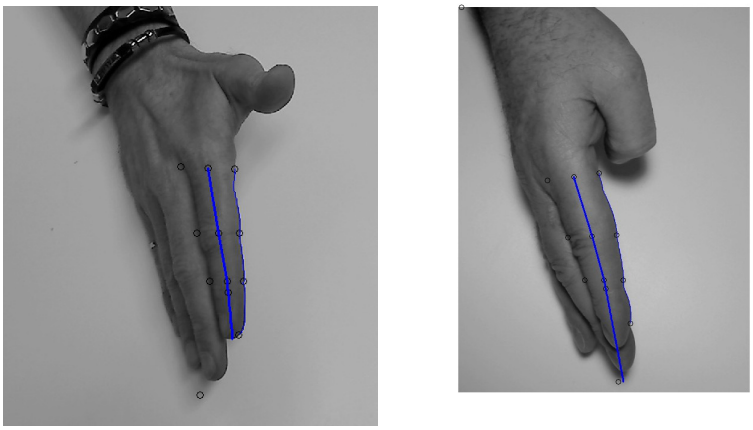

(a) 45° (b) 70°

Figure 68: DIP and PIP joint angle, lateral view

intended to show potential error between actual and the automated algorithm measurements as joint angles increase. The third position is shown in Fig. 69. The resulting measurements

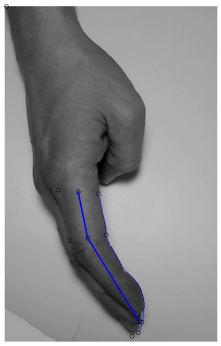

Figure 69: Third lateral pose examining flexed DIP and PIP joints

are provided in Table 19 and displayed in chart format for convenient viewing. The error for hand images in this pose are much lower than the previous case for the top view, with a mean value of 1.38° and variance of 0.44°. The largest error relates to the DIP joint measurement for the flexed position. This resulted in an error of 2.5°, which is significant for this particular measure considering that is a 29% error of the total. Smaller joint angles are subject to greater error as a function of resolution with both a goniometer that has low precision (+/- 0.5°) and software with potential noisy input (i.e. a 0.5° error from

Subject	Joint Angle	Algorithm	Goniometer	Error
Subject 1 - 45°	DIP	4.75°	3.5°	1.25°
Subject 1 - 45°	PIP	2°	1°	1°
Subject 2 - 70°	DIP	4.5°	3°	1.5°
Subject 2 - 70°	PIP	2°	1.5°	0.5°
Subject 3 - flex	DIP	8.5°	6°	2.5°
Subject 3 - flex	PIP	20°	18.5°	1.5°

Table 19: Lateral pose, DIP and PIP joint angle measurements

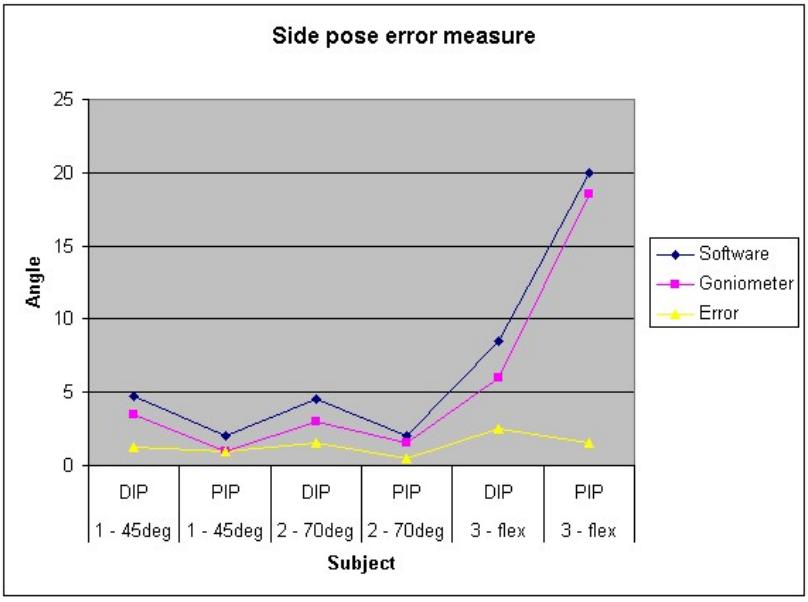

Figure 70: Error between software and goniometer measurements

a 1 or 2° angle is significant). However, consistency in the error is important, there is minimal fluctuation compared with the top view perspective. There are several reasons why we are seeing improved performance. First, with only one hand in the field of view, the subject is able to more readily situate themselves in the centre of the camera field of view, ensuring an optimal viewing angle. This also comes with the added benefit of avoiding much of the shading issue faced in the previous pose. Finally, without requiring a set of manually discovered landmarks to position a skeleton structure, this algorithm is able to avoid that potential source of error. The results support these facts and follow the algorithm measurements closely, with some variation for the subject exhibiting finger flexion. Less error would be preferable but most importantly, change is readily measured and this holds

promise for monitoring potential early warning signs of deformities that can manifest in the hands resulting from RA.

4.7 Range of motion - top view

The final hand pose revisits the top view, restricted to the dominant hand in the field of view. The reason for selecting the dominant hand is that it will receive the bulk of the work from an individual and most likely to exhibit signs of wear and tear. When discussing range of motion there are two types, active where the individual activates the joint under their own power or passive where a trained individual will manipulate the joint instead [98]. Considering our target audience is intended to operate from both a clinic and in a home-based setting, the choice of active range of motion (ROM) measurements are best suited.

The angles we are interested in measuring are the angle of abduction for each of the fingers and thumb on the dominant hand. Abduction implies stretching away from the centre of something and for our case, it is the fingers stretching away from the centre of the hand [98]. We are interested in any change for how much the patient is able to abduct the extended fingers from the centre of the hand which may indicate potential underlying problems associated with pain or stiffness as a function of RA [76].

For verification purposes, three example hand poses are used, including Fig. 14. All three will be compared with standard goniometer measurements. The challenge in these images is to locate the hand structure and build the skeleton with representations for the main axes of each finger and also for the centre of the hand in between the middle and ring fingers. This can be seen overlaid on the final output. The results from the ROM tests are shown in Table 20, all goniometer measurements were made using the $Baseline$ goniometer on unmarked, printed images of each hand pose. Results from the software provide a copy of the image and the angular measurement lines are overlaid on top (see Fig. 72). The discrepancy between the software and goniometer measurements are presented in an accompanying chart to help visualize the results (see Fig. 73). The error quantities are once

Figure 71: Top view for measuring ROM

Subject	P-t-m	R-t-m	M-t-m	I-t-m	T-t-m
Measured by software					
Subject 1	28.85°	5.7°	4.13°	19.38°	55.08°
Subject 2	24.19°	8.1°	5.24°	20.05°	49.37°
Subject 3	22.67°	4.93°	6.18°	15.57°	68.86°
Measured by goniometer					
Subject 1	27°	6.5°	5.5°	21.5°	57.5°
Subject 2	24°	9°	5°	18.5°	48°
Subject 3	21°	5.5°	6°	17.5°	69°

Table 20: Range of motion angle measurements via software and goniometer

again significantly lower than the first hand pose and more consistent with the lateral view hand pose. The mean error value between the ROM measures is 1.15° and the variance is 0.6°. This is in part likely due to a simpler configuration for measuring with the goniometer. More complicated poses require careful precision with the goniometer and can add human error, increasing the discrepancy. The ROM measure still requires a degree of precision when measuring and the greater discrepancy exhibited between the measurements for subject 1 can likely be explained by operator error. The greatest error present in the measurements comparing actual with the software is 2.42° for the first subject, measuring from the thumb to the mid-line, yielding a 4.2% discrepancy. Considering that acceptable rates of angular measurement error are typically reported as fluctuating between individual raters and up to as much as 5°, my software is within that limit when representing the ROM

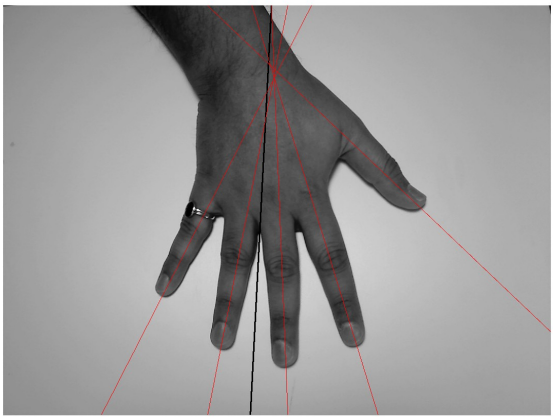

Figure 72: Results of software measuring ROM angles, overlay

measures. In addition, there will be no variability from one data set to the next, the measurements will always be taken the same way using software, guaranteeing repeatability.

5 Results and Discussion

This section contains results compiled from experiments using the telerehabilitation gaming system. They were designed to explore the range of reporting with the movement performance feature set and provide a basis for accompaniment by the visual features. Unfortunately when the experimental work took place, the visual feature extraction methods were not completed. However, separate experimental work and testing was done during the verification stages, demonstrating their potential and future direction.

5.1 Visualizing outcome measures

The resulting data from a gaming session is a rich source of information and not easy to make sense of until post processing occurs to separate important details and extract features of interest. In this section, we look at how movement is separated, processed and how features are extracted.

The starting point consists of capturing user movement as a continuous stream, that

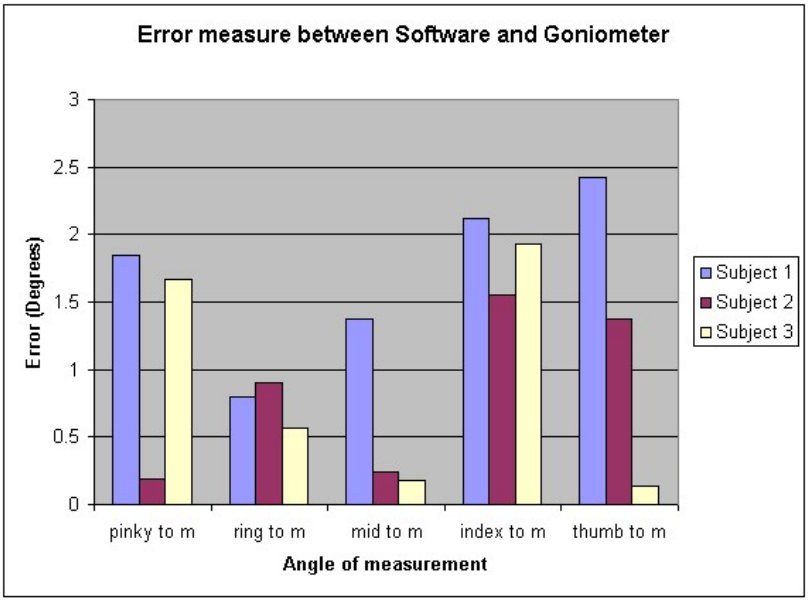

Figure 73: Discrepancy between software and goniometer measurements

information is parsed and broken up into movements coinciding with events. Game events are linked to the life of targets that users are required to destroy by running the paddle into them. The life of a target begins when it appears on screen, until the time it is either destroyed or leaves the screen comprising one complete game event. During that time, movement information is captured for everything on the game screen so it is possible to re-create what occurred during individual events. When looking at separating data, movements are broken up into separate bins based on distance that the paddle moved during the game event. The size of movement categories were classified as small, medium and large which corresponds to distances of $0-\frac{1}{3}$, $\frac{1}{3}-\frac{2}{3}$, and $\frac{2}{3}-$fullscreen. Separation into categories helps reduce the amount of movements considered at one time as it is possible to have hundreds of movements during a game session depending on game settings. The movements are further separated into categories by the direction of movement. For experimental purposes, the movements we used were 1D, so either left-right or up-down depending on the screen configuration and the input control object employed. A sample collection of game movements and the process of event and movement separation is shown in Fig. 74.

Each separate signal corresponds to a movement in the game, the green stars indicate

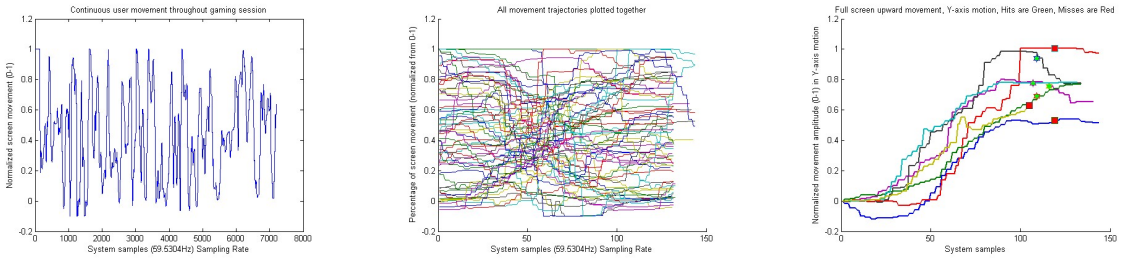

Figure 74: Movement parsing process

successful events where the target was destroyed and any red squares indicate a failed event where the target was missed. Considering that this is one of six separate categories of movements, it is easy to justify their separation.

The movement performance features are derived from these trajectories. The starting point is looking at movement accuracy when a client misses a target. Besides absolute accuracy, we include two additional performance metrics, overshoot and undershoot. The plot shown in Fig. 45b demonstrates a set of movements that exhibit a number of unsuccessful events, with both overshoot and undershoot errors plotted. These measures provide part of the resulting user performance profile for accuracy. Next, in Fig. 45a, the temporal measures are shown, they consist of rise time and reaction time for the individual and represent how quickly they complete the bulk of the movements and also how fast they respond to the onset of an event. The next category of movement performance measures rate efficiency, this include the path length, which examines how much variation there is between samples, more erratic movements will result in higher values, indicating more coarse or less well controlled movements. This is readily visible in comparing movements in Fig. 75 with the movements in Fig. 74. The other efficiency measure is the residual error. This is the difference between user movements and an average healthy movement trajectory. The average movement trajectory was built from a number of individual experiments with healthy subjects and discussed in detail in Sec. 4.2. Although this can be considered an accuracy measure, it is measuring the distance between user average movement and typical healthy human movement. The characteristics of the average movements are usually well

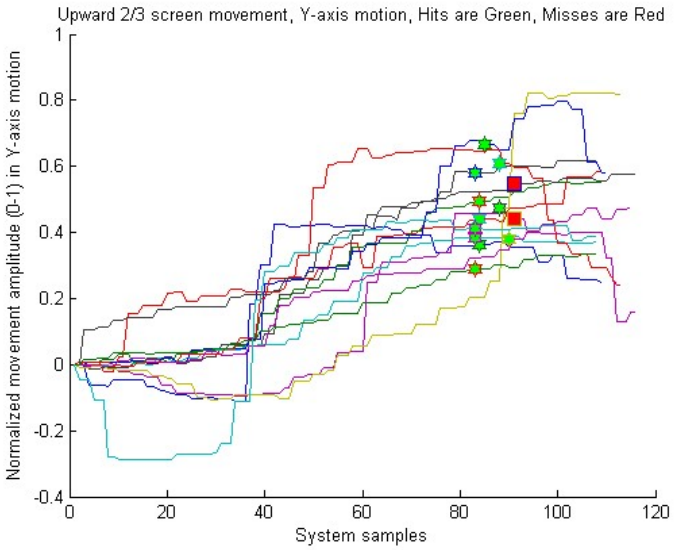

Figure 75: Movement data exhibiting lower movement efficiency

formed with smooth control (see Fig. 19), comparisons will demonstrate variations from the smooth movement, representing degree of efficiency. Next, the coarse scoring measures are grouped together to provide an overall performance measure, this is made up of the score, number of hits and number of misses. Finally the symptomatic or questionnaire measures for pain and stiffness make up the final component in a user performance profile after a game session. This provides a means to organize result categories for a broad view of user performance when making comparisons if desired.

Category	Movement performance features
Accuracy	Overall accuracy, Overshoot, Undershoot
Temporal Measures	Reaction & Rise time
Efficiency	Path length, Residual and RMS Residual error
Performance	Score, Hits, Misses
Symptoms	Pain, Stiffness

Table 21: Five categories of movement performance features

The additional measures discussed in the background details, Sec. 2.3 include the phase plane plots that contain the position vs. velocity information. These are a great supporting tool for examining average movement performance at a glance. They were not included as part of the main profiling, but as a secondary source of information they can be produced

for an individual in the sample population as needed. Collectively, the Accuracy, Temporal, Efficiency and Performance measures along with the pain and stiffness markers form a report-card for the individual after a telerehabilitation session. This leads into the discussion of results from experiments conducted using the telerehabilation gaming system.

5.2 Telerehabilitation gaming results

There have been several experiments using the telerehabilitation gaming system described herein. Included are examples with RA patients as well as some normative cases to provide a comparison. In each case, the experimental setup is described for each situation, followed by a brief look at the results.

5.2.1 Experiment 1 - RA patients n = 30

The experiment described in this subsection was conducted by my collaborating partners at the College of Rehabilitation Sciences. The telerehabilitation gaming system was used with a group of RA patients (n = 30). The participants ranged in age from 30 to 60, all with a recent onset of at least two of the symptoms listed in Table 22.

Number	Rheumatoid Arthritis Symptom
1	Morning joint stiffness duration $\geq$ 30 minutes,
2	Six or more tender joints,
3	Three or more swollen joints,
4	Erythrocyte sedimentation rate (ESR) $\geq$ 28mm/hr.

Table 22: Rheumatoid arthritis symptoms

Similar to work done in [53], two visits were required for a test-retest analysis, providing feedback for multiple visits. Selection was made from a pool of eight control objects for a given task. The selection criteria chosen by clinicians was based on duration of a session, fatigue and pain reported by the subject. Some objects provided limited use as they were too difficult to map a full range on-screen due to patient disability. To help focus

individual action on finger-hand function, a padded arm rest with a velcro wrist strap was used to limit assistance from the upper limb.

Preliminary results were gathered from the trials and have been examined to look for the ability to monitor patient performance. A pair of plots are included here to demonstrate that ability of the individual can easily be seen in the context of the exercise and task setting (see Fig. 76). From these plots it is readily visible that the performance on the left

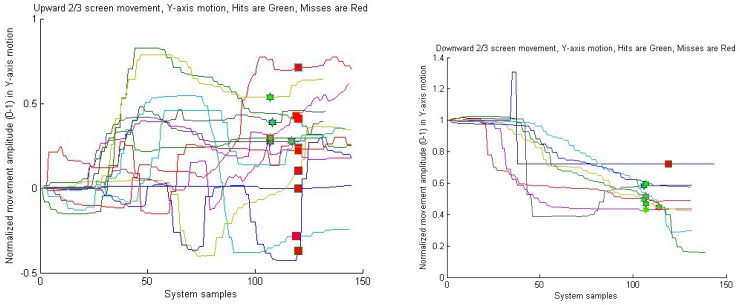

(a) Poor RA patient performance (b) Good RA patient performance

Figure 76: Preliminary results from RA patients shows poor/good performance

represents a more difficult task for the individual making the movements. The movement trajectories do not exhibit the smoother similarities exhibited in the plot on the right. These were demonstrated to provide some insight into how it is useful to have access to the movement trajectories and graphical or visual representation of the movements and movement performance features. Delving deeper into the performance measures will provide a more verbose examination of patient performance. Two example cases are discussed in more depth where the subject performs the same test but on two separate visits for test-re-test comparison.

First, the in-game parameters are presented, which were kept uniform between the two sessions for comparison. This applies across variations of the game in either the horizontal or vertical orientation.

Parm1. Game duration is limited to 90 seconds,

Parm2. One target on the screen at a time - a circle,

Parm3. Use full screen (as opposed to windowed play),

Parm4. Paddle size = 100%,

Parm5. Target size = 3, for horizontal play,

Parm5a Target size = 6, for vertical play,

Parm6. Target speed = 3, for horizontal play,

Parm6b. Target speed = 4 for vertical play,

Parm7. Minimum distance to target = 0.4,

Parm8. No distractors during game play.

Using these parameters, we report on large and medium movements. Small displacements were restricted early on in the testing phase of the gaming platform as they often provided little useful information as very small movements of the paddle (sometimes almost none) was required to reach the target during an event. Also, there were no distractors to avoid adding any extra requirements on the cognitive process that would affect movement due to multiple things to consider on the game screen at once. The input control objects differ between the two individuals. Subject one used an instrumented wine glass, tilting it forward and backward to control the paddle in a vertical orientation. Subject two used an instrumented coffee cup, rotated left and right to play the game in a horizontal orientation (see Fig. 77). Selection of the input control object was made by the clinician and was intended to match therapeutic movements with object movements, slaved to the game paddle. The amount of resulting data is extensive and to avoid including large amounts of data in the body of this document, examples have been relocated to the appendices. However, each of the five categories of movement performance discussed in Sec. 5.1 (from Table 21) are presented for two subjects during their first and second sessions. All data is kept anonymous and any identification except for numbers have been removed from the data files.

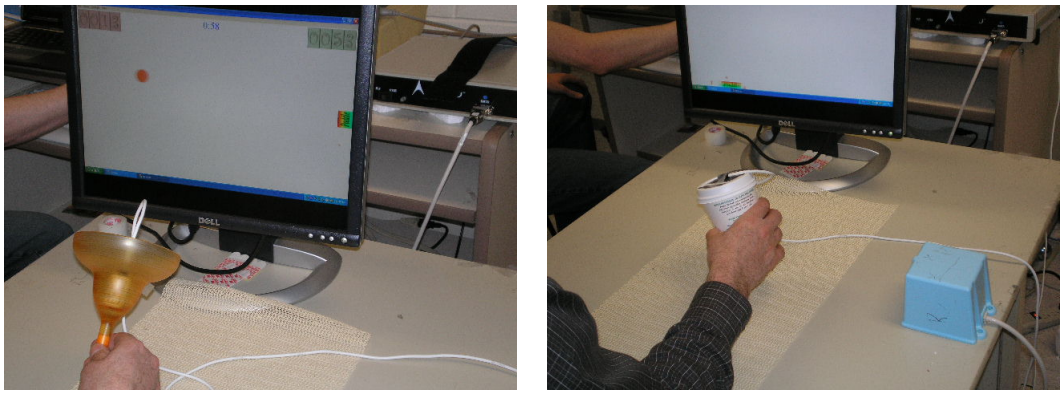

(a) Wine glass (b) Coffee cup

Figure 77: Instrumented input control objects for the rehabilitation gaming platform

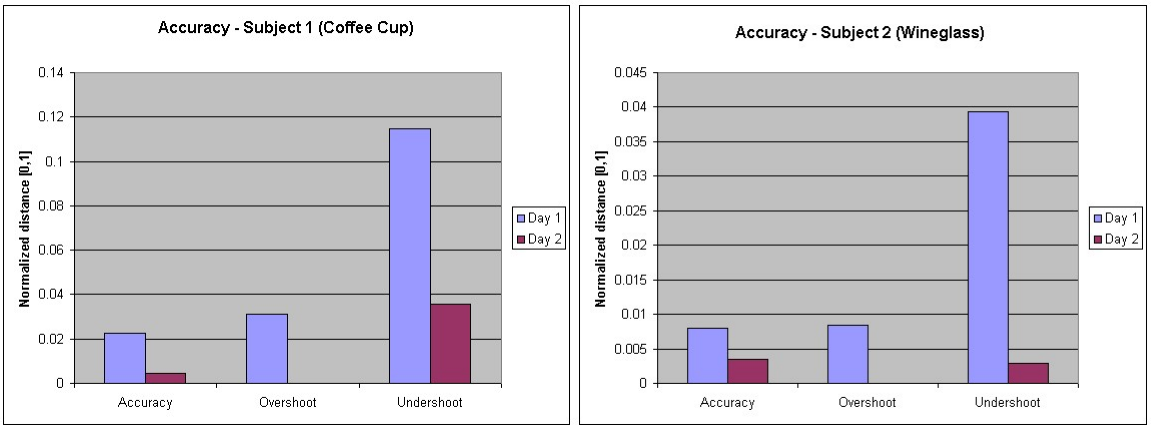

(a) (b)

Figure 78: Accuracy measure from RA patients, subject 1 - coffee cup, subject 2 - wineglass

Charts are provided to help demonstrate trends in performance using the movement performance metrics and the pain and stiffness pop-up windows. An immediate observation for both cases are improvements in most aspects for the second day. The accuracy error levels are low, reporting less than 1% of the screen distance on average. Reaction speed and rise time both improved from day 1 to day 2. The values reported are well within the range of healthy reaction speed, discussed in Sec. 2.3 and Sec. 3.4. The amount of improvement on the second day improved by 3 and 20% for reaction speed and 30 and 45% for rise time for subjects 1 and 2 respectively. This coincides with learning the task

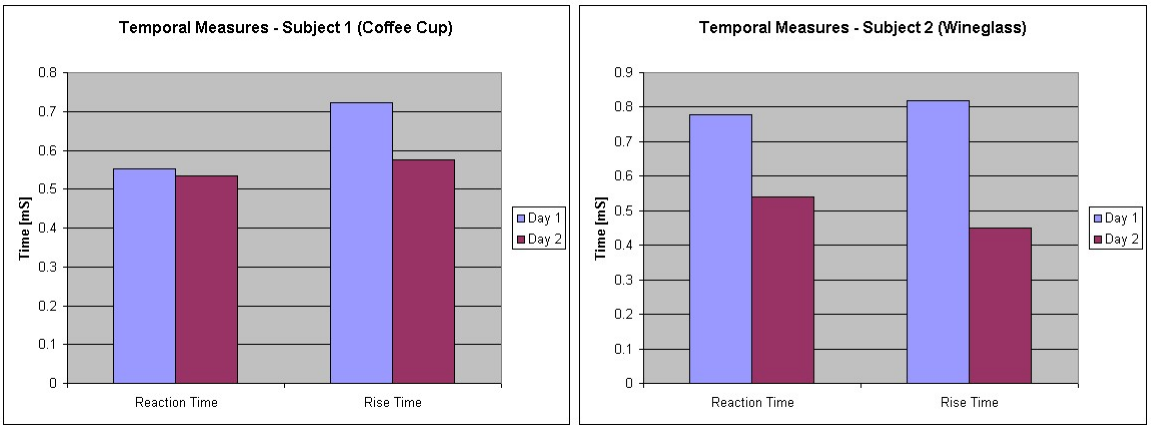

(a) (b)

Figure 79: Temporal measure from RA patients, subject 1 - coffee cup, subject 2 - wineglass

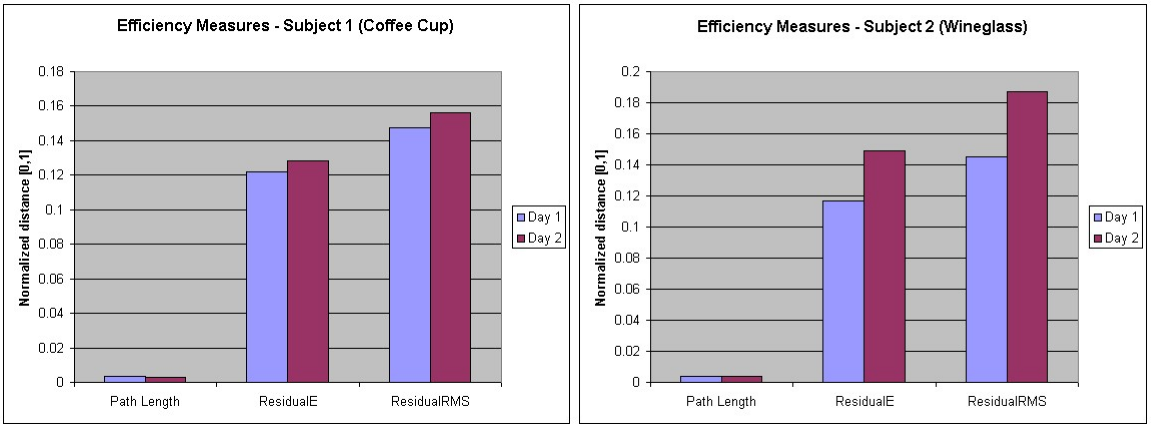

(a) (b)

Figure 80: Efficiency measure from RA patients, subject 1 - coffee cup, subject 2 - wineglass

and becoming familiar with the movements. The efficiency measures are the one distinct area that appears to worsen on the second day compared to the first day. Specifically the residual error measures increased by 22% for both. However, the other efficiency marker, path length appears to improve slightly or remain steady in both cases. This implies that although the subjects might be making their movements somewhat abnormally, the degree of control is still smooth. The performance measures improved consistently from day 1 to day 2 for both subjects, likely from learning the task and familiarity. Finally, the chart

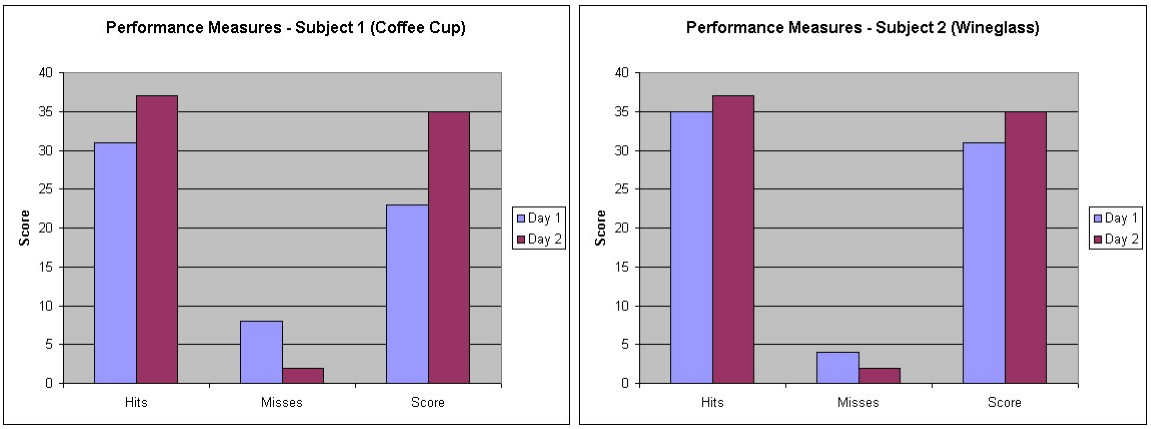

(a) (b)

Figure 81: Performance measure from RA patients, subject 1 - coffee cup, subject 2 - wineglass

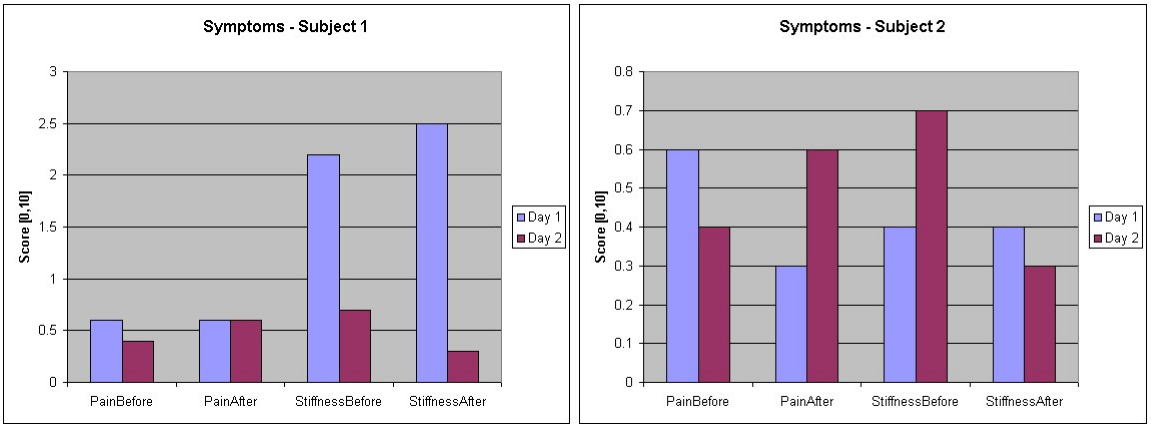

(a) (b)

Figure 82: Symptom measure from RA patients, subject 1 - coffee cup, subject 2 - wineglass

containing the symptom description, or pain and stiffness dialogue box results, drops in value for subject 1 but there is a slight increase in subject 2's values from day 1 to day 2. They remain less than a value of 1 so it is not overly concerning, considering that the popup windows from Fig. 12 contain sliders that range from 0 to 10. More concerning results coincide with larger values or when pain and/or stiffness increase during a session. For this case, the increase is 0.2, representing a very slight change in pain level. To provide

another source of information on a subject's performance, it is possible to make use of the phase plane plots discussed earlier. For this case, we can examine the plot for subject 2 to see if there are any unusual anomalies in their velocity profile (see Fig. 83). The position

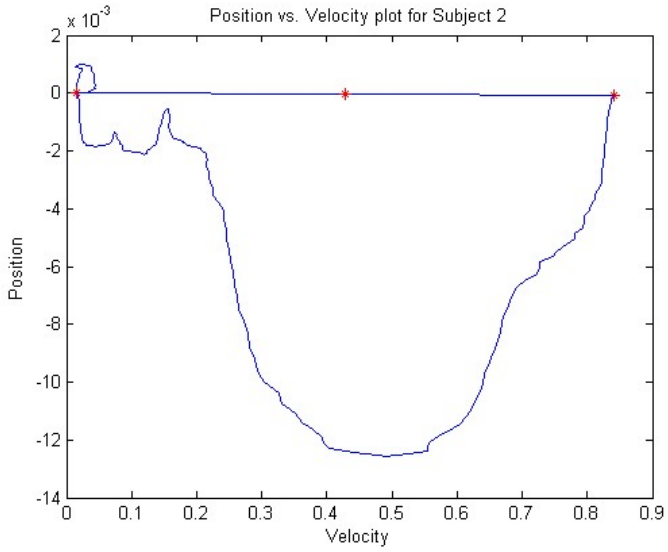

Figure 83: Velocity vs. position plot for subject 2

vs. velocity plots are typically bell shaped, symmetric plots (see Sec. 2.3), the more skewed and erratic the plots are, the worse the average quality of the movements are. As we are only dealing with one direction of movement (e.g. one way movement, not returning the paddle to the starting position), only half of the movement cycle will be shown, which is why there is only half of a bell shape present in the plot. Considering the quality of the velocity profile, the indications are that the movement performance is good as it is very similar to the desired bell shape of optimal movements, unlike the example phase plane plots shown in Fig. 5. The smoother and more controlled movement becomes, the smoother the position vs. velocity curve will be. Phase plane plots can be a useful tool to provide confirmation if other data has anomalies or suspicious outliers in it, a quick look at a phase plane plot can help provide a good $at - a - glance$ second opinion on the quality of movement.

Collectively, the performance metrics of the 2 individuals reported here demonstrate in a general sense, "$good$" performance. The earlier movement trajectory plots that demon-

strate poor performance as well are most certainly for a more challenging task or the subjects are experiencing worse symptomatic conditions. There are other input control objects that require fine precision control with some resistance and that can cause similar problems for anyone. This concludes the discussion relating to movement performance measurements and the first experiment. Next we look at a smaller group but with more variable performance.

5.2.2 Experiment 2 - RA patients n = 4

The second experiment was also conducted in cooperation with the College of Rehabilitation Sciences at the University of Manitoba. The telerehabilitation gaming system was employed as part of an open clinic with a smaller group of RA patients interacting with the gaming platform using a variety of input control objects during a single session. The individuals that took part in this experiment were considered beyond the early onset stage of the disease and in some cases exhibited much greater signs of prior disease activity (deformities) than expected for our target demographic. The outcome measures reflect the change in condition of the individuals when comparing to the previous results of the early onset subjects.

The game parameters were kept similar to aid in comparison and post-analysis. The single target on-screen restriction, target size, speed, difficulty, game orientation and paddle size all follow the plans set out from the first experiment. The duration of the game varied between 1-3 minutes depending on the individual and the task. There were other datasets beyond n=4 but unfortunately the quality of the data made it unusable due to limitations of user ability. The other distinction to note is a single visit protocol was employed, resulting in no temporal progression to measure. However, varied performance in the group points out how through profiling we are able to report on individual aspects of user performance and can provide warning when markers change suddenly or exhibit concerning trends. Each subject played the game 5 times with a different input control object each

time. The instrumented objects they used included a wooden dowel, clothes peg, wine-glass, spray nozzle and a weighted wooden dowel where it is inserted into a softball and supported for rotational control (shown in Fig. 84).

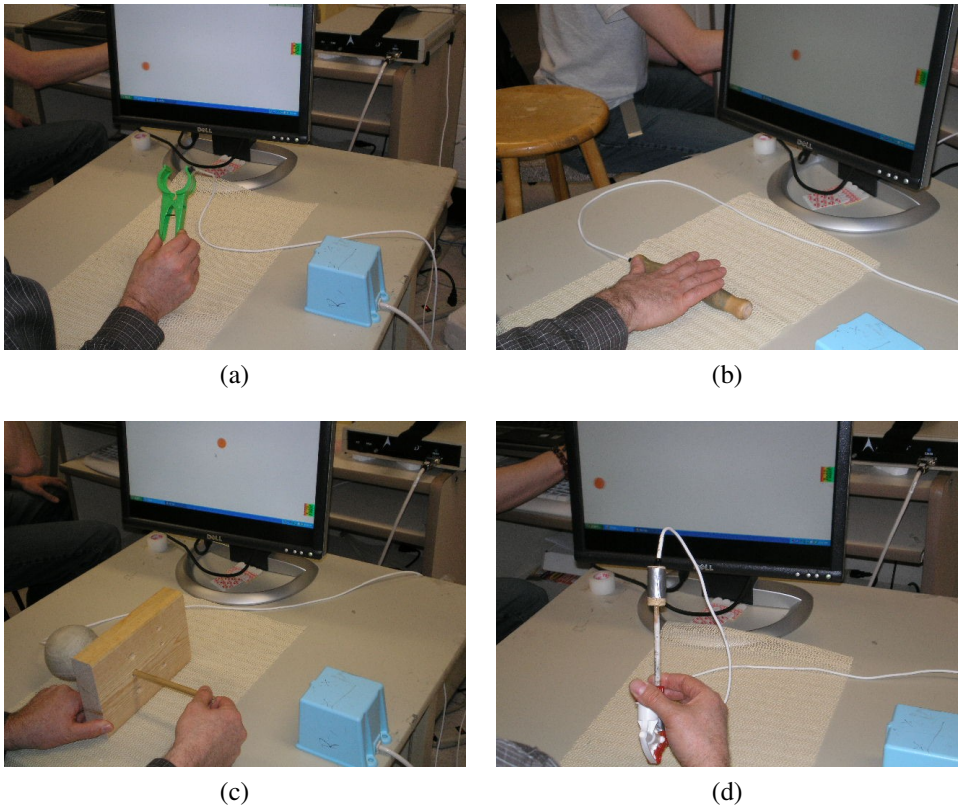

(a) (b)

(c) (d)

Figure 84: Instrumented input control objects

Similar to the previous experiment, two of the test case results are presented here to keep the discussion manageable. Further information can be found in the appendices. Once again, all data is anonymous and contains no identification information in it. The two examples cases presented are the first and fourth test subjects and they exhibit a range of interesting values for the measured game parameters. Both subjects use the same set of input control objects in succession (5 trials), using the same game settings with the exception of duration or length of the game session. The game sessions were shortened at the discretion of the clinician if the control object was deemed more challenging to manipulate.

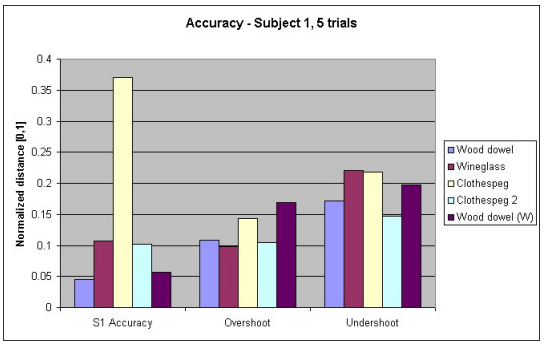

(a)

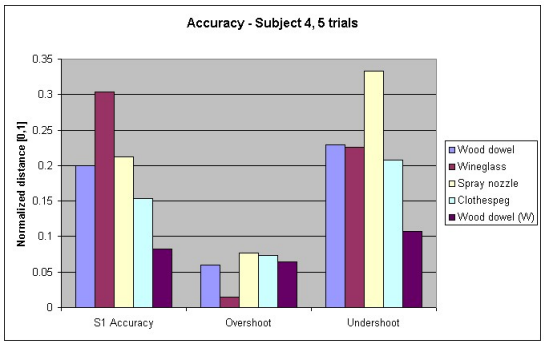

(b)

Figure 85: Accuracy measure from RA patients

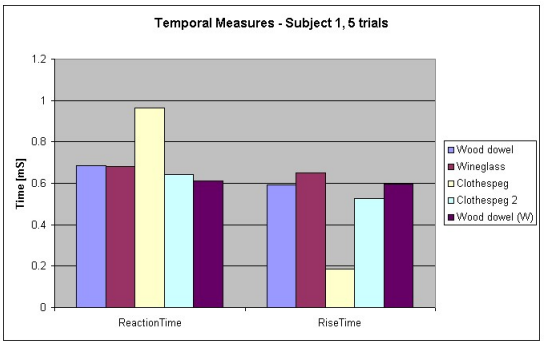

(a)

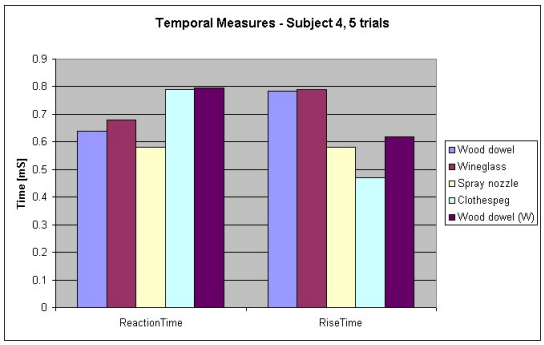

(b)

Figure 86: Temporal measure from RA patients

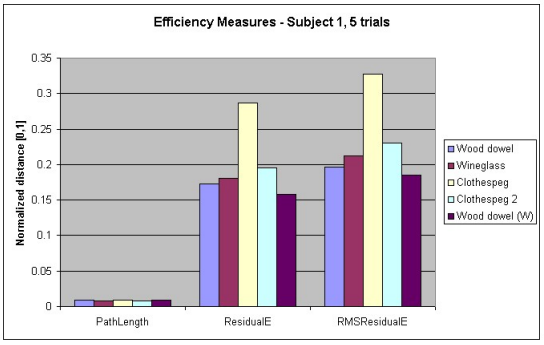

(a)

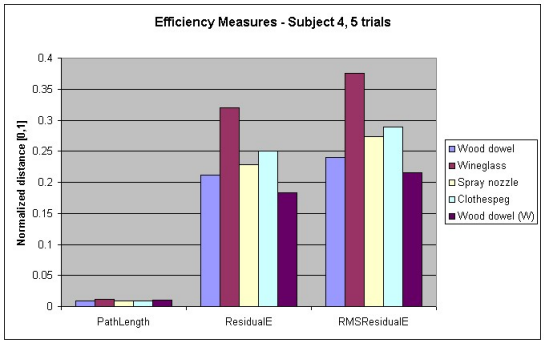

(b)

Figure 87: Efficiency measure from RA patients

The first comparisons made are between the two subjects. There are 5 separate trials reported on each plot, each corresponding to a different input control object. From the

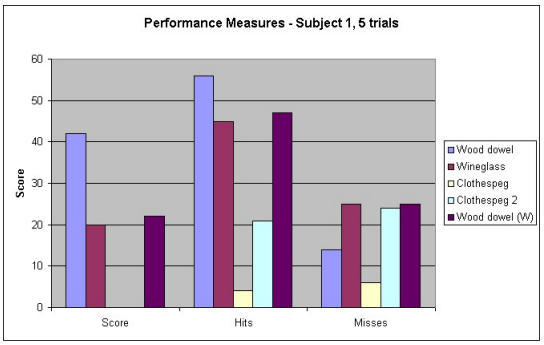

(a)

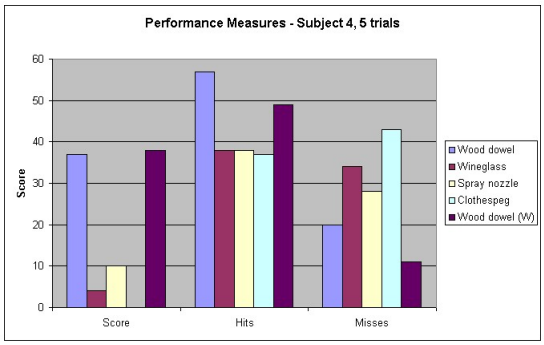

(b)

Figure 88: Performance measure from RA patients

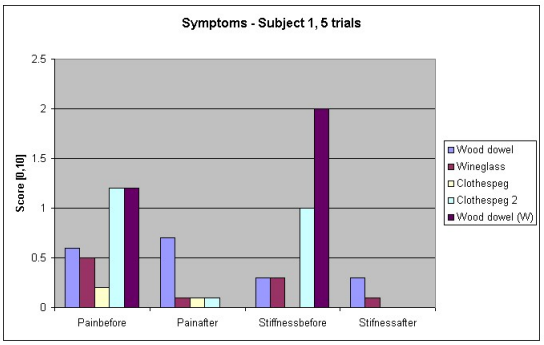

(a)

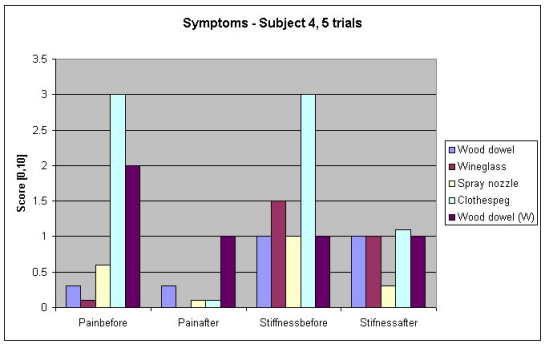

(b)

Figure 89: Symptom measure from RA patients

accuracy measures, it is easy to see that the absolute error measure demonstrates that subject one is performing significantly better than subject four. The total difference between the accuracy measure is 6.8% in favour of subject 1. The overshoot and undershoot errors alone would disagree, but the average error indicates that it is likely there are more cases that contribute to the overshoot and undershoot measures for subject four. This brings up an important point about overshoot and undershoot errors, these are more about defining game strategy than measuring the overall accuracy. Often there are fewer of either overshoot or undershoot errors making the average appear large compared to the overall measure. More direct comparisons use the absolute error first and then expand to include the overshoot/undershoot information to provide a more detailed analysis of missed-target events.

The temporal measures exhibit the opposite trend, where reaction times are shorter on average for subject four (in the order of 2.6% faster). The rise times were significantly shorter (17%) for subject one, indicating that they made the bulk of their movement in less time on average. The efficiency measures were not as easy to separate, the path length measure values differed by less than 1%, and were both low, indicating smooth, controlled movements. However, the residual error demonstrates that there is between a 20-25% discrepancy with average healthy movements. This could be in part related to difficulty associated with manipulating the input control object and also the condition of the individual performing the task. Next, we look at the performance measures, which are harder to gauge for discerning between the two test subjects. Up until Fig. 88, the metrics all point to subject 1 as performing better overall, however, the coarse score measures demonstrate a problem that can be found in many traditional gaming platforms that are more likely to measure score and other coarse parameters when gauging performance. For this case, the average scores of subject four are better, this is due to longer game play where more targets were hit. The number of misses was also larger for subject four but the percentage of success outweighed the number of misses to provide a better overall score. Finally, both subjects displayed symptoms associated with RA, in the pain and stiffness measures. Compared to previous results, the values were generally higher. The trend seems to be that after-session pain and stiffness values are typically lower, even if only by a small amount. This was expected and agrees with information presented in the literature that exercise can ease joint pain and stiffness for those affected by arthritis [76].

As a point of interest similar to the previous experiment and to demonstrate the difference in movement quality, a position vs. velocity plot was generated for both subject 1 and subject 4 (see Fig. 90). These plots represent large, downward oriented movements in a North-South oriented game. The quality of movement is quickly discernible as much worse in the phase plane plot for subject four. The plot is skewed and does not exhibit the desirable bell-shaped velocity curve. The movements used to generate these plots are

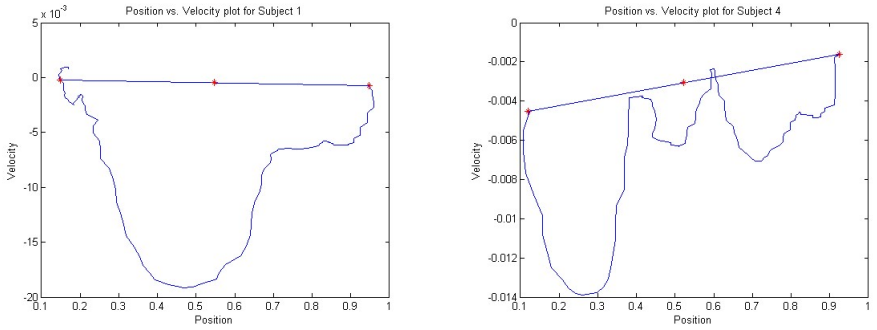

(a) (b)

Figure 90: Phase plane plots for Subject 1 and 2

derived from the first task, using the wooden dowel in the non-weighted configuration from Fig. 84. The remaining results not included in the body of this document demonstrated that the first control object (wooden dowel) typically demonstrates better performance from each of the participants. This also highlights the utility of the phase plane plot as a tool available through the telerehabilitation gaming platform outcome measures.

Comparisons between the first and second experiments are more challenging as the tasks, duration of the games and test subjects differed in parts. One of the driving forces behind the telerehabilitation gaming system design was to compare current performance with prior sessions from the individual to monitor improvements or degrading performance. Comparisons are still possible between users but performance levels in patients are likely to be variable similar to healthy individuals. The second trial for experiment two makes use of the wineglass and that is the input control object used in experiment 1 for subject 2. Generalized comparisons point out that the accuracy measures agree with the statement that the subjects in experiment 2 were more restricted or limited in their movement capabilities than those from the first experiment. However, it is difficult to comment on the temporal measures as the second test on day 2 reveals much improved performance. The path length measures show little discrepancy between subjects however the residual error demonstrates significant change, the test subjects in experiment 2 exhibit 50 and 60% greater error re-

spectively when comparing their performance to average healthy movements. Comparing performance measures will be a generalization when looking from one subject to the next if game parameters have changed. The percentage of success or score can be used as a metric and it points out that the subjects in the second experiment had considerably less success (subject 1 hit 48% of all targets and subject 2 hit 40% of all targets) in destroying targets with the wineglass control object. The symptomatic measures show greater activity in the second experiment which may be a contributing factor for why performance was considerably worse than subject 2 from the first experiment as the patients exhibited more advanced stages of RA progression. In each case, the pain and stiffness markers dropped by the end of a session, but at the start they appear to be more pronounced.

One final item about this experiment was reception of the telerehabilitation game by patients using the system. I was present for some of the experimental work and when asked, the majority had favourable reviews with regards to playing a game as part of a therapeutic regimen. This included individuals that would classify themselves as non-gamers (either from lack of experience or prior interest).

5.2.3 Experiment 3 - normative subjects n = 10

Prior to the experiments involving RA patients, earlier work was done with normative cases or healthy volunteers to test the system for preparedness and provide feedback. One of the important experiments that has been described in detail already was development of the residual error measure and the average trajectories. The goal was to develop four average movement trajectories from a collection of gaming sessions yielded by a group of 10 individuals. This has been mentioned already in Sec. 4.2. A few additional details are provided here along with some example results of normative data to accompany what has already been demonstrated via the groups of RA patients.

The normative group was a sample population of students and friends that volunteered to take part in the experiment. The group of 10 ranged in age from 22 to 38, consisting

of half male and half female participants. The game settings have already been mentioned in the first experiment discussion and were kept constant for this case. The input control object recommended was the mouse or any alternative device that the participant was very comfortable using. The intent was to have 10 sources of smooth game play that generate reasonable average movements when examined collectively. Although the game settings were set to a medium difficulty level, the amount of targets on screen was restricted to one and the time between targets was enough that very few targets were missed during these experiments, providing greater amounts of useful data. The participants played the game twice a day for five days, producing output data from their sessions in two orientations, horizontal movements and vertical movements. Engaging in one session-orientation of each per day, provided a significant source of data to generate average movement trajectories for the varied combinations of movement distances and orientations needed for the telerehabilitation gaming system. All data was returned for post-processing and the movements were parsed into separate categories, medium, large and direction for a total of eight collections to represent the average movements. Lastly, averaging took place to establish a normative trajectory for each case. The averages were derived from over a 1000 moves in each category and the end result contained 8 smooth average trajectories, one for each case.

To provide more insight into normative data for comparison with the prior experimental results, the accuracy, temporal, efficiency and performance measures are included along with example phase plane plots for three normative cases.

The phase plane plots exhibit profiles close to the ideal bell shape or smooth curve expected from fine control during the movement phases (initiation, ballistic and correction) [10, 94]. There are no pain or stiffness results for obvious reasons, but the other measures shed a little more light on some of the performance metrics. Accuracy is the least surprising of the group, as we expect to have predominantly low values in these categories. One of the normative cases exhibited some overshoot and undershoot but a value of 2.5% of the screen distance for overshoot error and 1.4% for undershoot is very small consider-

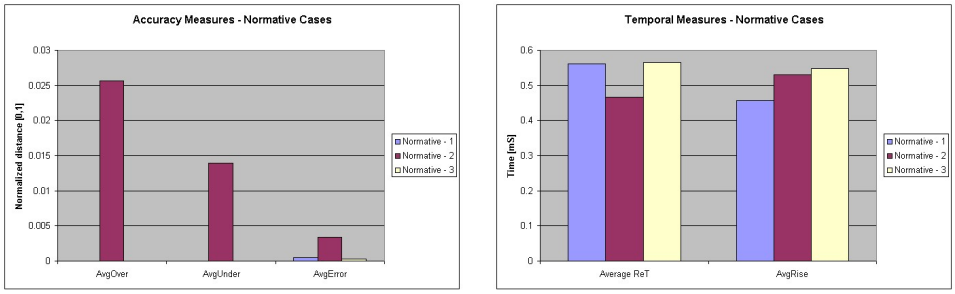

(a)

(b)

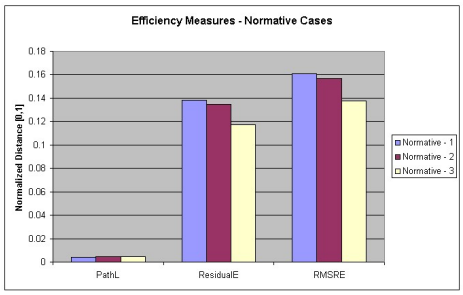

(c)

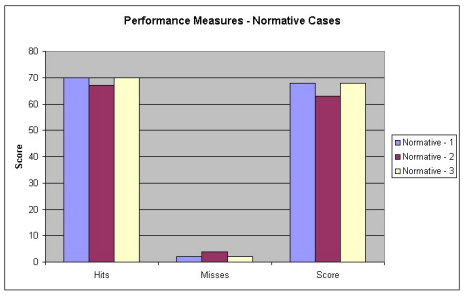

(d)

Figure 91: Movement performance for normative subjects

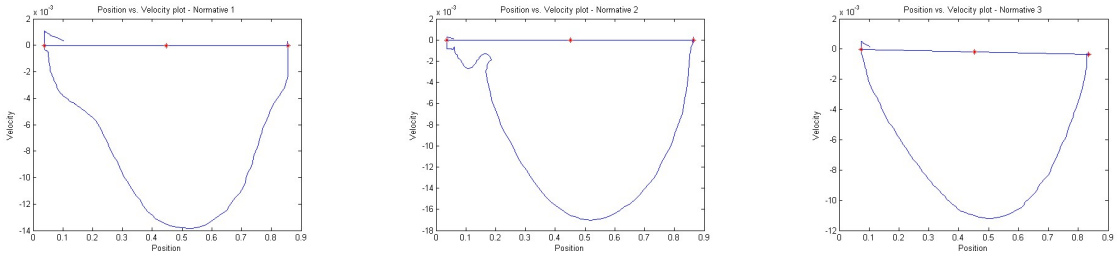

Figure 92: Position vs. velocity plots - normative subjects

ing there were only 4 missed targets. The temporal measures exhibited values within the normal range for reaction and rise times. Also, performance measurements represent expectedly high hits and game scores while missed events are low. There was one unexpected result in the residual error measurements. Considering the normative cases were part of the group that make up average movements, it was interesting to see that their residual errors ranged from 0.12 to 0.14 of normalized screen distance error. That is still considerably less than the previous two RA experiments, but it sheds some light on movement strategy and how it can make a difference from the average if you choose an alternative strategy

(e.g. wait until the target is close to the bottom of the screen and then move quickly to intercept vs. start movement shortly after a target appears and gently cross the screen until you intercept). Collectively, these are measures of task difficulty, stemming from research on precision, goal-directed aiming tasks [10, 88, 94, 95]. This points out the importance of using measurements like these to compare relative to one's own performance. Comparing with others is valuable, but to gauge whether you have improved or deteriorated, it is necessary to look at past performances.

5.3 Further discussion

The results presented to this point have encompassed the telerehabilitation gaming platform implemented and tested as part of several experimental setups. There has been a great deal of work done to develop this platform that is able to provide a rich source of data for extracting movement performance features from research based on goal-directed, precision aiming tasks to report on client performance and condition based on measures of task difficulty. Part of the process has resulted in generating several publications for both the telerehabilitation gaming system development [80, 81, 112] a home based pilot study [138] and recent interest from industry.

One aspect of the system that has been dealt with somewhat less to this point is the use of a content management system (CMS). This has purposefully been left in the prototype phase as the concept is better suited for a production level system. I built a prototype based on the $Joomla!^{®}$ platform and scripting languages to provide a web interface as a front end. In addition, the back end of the server has a listener that waits for gaming data files to be uploaded once they are completed. The gaming platform has client software written into it, allowing users to select the option of uploading data upon session completion. Once data is uploaded and categorized into appropriate user directories (stores all results for an individual separate from others), automatic data processing occurs on the server side, populating a MySQL database with the extracted feature values that have been described

in the previous experiments. The front end allows registered users to log in and generate reports and plots to examine patient performance from individual gaming sessions, similar to what has been presented in this chapter. Before finishing with the prototype CMS, additional work was done to provide automatic notifications with set thresholds for performance parameters. This is intended to automate monitoring for potential problems arising that can be found in the movement performance features. When out of control parameters are recognized from post-analysis, the CMS is able to send an email to a contact person indicating the problem. The basic functionality is in place, but to expand to full scale trials, production level refinement of the code and the process needs to be addressed.

The alternative means for post-session analysis is to use software tools on a local machine that I developed for feature extraction. Each of these tools provides a friendly GUI that presents users with options (e.g. movement onset, filtering frequencies, storage locations) when processing the resulting gaming data from a session. The ability to manage multiple data files, or batching has been added to each tool so that any number of files can be processed at once. The type of gaming session described in my work has been restricted to the episodic game play where users manipulate the paddle and destroy targets that appear in random locations. The alternative, mentioned briefly in Sec. 3.2 is the deterministic movement or sinusoidal mode of game play. This involves having a target move up and down or left and right on the game screen, having users follow the movement as closely as possible to emulate the periodic or pendulum motion. A complete analysis and feature set was built for this game mode as well. As an example, Fig. 93 demonstrates resulting output from the sinusoidal game mode. The features extracted from the movement trajectory that follows along with the reference signal include a number of variables, both amplitude and temporal based to closely examine individual performance. This mode of game play was intended for a clinical setting where user movement is being studied and not as much for the remote alternative. Although it can be used remotely, I would anticipate most people would quickly tire of the simple task of moving the paddle up and down on the screen.

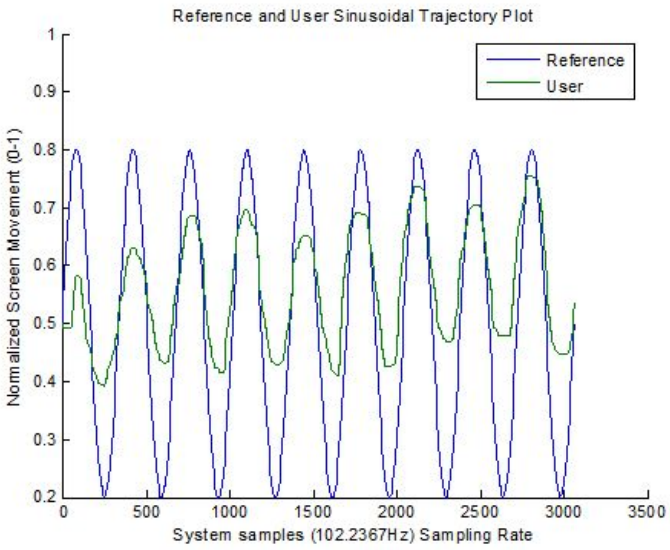

Figure 93: Resulting movement data from sinusoidal game mode

More details about the features that are extracted can be found in the appendices, along with the instruction documentation for each of the separate analysis tools that were built for post processing gaming session data. Output data from the GUI-based analysis tools are formatted for spreadsheets and can be imported and managed as needed.

Unfortunately the visual feature analysis methods were not in a state of readiness in time for the experimental work. The bulk of time was spent working through the problem with camera perspective error. The original decision to have one hand pose with both hands was intended to limit the amount of pictures required and make the experience as simple and quick as possible for the end user. However, the poor imaging results create more error in the data collected, implying that it is not the best approach. Since feature extraction is a higher priority element of the system, a compromise was necessary. The single hand pose images exhibited far less error and were considerably more manageable. This led to the consequence that without specialized camera equipment, a two-handed pose is unrealistic for the home-based telerehabilitation system. Within a clinical setting, it could be more realistic to consider multiple camera setups or wide-angle lenses where cost and the necessary training/knowledge for operation is less problematic. However, for home-

based or use in a private practice, inexpensive camera equipment will suffice if one hand is in the field of view per image. Moving forward, I think it makes most sense to eliminate the two-handed pose and re-purpose the code to process one hand at a time. Work is ongoing to solve this problem.

The other two hand poses provided encouraging results and have gone through testing and experimental work with several subjects. Preliminary results provided in Sec. 4 show promise for both the ROM and lateral view hand pose. These are both aspects of goniometry that provide useful information to accompany movement performance for an individual as it is able to provide an extra degree of insight into the current state of the hands and if there are any significant changes that could indicate problematic conditions. Goniometry has been commonly measured through the use of manual tools and visual estimation or more recently by making those same measurements on photographic imagery of the subject in various poses. Recent research in the area has been ongoing in developing smart tools to extract the same information. One study that focused on goniometry of the the knee is reported in [37]. Another example that is closer to what we are interested in is reported in [135] where joint angles and panning angle are discussed in the context of a Dupuytren's Contracture (affecting the hands). In addition there have been studies to validate using photographic evidence for goniometric measurements [8]. The area where my methods introduce novelty are that I have yet to come across a proposed full assessment of the hands, including joint placement, joint angles, size, redness and texture to provide a more complete picture of hand and joint health. There has been a large body of work done with biometrics of the hand relating to geometry, although typically the joints are not as well studied as fingerprints and creases in the palm (for hand scanners) [68, 133]. Often pegs are used to place and help separate the fingers, which could cause deformation through pressing on the skin surface, affecting joint information and angles [133]. Although what I set out to do is still in the developmental stages with hand imagery, a solid foundation has been built and lessons learned through working on both the one and two-handed poses with

regards to hand geometry and extracting features of interest to complement the movement performance profile. With continued efforts, this has great potential to help improve on reporting changes that can occur as a function of disease activity in RA patients.

Telerehabilitation and rehabilitation gaming have become quite popular recently. There have been a number of publications that refer to *Serious Games* for rehabilitation [45]. One aspect brought up in a discussion on taxonomy in [120] mentions key aspects in design of rehabilitation games, that of performance and progress monitoring. The main idea is to provide feedback from a game developed for rehabilitation specifically for the user and other stakeholders. This applies across all application areas, not just for our target demographic (RA patients). Furthermore, Luft hints at standardizing measurement outcomes in neurorehabilitation [82] as a means for comparison and advancing technology in the field. Through examining recent publications in telerehabilitation gaming [17,20,70,97,108,118, 132], it is easy to see that the performance metrics are quite variable, different platforms capture different elements of movement and process data by various means. Some aspects will relate to a specific demographic as it is impossible to have a generic group of features that will suit all problem areas. However, for movement performance, the group of features that we use are characteristic of the research behind precision, goal-directed aiming tasks, implying that they are not only useful for RA patients, the system can and has been used for other demographics as well. The raw data provided by our gaming platform from any given session (see Fig. 18) provides all the information needed for extracting the movement performance features. Using an approach like this to generate movement data from sessions is one possible avenue for dealing with the challenging problem of standardizing rehabilitation gaming output measures since presenting movement data in the same format as our platform would imply that the analysis tools will provide the same performance metrics.

In addition, there are a couple of other areas that our approach to telerehabilitation gaming differ from others. In the literature there are very few reports of telerehabilitation for rheumatoid arthritis patients. The work in [148] outlines an online system that pro-

vided an intervention through an Internet-based physical activity program. Their approach was more of providing information for an individualized exercise regimen to educate the users on maintaining activity levels, strength and conditioning. This was done through email communications with questionnaires used for feedback [148]. More recently, a novel approach with the Microsoft® Kinect was reported for RA patients with the intent of measuring gross-movement [87] and promoting ROM and cardiovascular health as part of the rehabilitation process for RA patients, although without mention of progress tracking or performance measures. Other alternatives are not as visible with regards to our target demographic and telerehabilitation, perhaps this might be in part related to rehabilitation being concerned with having a resolution or final outcome where the process ends or is no longer needed in the same capacity. Since RA is an autoimmune disease with no known cure, treatment programs are for life.

The other things to consider where the telerehabilitation gaming platform provides a novel aspect to a treatment plan is that it is able to support a wide range of therapeutic movements through varied input control devices. These are selected by the physiotherapist based on the object properties (size, shape, weight and grip/grasp type) to provide the necessary therapeutic movement for the individual. The in-game parameters allow for altering the sensitivity of the control device to provide whatever scaling is needed to suit the input control object, from large scale movement down to fine control, maintaining high-fidelity and thus providing the best possible in-game experience, regardless of degree of disability. This implies that the system can be used not only for rehabilitation but also for training fine movements such as a surgical training application. Also, a number of systems that employ telerehabilitation gaming have a suite of games or perhaps a single game (as in our case), but in order to expand to other titles, they need to either build a new module or develop new software. For our case, the measurement tool stays the same, but during a therapy session, individuals use the game for a short duration (at most 3 minutes), before they can move on to other games of their choice using the same input control device. This is intended to help

retain motivation especially for the case of long term treatment plans and promote use of the telerehabilitation gaming platform as a measurement tool. Lastly, the element of cost can be prohibitive when it comes to telerehabilitation systems. Healthcare insurance only covers certain amounts and not everyone may have access to expensive customized equipment for the home. Our main requirements are a computer at home, a camera that will capture still imagery at a reasonable resolution (preferably 1MP or greater) and a wireless device such as the Gyration Air Mouse to instrument input control objects. The cost of these elements is relatively inexpensive considering most individuals will have a camera and computer at home already and the air mouse is less than $100. A number of designs in the literature provide similar function but using more expensive technology that could potentially be prohibitive for the end user, some examples include setting up a virtual reality environment with data gloves [13, 15, 47, 57] or robotic assisted technology [72, 134]. There are other low cost solutions but typically they sacrifice other elements such as the input control device, using either pre-fabricated controllers or customized versions with only one intended use [20, 67]. Another alternative is publicly available gaming consoles, which is where the term $Wii - habilitation$ comes from. There are a number of studies that have cited use of the Wii and Microsoft® Kinect as rehabilitation tools [70, 74, 140]. Unfortunately they are not suitable for fine, precision controlled movements such as that of finger-hand function which is why we avoided that route and chose a custom telerehabilitation gaming platform design.

6 Conclusions and Recommendations

This thesis outlines the design and development of a telerehabilitation gaming platform intended for RA patients. There were several goals targeted during system development. The first directive was development of a set of digital features to profile or report on finger-hand function. Next was building a gaming platform to suit the needs of a rehabilitation program

for our target demographic, early-onset RA patients. The third directive was development of a collection of movement performance metrics to report on precision goal-directed aiming tasks. The fourth directive was to build a means to automatically process outcome measures from resulting data and provide them in a convenient format for post-analysis. The final directive was to expand the database of features into the visual domain to establish reporting on the condition of RA patients from still imagery of the hands. These elements have all been carefully described in the sections on architecture, verification and experimental work. The three main components in this body of work are the rehabilitation gaming platform, development and processing of outcome measures for movement performance metrics, and feature extraction from selected hand poses of still imagery.

6.1 Conclusions

Designing and building a telerehabilitation gaming system for a target demographic is a large undertaking that requires knowledge in a number of key areas to make a meaningful contribution. These include, researching the target demographic to understand the disease and how it progresses. Coming up with a means to implement that knowledge into a contained system that supports a physical rehabilitation program which is part of the treatment process for RA patients to help maintain strength and range of motion in their joints. Then to provide the ability to report on key performance parameters and other supporting measures that describe a patient session in detail. The ability to monitor session parameters over time for comparison is of great importance as one aspect of RA is that the symptoms tend to fluctuate and may be either active or appear in remission depending on the individual [76].

My contributions to the project start with the rehabilitation gaming platform. Development of the gaming platform expanded from insights and experimental work taken on by collaborating physiotherapists from the College of Rehabilitation Sciences. The development cycle progressed through many stages and revisions that included additional elements

such as an additional game mode with learning methods. Both classical and reinforcement learning algorithms were experimented with to adaptively adjust game settings during a session to optimize the challenge of playing the game. Additionally, a force-feedback tele-operated mode was added, where remote administrators could monitor game play in real time and send force feedback signals to indicate specific events during game play. This provides the ability to send a stimulus to the user to make them aware of a specific situation that may occur during the game. I also created a sinusoidal game mode where there is only one indestructible target that users are asked to follow with the paddle as close as possible for predictive movement analysis of pendulum motion. In addition, the basic game was refined by adding a range of various adjustment parameters for the paddle, targets, score-board, and various other in-game settings. These were all part of the refinement process in establishing a game that is intended to support 1 or 2-dimensional planar movements tai-lored to specific input control objects that are instrumented as control devices. The result provides a platform for monitoring and measuring progress of therapeutic movements that are part of a rehabilitation program.

To report on what transpired during a game session, sequential output of all on-screen movement is captured, providing a rich data source that is able to detail movement perfor-mance with a variety of metrics. I was involved in researching and developing movement analysis techniques for the telerehabilitation gaming system. This required becoming fa-miliar with precision, goal-directed aiming tasks and how they are studied and reported. Followed by design and development of software tools to implement a select group of movement performance features that are able to provide a comprehensive picture of what occurred during a gaming session. This included looking at accuracy, temporal, efficiency and performance measures. Additionally, part of the process for tailoring the system to our target demographic involved the inclusion of pain and stiffness pop-up windows. These provide self-reported conditions on two common symptoms that are often reported by RA patients as a function of disease activity. Originally efforts were directed into learning about

clinical instruments or questionnaires as they are commonly used to report on disease activity, however to avoid frequent lengthy surveys that could affect long term adoption rates, this aspect was limited to two direct questions about the current degree of pain and stiffness an individual is experiencing.

To complement movement performance metrics, efforts were then directed into addressing visual symptoms of RA patients. This required revisiting prior research on the target demographic and establishing key symptoms that have elements that could be detected from still imagery. This also required becoming familiar with the study of goniometry, measuring joint angles with the intention of looking for the potential onset of problems leading to deformities that can result from damage to joints. Varied hand poses were included to provide specific views relating to problematic conditions that can occur in RA patients. A top view with both hands was included to examine joint condition and joint angles at the DIP, PIP and MCP joints paying particular attention for signs of inflammation and early warning of changes in joint angles that can indicate the presence of joint damage. This view is intended to monitor ulnar deviation occurring at the MCP joints [76]. The second hand pose from the lateral view was included to examine the DIP and PIP joint angles of the index finger. This is due to a potential complication of RA where tendons become slack and joint damage occurs, which can lead to the eventual fusion in an abnormal flexed or extended position [76]. A final view was added to monitor range of motion for the dominant hand as one of the key symptoms of inflammation is loss of function [127].

The telerehabilitation gaming platform and movement performance metrics have been tested successfully with both RA patients and normative subjects. This demonstrated the ability and utility of the system design to ably perform the duty of reporting on precision goal-directed aiming tasks and provide a verbose account of user performance after a session and also between multiple sessions. Unfortunately the visual elements were not ready in time for the experiments and were limited to verification trials. Verification confirms that including a single hand in each pose is the optimal approach. Thus reducing additional

error from camera perspective, shading and simplifying the hand poses.

To complete the telerehabilitation system, a content management system (CMS) was built in a prototype format. This demonstrated the concept of central data storage for results from various clients using the telerehabilitation gaming platform. All post-processing to extract movement performance features can be done on the server and stored in a database for querying and automatic notifications providing updates on performance or potential problems as they occur, to both patient and care provider. In a sense, I see this as a first step in the automation of repeating therapy sessions where prescribed movements are performed on a regular basis at home by the patient. Instead of a home session completed in an unmonitored fashion, the telerehabilitation system is able to track progress and provide updates to patients and care-givers. Although the system design is intentional, my initial ideas were of a ubiquitous nature where the patient may not necessarily be aware that they are taking part in something that is being monitored (other than being told that they are) and that they will receive notifications when out of the ordinary conditions arrive in a preventative maintenance approach as opposed to reactive. This was intended to support the idea of building an environment that takes care of its inhabitants.

6.2 Recommendations and future work

The telerehabilitation gaming platform is a project that is never really complete as there are always aspects that can be improved upon or added to provide greater functionality. An important area of research in telerehabilitation is the discovery of digital features for monitoring progress/performance of patients. There are a number of features that are universal in movement analysis but once you go beyond and look at features specific to a target demographic then they become more unique. One of the early indicators in disease activity for RA is warmth, and that is why I decided to include the joint features (redness, swelling and texture). These features are useful for cases that readily exhibit external signs of inflammation, however, this will not always be the case as some individuals don't present

with much outward signs from a visual perspective. A current topic of interest in arthritis research is investigating thermal or heat signature of the joints [43]. From experience using a thermal camera, this has potential to be advantageous and provide early warning at the first sign of disease activity instead of once inflammation is presenting with the aforementioned symptoms. The reason that we did not start with thermal imaging is the cost associated with the technology. The least expensive cameras with the poorest resolution at the time were in the order of 1000s of dollars, making them unsuitable for anything but a clinical setting with a larger budget. As our planned utility is intended also for a day-to-day basis in a home setting, the associated costs would not be appropriate for the application. More recently there have been developments to bring a thermal imaging camera to market that is inexpensive in the form of an attachment for a smartphone or tablet. Their specifications provide enough resolution (-66°C - 90°C) that this could be a viable means to report on joint condition at a more reasonable estimated cost of $325 [101].

Another possible avenue to extend the research of the telerehabilitation gaming platform relates to the outcome measures. Development of a $listener$ module that runs in the background of an operating system during a telerehabilitation gaming session could potentially extend the functionality to any platform providing useful information without requiring use of our game exclusively. This is a complex problem as it would require operating as an overlay, waiting for indications of event starts, then tracking cursor position and listening for event ending conditions. The reporting would likely not be as verbose as the built in alternative that has been discussed in my work although it could be a potential avenue to provide greater amounts of data and extend the selection of games without requiring writing unique applications (a time consuming process). The potential limiting factor would be that each game would need to be modified to present starting and ending event information to the listener. As most games are proprietary and not open source, this would require cooperation and support from game developers for this task.

The next steps moving forward for my work include revisiting the first hand pose to

address one hand in the field of view at a time. The complexity of examining both hands presented many problems with lighting, cameras, hand position and a host of other variables to consider. Eliminating one hand from the field of view will limit the potential problems at the cost of an additional image required per session. Once the investigation of a single hand pose from the top view is complete, I plan to revisit the nearness measure for selecting the joint area to look for signs of similar patterns in other areas of the hand. My reasoning for this is that I believe it is possible to use these measures to discover similarities in areas that are more challenging to locate geometrically such as in-and-around the MCP joints and the wrist which are both commonly affected areas in early onset RA patients [76]. Using the nearness measure allows us to be selective and choose areas that adhere only to features of interest that represent similarities with current (or worse) conditions in the hand through parameter adjustment (the ϵ and r values). Finally, additional verification and experimental work to stress test the system and examine the response to as many input conditions as possible is essential. This technique was used for each of the different stages of development for the telerehabilitation gaming platform, the performance measures and reporting system and has provided a more robust design that is well suited for telerehabilitation in support of a physical therapy program for RA patients.

A Appendix A - Terminology

6-DOF - 6 Degrees of Freedom: The ability to move/track in linear X, Y, Z and angular X,Y,Z axes

ACPA - Anti-Citrullinated Protein Antibody: An autoantibody commonly found in rheumatoid arthritis patients' serologic test

AHFT - Arthritis Hand Function Test: Clinical instrument to report on hand condition of arthritis patient

ATA - American Telemedicine Association: A governing body responsible for developing guidelines and policies for telemedicine

CMS - Content Management System: A virtual location to store data with a web-based front end and support for database storage

CRP - C-Reactive Protein Test: Blood test that looks for protein content in the blood, a sign of inflammation

DASH - Disability of the Arm, Hand and Shoulder Questionnaire: A common instrument to report on upper limb disability

DAS - Disease Activity Score: A clinical instrument developed in the Netherlands to comment on disease activity

DIP - Distal Interphalangeal Joint: The joint at the end of the fingers/thumb between the distal and intermediate phalanx

DMARD - Disease Modifying Anti Rheumatic Drug: Often one of the first drug choices in treating RA

ESR - Erithrocyte Sedimentation Rate: Inflammation marker, how quickly red blood cells fall to the bottom of a test tube

GAT - Grip Ability Test: A set of clinical tests to report on grip

GLCM - Gray Level Co-Occurrence Matrix: Matrix containing probabilities of pixel proximity occurrence in an image

GUI - Graphical User Interface: User friendly interface to access underlying code

HAQ - Hand Assessment Questionnaire: A clinical instrument tailored to RA patients for hand function

JHFT - Jebsen Hand Function Test: A set of clinical tests to report on hand function

MAT - Medial Axis Transformation: A computer vision algorithm that establishes the skeleton of a structure

MCP - Metacarpophalangeal Joint: The joint at the base of the palm between the proximal phalanx and the metacarpal bone

MHQ - Michigan Hand outcomes Questionnaire: A clinical instrument to report on hand condition

NSAID - Non-Steroidal Anti-Inflammatory Drug: A drug to reduce inflammation without using steroids

PIP - Proximal Interphalangeal Joint: The joint in the middle of the finger between the intermediate and proximal phalanx

RA - Rheumatoid Arthritis: A chronic, systemic, autoimmune inflammatory disease

RF - Rheumatoid Factor: A serologic test looking for autoantibodies in the blood

ROM - Range of Motion: the angular distance of separation between the fingers and a mid-line

TNF - Tumor Necrosis Factors: Refers to a group of cytokines in the body that can cause cell death [46]

A Appendix B - Telerehabilitation Gaming Data Analysis Manuals

Game Data Analysis GUI – Overview

Introduction: This GUI allows processing of resulting data files from gaming sessions using the paddle based gaming software. The output presents six files for every one input file. They consist of a stats file, movement trajectory files broken up into four separate distinct movements (right/up, left/down, for both large and medium moves) and a separate file that contains all movements in one column.

The output files are named according to the input filename but with a new added extension based on content. For example, with an input filename of ra1t1.txt, the output files will be as follows:

Stats file: ra1t1stats.txt

Left large movements file: ra1t1lfmov.txt

Left medium movements file: ra1t1lmmov.txt

Right large movements file: ra1t1rfmov.txt

Right medium movements file: ra1t1rmmov.txt

Total gaming movement file: ra1t1totl.txt

The GUI has been constructed to provide a small degree of customization in processing the data files (see Fig. 1 for a screen capture).

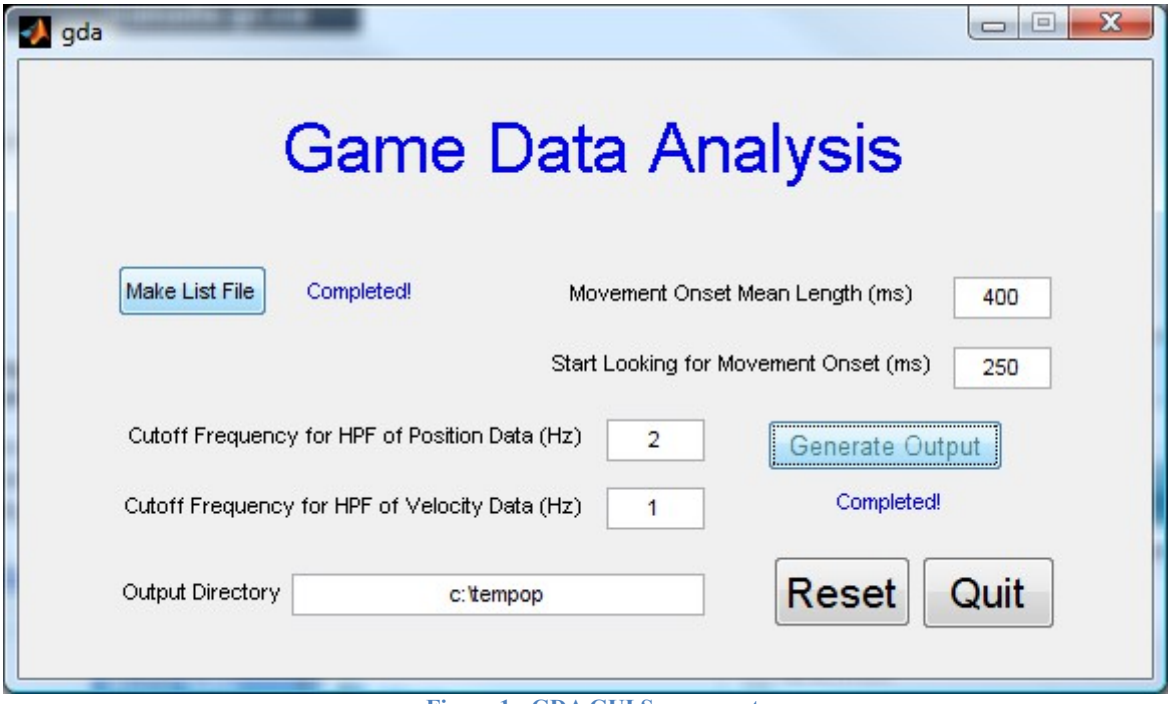

Figure 1 : GDA GUI Screen capture

How to use the GUI: There are eight additional files that must be included along with the 'gda.m' and 'gda.fig' files. They consist of the normative, average movement trajectories for both the horizontal and vertical directions. The files are as follows:

Havglf.txt – horizontal orientation, average movement trajectory for left large movements.

Havglm.txt – horizontal orientation, average movement trajectory for left medium movements.

Havgrf.txt – horizontal orientation, average movement trajectory for right large movements.

Havgrm.txt – horizontal orientation, average movement trajectory for right medium movements.

Vavglf.txt – vertical orientation, average movement trajectory for left large movements.

Vavglm.txt – vertical orientation, average movement trajectory for left medium movements.

Vavgrf.txt – vertical orientation, average movement trajectory for right full movements.

Vavgrm.txt – vertical orientation, average movement trajectory for right medium movements.

Each of these files must be in the same directory as the 'gda.m' and 'gda.fig' files before you start processing data. The input and output directories where the existing and processed data will reside can be specified in the GUI.

Step 1: Set the 'Current Directory' to the location where the GUI and average movement trajectory files are located. Enter *gda* at the command line prompt in MATLAB. The resulting view of the gda GUI should appear like Fig. 1 (above).

Step 2: Next, click on the 'Make List File' button to bring up another pop-up window that allows you to enter the location of the data files you would like to process. You can enter the location (i.e. *C:\data_location\test_files\)* and then click on 'Ok' to submit the location of your input files. A list file will be generated and if it is successful, a blue message that says, 'Completed!' will appear next to the button indicating that a list file has been made that contains all of the data files you want to process.

Step 3: Next, you must fill in the edit boxes with the values for five parameters.

3a: Movement Onset Mean Length (must be specified in milliseconds). This is the amount of signal to average when looking at developing a baseline for determining the official movement onset.

3b: Start Looking for Movement Onset (also specified in milliseconds). This is the amount of time to skip at the beginning of the signal before looking for a legitimate trigger indicating the start or reaction time for user movement (avoids false triggering via noise).

3c: Cutoff Frequency for HPF of Position Data (specified in Hertz). This is the filter cutoff

frequency for filtering the position data in preparation for taking the derivative to get the velocity.

3d: Cutoff Frequency for HPF of Velocity Data (specified in Hertz). This is the filter cutoff frequency for filtering the velocity data in preparation for taking the derivative to get the acceleration information.

3e: Output Directory. This edit box requires you to specify a separate output directory where to store the processed information.

Step 4: Once all of the edit boxes contain the appropriate values, the next step is to generate output. Click on the 'Generate Output' button. There will be a progress bar in the main MATLAB command window that will scroll from 0-100% for each of the individual files. Once all of the files are processed, a blue, 'Completed!' message will appear under the Generate Output button. At this point there will be six output files (as discussed earlier) for every input file, located in the output directory that was specified in step 3e.

Step 5: Upon completion, you have the choice of either using the Reset button to process another directory of input data or click on the Quit button to close the GUI and finish your session.

Analysis GUI Output Legend

The column headers found in the output file from the Analysis GUI for processing gaming data files are briefly described in this document. Each of the headers is listed along with a semi-verbose description of what the numerical quantity relates to.

Filename – This column contains the filename corresponding to the data contained in the corresponding row.
ARTLF – This column contains the Average Response Time for Left Full-Screen movements.
ARTL23 – This column contains the Average Response Time for Left 2/3-Screen movements.
ARTL13 – This column contains the Average Response Time for Left 1/3-Screen movements.
ARTRF – This column contains the Average Response Time for Right Full-Screen movements.
ARTR23 – This column contains the Average Response Time for Right 2/3-Screen movements.
ARTR13 – This column contains the Average Response Time for Right 1/3-Screen movements.
Score – This column contains the total score for the corresponding game, this value is derived from the total # of misses subtracted from the total # of hits.
ABSLF – This column contains the Absolute Average Value of the Error contained within all Left Full-Screen movements (includes both Overshoot and Undershoot).
ABSL23 – This column contains the Absolute Average Value of the Error contained within all Left 2/3-Screen movements (includes both Overshoot and Undershoot).
ABSL13 – This column contains the Absolute Average Value of the Error contained within all Left 1/3-Screen movements (includes both Overshoot and Undershoot).
ABSRF – This column contains the Absolute Average Value of the Error contained within all Right Full-Screen movements (includes both Overshoot and Undershoot).
ABSR23 – This column contains the Absolute Average Value of the Error contained within all Right 2/3-Screen movements (includes both Overshoot and Undershoot).
ABSR13 – This column contains the Absolute Average Value of the Error contained within all Right 1/3-Screen movements (includes both Overshoot and Undershoot).
AVGMissLF – This column contains the Average amount by which the user missed for all Left Full-Screen movements. (note: values are both positive and negative)
AVGMissL23 – This column contains the Average amount by which the user missed for all Left 2/3-Screen movements. (note: values are both positive and negative)
AVGMissL13 – This column contains the Average amount by which the user missed for all Left 1/3-Screen movements. (note: values are both positive and negative)
AVGMissRF – This column contains the Average amount by which the user missed for all Right Full-Screen movements. (note: values are both positive and negative)
AVGMissR23 – This column contains the Average amount by which the user missed for all Right 2/3-Screen movements. (note: values are both positive and negative)
AVGMissR13 – This column contains the Average amount by which the user missed for all Right 1/3-Screen movements. (note: values are both positive and negative)
LFOver – This column contains the Average Error for all Left Full-Screen Overshoot movements.
LFUnder – This column contains the Average Error for all Left Full-Screen Undershoot movements.
L23Over – This column contains the Average Error for all Left 2/3-Screen Overshoot

movements.
L23Under – This column contains the Average Error for all Left 2/3-Screen Undershoot movements.
L13Over – This column contains the Average Error for all Left 1/3-Screen Overshoot movements.
L13Under – This column contains the Average Error for all Left 1/3-Screen Undershoot movements.
RFOver – This column contains the Average Error for all Right Full-Screen Overshoot movements.
RFUnder – This column contains the Average Error for all Right Full-Screen Undershoot movements.
R23Over – This column contains the Average Error for all Right 2/3-Screen Overshoot movements.
R23Under – This column contains the Average Error for all Right 2/3-Screen Undershoot movements.
R13Over – This column contains the Average Error for all Right 1/3-Screen Overshoot movements.
R13Under – This column contains the Average Error for all Right 1/3-Screen Undershoot movements.
TOver – This column contains the Total Average Error for all movement categories for Overshoot movements.
TUnder – This column contains the Total Average Error for all movement categories for Undershoot movements.
PHits – This column contains the number of times the paddle was hit by distractors during game-play.
AResLF – This column contains the Average Residual Error for Left Full-Screen movements.
AResL23 – This column contains the Average Residual Error for Left 2/3-Screen movements.
AResL13 – This column contains the Average Residual Error for Left 1/3-Screen movements.
AResRF – This column contains the Average Residual Error for Right Full-Screen movements.
AResR23 – This column contains the Average Residual Error for Right 2/3-Screen movements.
AResR13 – This column contains the Average Residual Error for Right 1/3-Screen movements.
TRes – This column contains the Total Average Residual Error for all movements.
TRMSRes – This column contains the Total Average Residual RMS error for all movements.
LFRiseT – This column contains the Average 90% Rise Time for all Left Full-Screen movements (in mS).
LFRiseP – This column contains the Average 90% Rise Time for all Left Full-Screen movements (in percentage).
L23RiseT – This column contains the Average 90% Rise Time for all Left 2/3-Screen movements (in mS).
L23RiseP – This column contains the Average 90% Rise Time for all Left 2/3-Screen movements (in percentage).
L13RiseT – This column contains the Average 90% Rise Time for all Left 1/3-Screen movements (in mS).
L13RiseP – This column contains the Average 90% Rise Time for all Left 1/3-Screen movements (in percentage).
RFRiseT – This column contains the Average 90% Rise Time for all Right Full-Screen

movements (in mS).
RFRiseP – This column contains the Average 90% Rise Time for all Right Full-Screen movements (in percentage).
R23RiseT – This column contains the Average 90% Rise Time for all Right 2/3-Screen movements (in mS).
R23RiseP – This column contains the Average 90% Rise Time for all Right 2/3-Screen movements (in percentage).
R13RiseT – This column contains the Average 90% Rise Time for all Right 1/3-Screen movements (in mS).
R13RiseP – This column contains the Average 90% Rise Time for all Right 1/3-Screen movements (in percentage).

SAnalysis GUI Documentation

How to operate:

1). Open MATLAB
2). Switch to working directory containing SAnalysis.m and SAnalysis.fig files
3). Type 'SAnalysis' on the MATLAB command line
4). You will see the following:

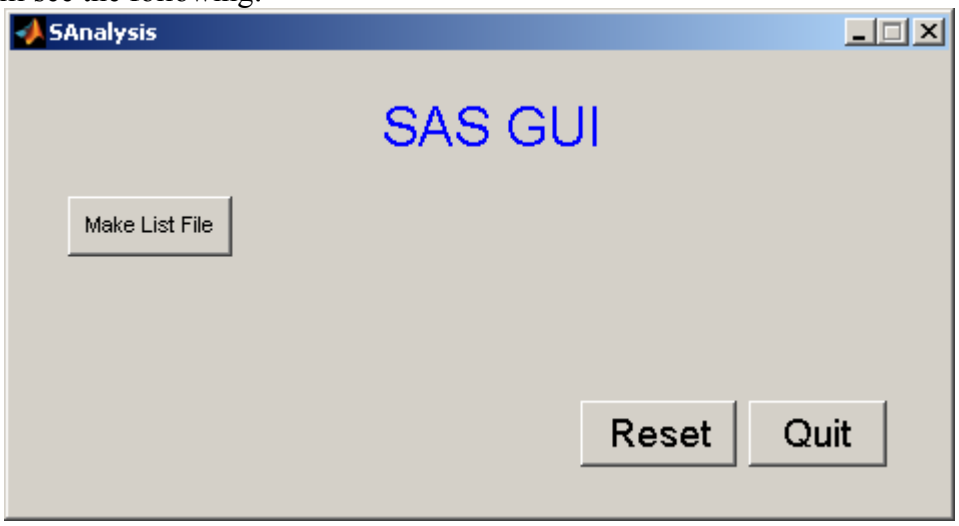

Fig. 1: SAS GUI on startup

5). Click 'Make List File' button, which will bring up another window, asking you for the directory that contains all of the data files that you would like to process (see below).

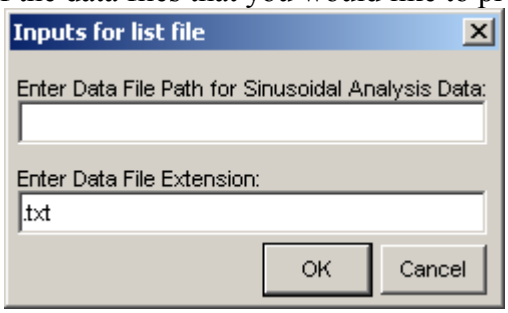

Fig. 2: File directory input window

6). Enter the data file path in the top edit box, for example, 'C:\documents and settings\user\desktop\sas_data\'. Then click the OK button. At this point a green completed! will appear along with a filtering cutoff frequency input and an output filename edit box, and the generate output button to process all of the files in the directory you selected (see image below).

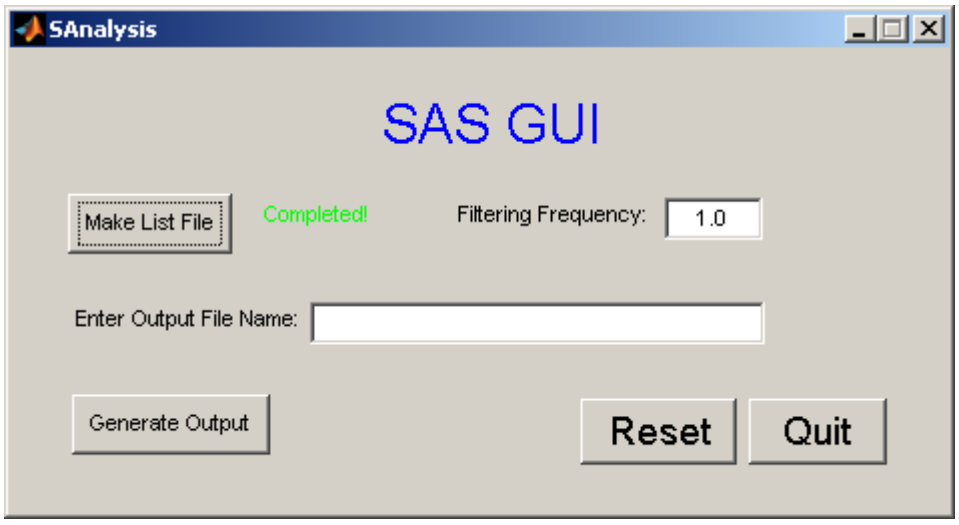

Fig. 3: SAS GUI after list file has been made

7). At this point, the default filtering cutoff frequency is displayed (1.0Hz). This frequency worked with most data but it can be changed as needed (when choosing a frequency you can test some of the data files being processed first with the original sas.m MATLAB script as it allows you to see how a single file responds to varied filter frequencies) to any decimal value above or below one but it must be greater than zero. Before clicking on 'Generate Output', please enter an output filename (i.e. 'C:\documents and settings\user\desktop\outputfile1.txt'). Once you have entered an output filename, click Generate Output and each input file will be processed individually and then added to a single output file with the name you specified. After all files have been processed another green completed! will appear next to the generate output button indicating that processing is finished and you can now examine the output data.

8). In the event that you want to restart and process some more data, click the RESET button, otherwise you can click QUIT to close the GUI.

9). The last step is to examine the output data, which is comma delimited. The files are included row by row with each one corresponding to an input file. The columns are all coded based on the data they contain. The legend below describes what each column heading stands for:

Filename – as the heading implies, this is the input data filename
MResE – This is the mean residual error of the user – reference signal (after peak 2)
RMSResE – This is the RMS residual error of user-reference signal (after peak 2)
APE(T) – This is the average peak error (temporal), in milliseconds
SDPE(T) – This is the standard deviation of the peak error (temporal) in mS
RMSPE(T) – This is the peak RMS error (temporal), in milliseconds
ATR(T) – This is the average trough error (temporal), in milliseconds
SDTE(T) – This is the standard deviation of the trough error (temporal) in mS
RMSTE(T) – This is the trough RMS error (temporal), in milliseconds
APtTE(A) – This is the average Peak-to-Trough error (amplitude)
SDPtTE(A) – This is the standard deviation of the Peak-to-Trough error (amplitude)
RMSPtTE(A) – This is the RMS Peak-to-Trough error (amplitude)
ATtPE(A) – This is the average Trough-to-Peak error (amplitude)
SDTtPE(A) – This is the standard deviation of the Trough-to-Peak error (amplitude)
RMSTtPE(A) – This is the RMS Trough-to-Peak error (amplitude)

PE(T)X – These correspond to the peak error (temporal) for peak X
TE(T)X – These correspond to the trough error (temporal) for trough X
PtTE(A)CX – These correspond to the peak-to-trough error (amplitude) for cycle X
TtPE(A)CX – These correspond to the trough-to-peak error (amplitude) for cycle X
RefPk(A)X – These are the reference signal peak amplitudes (for peak X)
UsrPk(A)X – These are the user signal peak amplitudes (for peak X)
RefTf(A)X – These are the reference signal trough amplitudes (for trough X)
UsrTf(A)X – These are the user signal trough amplitudes (for trough X)

1D/2D Event Processing GUI

To use the GUI, enter 'tdgui' at the command prompt when the files 'tdgui.m' and 'tdgui.fig' are located in the current working directory. You will be presented with the following interface (see Figure 1).

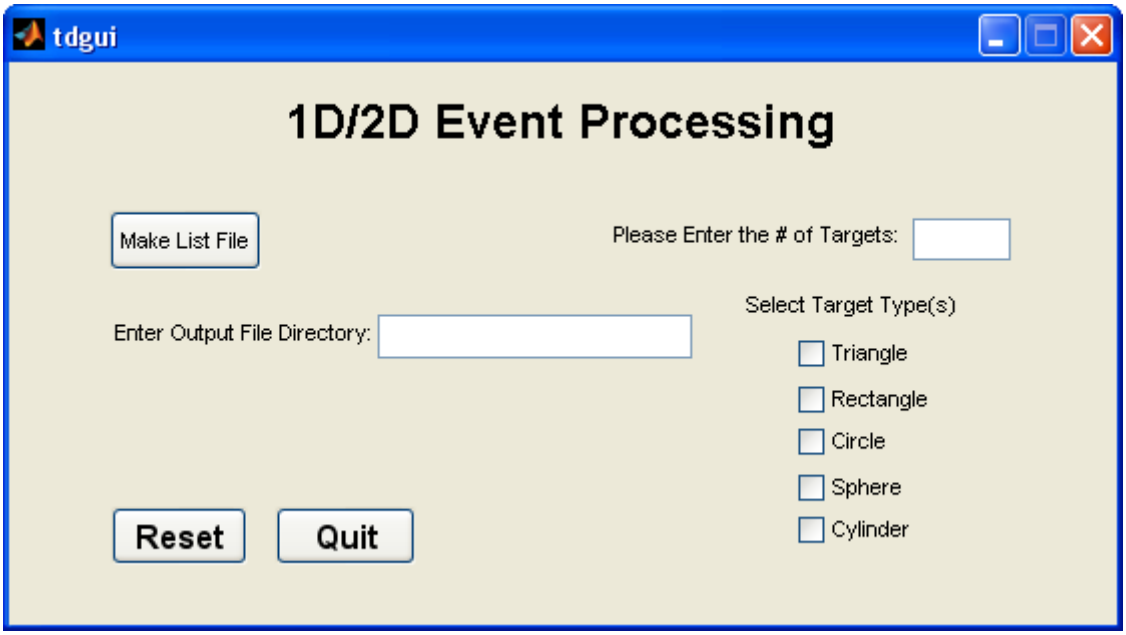

Figure 1: tdgui starting configuration

The first step in using this GUI is to generate a list file by clicking on the 'Make List File' button. This will bring up a smaller window for you to enter the location of the directory containing the gaming output files to be processed. The directory window can be seen in Figure 2.

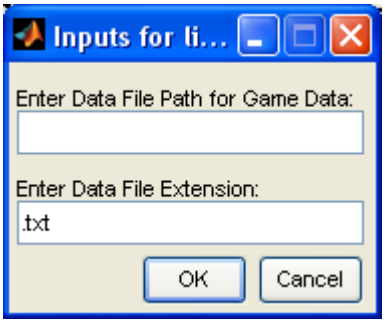

Figure 2: Window to enter data file path

Once completed, a 'Completed!' notification will appear next to the button. At this point, the 'Generate Output' button will also appear but is not used until the remaining information is entered first.

Next, please enter the number of targets (at present it can be anywhere from 1 to 5). Enter an integer value into the text box. Select which targets to include from the list of five presented

below the text box. The number of selected targets **MUST** coincide with the number of targets provided in the text box (only check those that apply!).

The last step before clicking on the 'Generate Output' button is to enter the location where you want the output files to be stored. Please enter a complete path (for example: c:\data\monday\session1\). Note that the final '\' must be included (see Figure 3).

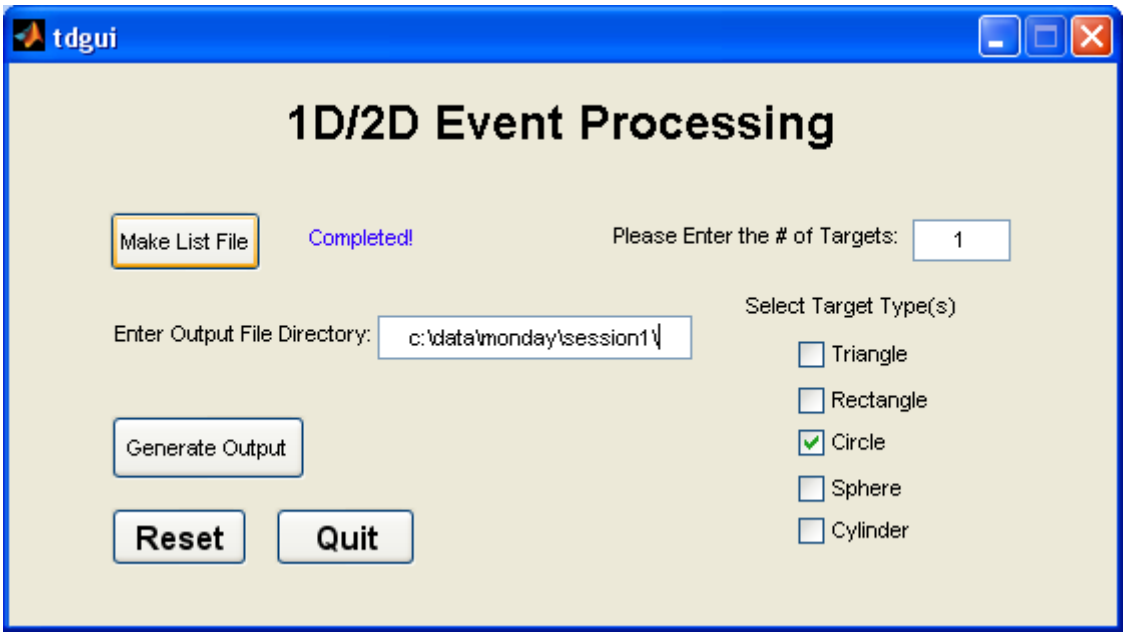

Figure 3: Ready to enter output directory and process files

Once these steps have been completed, all that remains is to click on the 'Generate Output' button and the process bars will appear in the MATLAB window until each file from the directory that you provided is processed at which point a blue 'Completed!' will appear next to the Generate Output button. The output files will be stored in the output directory that you specified and each of the filenames will be a modified version of the original data. The output filenames will take on the following form:

Input file: xxxxxxxx.txt
Output file: xxxxxxxxdata.txt

When you are finished, you can either 'Reset' the GUI by clicking on the Reset button and starting again, processing another set of data files or you can click on 'Quit' to close it.

MATLAB Data Analysis Tool, Quickstart Guide_v1

The data analysis GUI written in MATLAB requires the following files to operate properly:

gui_v1.fig
gui_v1.m
af4.m
chname.m
getsfreq.m
interpol.m
lpfip.m
mav.m
miv.m
smo.m

These files must all be places in the working directory for the GUI to operate properly.

Starting the GUI

To start the GUI, assuming that you are currently in the *working directory* containing the files mentioned above, type the command:

```
run gui_v1
```

This will start the user interface which will appear as shown in Fig. 1.

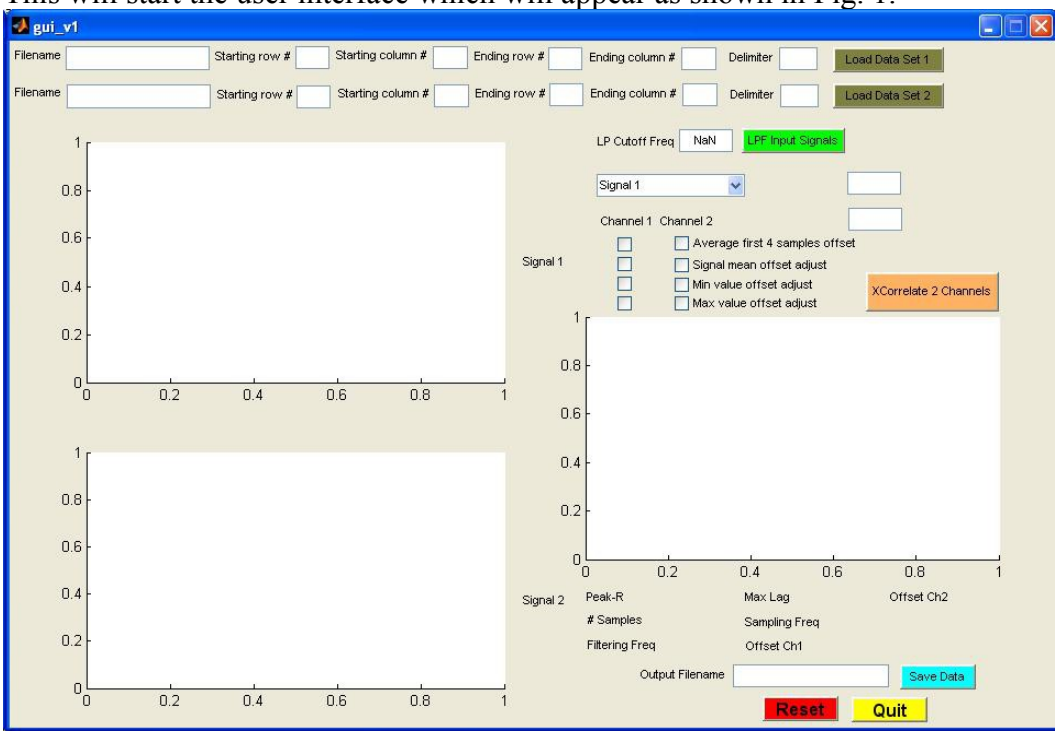

Figure 1: GUI Analysis Tool Starting Screen

Loading miniBIRD or FSA Data Files

With the GUI already loaded, the first step in processing data files is to load them into the interface. The text boxes at the top of the GUI allow for manual entering of the files in question.

Step 1: Enter a filename, which can be specified either as located in the working directory by just typing the filename, or you can specify the exact location by providing the drive letter and the directory location (e.g. c:\data\fsa\dl\dllip3.txt).

Step 2: Specify the starting row for data in the file you have selected. For example, miniBIRD files contain raw data and start at row 0. However, FSA files contain headers so they begin at row 1.

Step 3: Specify the starting column for data in the file you have selected. For example, miniBIRD files contain raw data and start at col 0. However, FSA files contain date and time stamps so the data begins at row 4.

Step 4: [Optional] Specify the ending row for data in the file you have selected. For example, if you are interested only in the middle part of a signal for analysis, after discovering how much of the signal you want to keep, specify the corresponding row in the 'Ending row #' edit box. This can be repeated in the GUI until you have the desired output.

Step 5: [Optional] Specify the ending column for data in the file you have selected. This allows you to choose the ending column to stop reading data. This was initially provided with the intent of allowing users to eliminate some data however after experimenting with the GUI, the value for the ending column must always be the number of columns provided in the data file in question (for a miniBIRD file, 11 and for an FSA file, 13).

Note: Step 4 and 5 are optional but if you plan to use an ending row you must also specify an ending column at present.

Step 6: Specify the delimiter for the data you are loading. For example, if you have a comma delimited file, enter a comma in the delimiter edit box; this works for any common character (e.g. , ; / ' " :). The one exception that is currently supported in this version of the GUI is tab-delimited data, enter `\t` in the delimiter edit box in that case.

Step 7: At this point, you are ready to load the data by pressing the corresponding 'Load Data Set' button (either one or two). Once pressed, the data will automatically be displayed in the appropriate axes below, referred to as signal 1 or signal 2 (see to the right of the two plots). When the data is displayed, the channels are provided with distinct colours with a legend. In addition to that, below the signal title, a number will appear showing the sampling frequency of the data.

Note: Repeat steps 1-7 for data set 2 to display a second signal (miniBIRD or FSA data)

Filtering the Input Data

Support has been provided to filter the input data using a low pass filter with a user specified cutoff frequency. A forward and reverse filtering technique is used to eliminate phase shift (the signal is run through the filter forwards and then the sequence is reversed and run through the filter again). A Butterworth filter design was used as it has the smoothest roll-off characteristics compared to the other types supported in MATLAB. The disadvantage is that it has a more gradual roll-off profile and as a result a 5^{th} order filter was designed to provide -100db/decade roloff-rate.

Step 1: To filter the data using the low pass filter, there is a restriction in the cutoff frequency that you can provide. The value must be less than half the sampling frequency. Enter the cutoff frequency in the edit box (LP Cutoff Frequency). Note that it is better to choose a higher cutoff frequency first and then revise it as necessary because the data is adjusted and cannot be returned without reloading the information.

Step 2: Once the cutoff frequency has been entered, pressing 'LPF Input Signals' will apply the 5^{th} order Butterworth low pass filter with the cutoff frequency you specified. The axes containing signal 1 and signal 2 are presently both linked to the filtering operation and will be updated accordingly in the axes display.

Step 3: In the event that the cutoff frequency chosen did not produce the desired result, repeat steps 1 and 2 until the filtered data appears as expected.

Selecting the Channels for Cross-Correlation

The next step is to choose which signal(s) you want to use for the cross-correlation procedure. There are three choices, either signal 1, signal 2 or both signal 1 and 2. Each of the signals contain channels displayed in the first two axes.

Step 1: Use the pop up menu to select one of the three options, 'Signal 1', 'Signal 2', or 'Signals 1 and 2'.

Step 2: Once you have selected the signal(s) for cross-correlation, the channel selection information will appear next to the two edit boxes where you enter which channel you want to use for comparison. For example, the values will be channels 3, 6-11 for miniBIRD files, corresponding to the reference channel and then the position channels (X, Y, and Z) and the rotation channels (X, Y, and Z). The FSA files will allow a choice of channels 8-10 corresponding to force sensors 1, 2, and 3.

Pre-Processing Channel Information and Cross-Correlation

The next step is to select which offset technique you would like to apply to the input channel (if any) before performing cross correlation of the two selected channels.

Step 1: Select any of the offset methods listed for channel 1 and/or channel 2. This is done by clicking the checkboxes for the techniques you wish to apply. Currently there are four possibilities, Average the first four samples, Signal mean, Minimum value and Maximum Value signal offset adjustments. Any, all or none of these methods can be selected (user defined).

Step 2: Once the desired offset methods have been selected (if any) the final step is to click the 'XCorrelate 2 Channels' button to perform the cross-correlation operation on the two signals.

Note: The two channels may not come from the same file which makes it very likely that the sampling frequency will not be the same. As a result, interpolation takes place to match the sampling frequencies. MATLAB provides support for several interpolation methods. The method currently in use is 'cubic spline' as it provides the smoothest interpolation but with the highest processing cost.

Step 3: At this point, the cross-correlation of the two channels will be displayed in the third set of axes. It is important to note that beneath the display there are facts about what is being displayed including the Peak R-value (from 0 – 1), the Max Lag (in samples), the total # Samples, the Sampling Frequency (in Hz), and finally the Filtering Frequency (if applicable) (in Hz). In the event that there was no LP filtering done on the input, the value is NaN (not a number).

Saving Data, Restarting or Ending the Program

Support has been provided to save the cross correlation information for further analysis or viewing. All files will be stored using a comma delimiter.

Step 1: Choose a filename to save your results in. You can specify the location anywhere on your computer or by just typing in the filename it will place it in the working directory.

Step 2: Once you have chosen your filename, click the 'Save Data' button to store a copy of your data. This stores a comma delimited file including all of the information provided below the cross-correlation window (Peak R-value, Max Lag, # Samples, Sampling Freq., Filtering Freq., Channel 1 and Channel 2 Offset) and the filename(s) that the data came from as well as the channel numbers (1 and 2). Note that if there were two separate signals, channel 1 always comes from signal 1 and channel 2 always comes from signal 2. In addition to the header, the first column contains all of the output cross-correlation data.

Step 3: Once you have saved your data (if applicable) and you are finished with the current information in the GUI, click the Reset (red) button to refresh the GUI and start the process again.

Step 4: When you have finished using the GUI Analysis Tool, press the Quit (yellow) button to close it.

A Appendix C - Example Output Data

The results in this section have been broken up into small tables for ease of viewing. There are 8 separate tables that all correspond to the data for the second experiment for the group of n = 4 RA patients.

Filename	% Success	# Distractor Hits	Response Time L U/R	Response Time M U/R
ra1t1.txt	80	0	0.650328	0.697769
ra1t2.txt	6.43E+01	0	0.631948	0.819989
ra1t3.txt	40	0	1.655447	1.103631
ra1t4.txt	4.67E+01	0	0.646104	0.760286
ra1t5.txt	6.56E+01	0	0.746517	0.569174
ra2t1.txt	8.48E+01	0	0.477389	0.520055
ra2t2.txt	8.15E+01	0	0.601349	0.718278
ra2t3.txt	40	0	0.771091	0.547586
ra2t4.txt	6.67E+01	0	0.835736	0.765534
ra2t5.txt	8.08E+01	0	0	0.57854
ra3t1.txt	6.43E+01	0	0.911707	0.771033
ra3t2.txt	7.39E+01	0	0.77793	0.726488
ra3t3.txt	75	0	0.794482	0.771009
ra3t4.txt	8.75E+01	0	0.782426	0.683283
ra3t5.txt	4.84E+01	0	0.911178	0.672685
ra4t1.txt	7.41E+01	0	0.575993	0.502382
ra4t2.txt	2.59E+01	0	1.050961	0.610082
ra4t3.txt	3.70E+01	0	0.478048	0.646198
ra4t4.txt	4.52E+01	0	0.577658	0.844587
ra4t5.txt	8.13E+01	0	0.738431	0.861148

Response Time L D/L	Response Time M D/L	Rise Time L U/R	Rise Time M U/R	Rise Time L D/L
0.697123	0.697769	0.643129	0.518158	0.562738
0.456562	0.819989	0.567918	0.479845	0.857445
0	1.103631	0.150495	0.256399	0
0.40103	0.760286	0.763071	0.576481	0.133677
0.566178	0.569174	0.587148	0.251635	1.044284
0.858822	0.520055	0.813948	0.536764	0.885556
0.701573	0.718278	0.751686	0.425196	0.250562
0	0.547586	0.575524	0.399515	0
0.651874	0.765534	0.384438	0.481384	0
0.969107	0.57854	0	0.428162	0.050126
0.765691	0.771033	0.398872	0.560913	1.068406
0.689743	0.726488	0.847219	0.667697	0.529118
0.40326	0.771009	0.598119	0.566972	0.589843
0.637731	0.683283	0.798503	0.75563	1.075389
0.954865	0.672685	0.705227	0.585757	0.405662
0.973902	0.502382	0.726253	0.57827	1.246594
0.450412	0.610082	0.846608	0.595783	1.151053
0.550311	0.646198	0.992227	0.497503	0.272376
0.890417	0.844587	0.560963	0.577462	0.406253
0.722559	0.861148	0.598095	0.496641	1.010748

Rise Time M D/L	Absolute Error L U/R	Absolute Error M U/R	Absolute Error L D/L
0.638329	0.083086	0.084738	0
0.699458	0.166997	0.0201	0.200443
0.334434	0.88606	0.017013	0
0.631622	0.083687	0.046615	0.16529
0.499914	0.093043	0.058639	0.070352
0.461415	0	0.036925	0.094488
0.485938	0	0.037485	0
0.656545	0.178417	0.200275	0
0.356581	0.068983	0.090166	0
0.595249	0	0.007596	0.04529
0.869294	0.143078	0.055972	0.02159
0.544866	0.284978	0.032816	0
0.590937	0.122618	0.015578	0.20009
0.608256	0.073784	0.081466	0
0.507219	0.124873	0.101829	0.18161
0.586196	0.440312	0.054436	0.258587
0.569271	0.580282	0.21718	0.24744
0.55587	0.285675	0.150567	0.28651
0.339472	0.269016	0.214249	0.05535
0.366152	0.020874	0.018691	0.251203

Absolute Error M D/L	Path Length L U/R	Path Length M U/R	Path Length L D/L
0.013263	0.008803	0.009304	0.009861
0.039723	0.012512	0.008197	0.006739
0.57636	0.003696	0.028568	0
0.110102	0.009847	0.005969	0.008907
0.004347	0.012676	0.00869	0.007976
0.068725	0.007356	0.006951	0.009172
0.011048	0.008044	0.008476	0.006402
0.091372	0.017456	0.009113	0
0.051447	0.025181	0.012095	0.009083
0.027508	0	0.005947	0.020252
0.123548	0.017835	0.008245	0.006734
0.022707	0.008729	0.004675	0.011091
0.077036	0.008901	0.006818	0.005144
0	0.012841	0.00794	0.008022
0.165737	0.012249	0.006286	0.010413
0.045238	0.006154	0.004781	0.017284
0.168412	0.013538	0.011389	0.010543
0.127	0.008359	0.006888	0.012034
0.076128	0.007617	0.010026	0.011645
0.03979	0.014441	0.009748	0.010608

Path Length M D/L	Residual Error L U/R	Residual Error M U/R	Residual Error L D/L
0.008194	0.133994	0.206143	0.175839
0.006157	0.182814	0.194668	0.222877
0.002568	0.559762	0.249074	0
0.008218	0.217474	0.200356	0.133208
0.006587	0.181043	0.192803	0.128385
0.00619	0.084659	0.133398	0.208119
0.007676	0.082518	0.163784	0.094352
0.011271	0.245107	0.291212	0
0.008043	0.204759	0.238461	0.097025
0.006612	0	0.169503	0.270378
0.008159	0.281766	0.191105	0.142066
0.00697	0.239227	0.244101	0.180491
0.008827	0.145965	0.159239	0.284337
0.006835	0.113657	0.156148	0.079717
0.006471	0.130132	0.206193	0.315143
0.005833	0.24311	0.19713	0.25685
0.009785	0.405479	0.254524	0.315753
0.009122	0.2556	0.224892	0.250312
0.005773	0.272905	0.278062	0.241936
0.008116	0.134044	0.214842	0.203844

Residual Error M D/L	RMS Residual Error L U/R	RMS Residual Error M U/R
0.173957	0.153625	0.234028
0.122596	0.234796	0.215675
0.336739	0.623898	0.2752
0.231596	0.258468	0.226756
0.130591	0.214438	0.221391
0.178758	0.099978	0.157741
0.142876	0.107879	0.187242
0.223384	0.318416	0.320953
0.17682	0.243175	0.278446
0.134533	0	0.188457
0.16344	0.345223	0.216155
0.188078	0.294158	0.272319
0.226707	0.170754	0.173536
0.100077	0.13139	0.189211
0.224742	0.14876	0.232558
0.148327	0.282574	0.218171
0.306024	0.467503	0.299009
0.182176	0.310066	0.253528
0.208921	0.317358	0.315115
0.179245	0.172213	0.237394

RMS Residual Error L D/L	RMS Residual Error M D/L	Overshoot	Undershoot	Hits	Misses
0.207336	0.191548	0.108719	0.17111	56	14
0.253043	0.144931	0.098345	0.22047	45	25
0	0.409471	0.14338	0.218115	4	6
0.156164	0.280887	0.1046	0.147535	21	24
0.152058	0.150621	0.16855	0.197001	47	25
0.237116	0.202964	0.022663	0.163369	56	10
0.12168	0.161382	0.139673	0.082591	55	12
0	0.256433	0.101476	0.246647	16	24
0.152512	0.206811	0.05697	0.10375	22	11
0.336971	0.156336	0.051343	0.061079	57	13
0.17742	0.193826	0.210941	0.250363	45	25
0.22118	0.206643	0.01826	0.215258	51	19
0.31182	0.258187	0.116359	0.181278	42	14
0.092541	0.119379	0.091545	0.232527	49	7
0.383575	0.261605	0.067632	0.214544	35	37
0.295903	0.16569	0.059607	0.229161	57	20
0.389764	0.344568	0.014418	0.226095	38	34
0.304834	0.227824	0.077168	0.332851	38	28
0.289782	0.231378	0.073104	0.207361	37	43
0.237575	0.21525	0.064321	0.107035	49	11

Score	PainBefore	PainAfter	Stiffness Before	Stiffness After	Object	Time
42	0.6	0.7	0.3	0.3	Wood Dowel	10:01AM
20	0.5	0.1	0.3	0.1	Wineglass	10:12AM
0	0.2	0.1	0	0	Spray Nozzle	10:31AM
0	1.2	0.1	1	0	Clothespeg	10:32AM
22	1.2	0	2	0	Wood Dowel	10:37AM
46	0.4	1.1	0.2	1	Wood Dowel	11:07AM
43	0.6	0	1.2	0	Wineglass	11:15AM
0	0.4	0.5	0.9	0.1	Spray Nozzle	11:23AM
11	0.3	0.3	1	1	Clothespeg	11:26AM
44	0.9	0.4	1	1	Wood Dowell	11:29AM
20	0.9	0.2	2	2	Wood Dowel	10:30AM
32	0.3	0.2	1.9	1.6	Wineglass	10:36AM
28	0.1	0.3	2	1.8	Spray Nozzle	10:41AM
42	0.2	0.1	2.1	2	Clothespeg	10:45AM
0	1.6	0.1	3.4	2.3	Wood Dowel	10:50AM
37	0.3	0.3	1	1	Wood Dowel	9:50AM
4	0.1	0	1.5	1	Wineglass	9:56AM
10	0.6	0.1	1	0.3	Spray Nozzle	10:02AM
0	3	0.1	3	1.1	Clothespeg	10:07AM
38	2	1	1	1	Wood Dowel	10:22AM

References

[1] A. K. Abbas, A. Lichtman, S. Pillai, Basic Immunology. Functions and disorders of the immune system, 4th ed., Saunders (Elsevier), 2012.

[2] M. P. H. I. Act, The personal health information act.
URL http://www.gov.mb.ca/health/phia/index.html

[3] D. Aletaha, T. Neogi, A. Silman, J. Funovits, D. Felson, C. Bingham, N. Birnbaum, G. Burmester, V. Bykerk, M. Cohen, B. Combe, K. Costenbader, M. Dougados, P. Emery, G. Ferraccioli, J. Hazes, K. Hobbs, T. Huizinga, A. Kavanaugh, J. Kay, T. Kvien, T. Laing, P. Mease, H. Menard, L. Moreland, R. Naden, T. Pincus, J. Smolen, E. Stanislawska-Biernat, D. Symmons, P. Tak, K. Upchurch, J. Vencovsky, F. Wolfe, G. Hawker, 2010 rheumatoid arthritis classification criteria, Arthritis & Rheumatism 62 (2010) 2569–2581.

[4] H. Anton, C. Rorres, Elementary Linear Algebra, 8th ed., John Wiley & Sons, 2000.

[5] A. T. Association, Telerehabilitation sig - american telemedicine association (April 2012).
URL http://www.americantelemed.org/i4a/pages/index.cfm?pageID=3328

[6] C. Atkeson, J. Hollerbach, Kinematic features of unrestrained vertical arm movements, The Journal of Neuroscience 5 (1985) 2138–2230.

[7] S. Bamberg, A. Benbasat, D. Scarborough, D. Krebs, J. Paradiso, Gait analysis using a shoe-integrated wireless sensor system, IEEE Transactions on Information Technology in Biomedicine 12 (2008) 413–423.

[8] D. Bionna, P. C. Zarkadas, J. S. Fitzsimmons, S. W. O'Driscoll, Validation of a photography-based goniometry method for measuring joint range of motion, Journal of Shoulder and Elbow Surgery 21 (1) (2012) 29–35.

[9] H. Blum, A transformation for extracting new descriptors of shape, Models for the Perception of Speech and Visual Form (1967) 362–380.

[10] R. Bootsma, L. Fernandez, D. Mottet, Behind fitts' law: kinematic patterns in goal-directed movements, Internation Journal of Human-Computer Studies 61 (2004) 811–821.

[11] R. Brown, Topology and Groupoids, 3rd ed., Booksurge Publishing, 2006.

[12] B. Bruce, J. Fries, The health assessment questionnaire (haq), Clinical and Experimental Rheumatology 23 (2005) 14–18.

[13] G. Burdea, V. Popescu, V. Hentz, K. Colbert, Virtual reality-based orthopedic telerehabilitation, IEEE Transactions on Rehabilitation Engineering 8 (2000) 430–432.

[14] M. Cadogan, C. Nickson, Life in the fast lane: Radiology image database, URL: http://lifeinthefastlane.com (2014).

[15] M. Cameirao, S. B. i Badia, E. Oller, P. Verschure, Neurorehabilitation using the virtual reality based rehabilitation gaming system: methodology, design, psychometrics, usability and validation, Journal of Neuroengineering and Rehabilitation 7 (2010) 1–14.

[16] C. Carignan, H. Krebs, Telerehabilitation robotics: Bright lights, big future?, Journal of Rehabilitation Research & Development 43 (5) (2006) 695–710.

[17] G. A. Caurin, A. A. Siqueira, K. O. Andrade, R. C. Joaquim, H. I. Krebs, Adaptive strategy for multi-user robotic rehabilitation games, in: 33rd Annual International Conference of the IEEE EMBS, 2011.

[18] G. G. Celesia, Visual perception and awareness, Journal of Psychophysiology 24 (2) (2010) 62–67.

[19] P. Chandrasoma, C. R. Taylor, Concise Pathology, McGraw-Hill, 1998.

[20] C.-M. Chang, Y.-C. Chang, H.-Y. C. L.-W. Chou, An interactive game-based shoulder wheel system for rehabilitation, Patient Preference and Adherence 6 (2012) 821–828.

[21] S. C. Chapra, R. P. Canale, Numerical Methods for Engineers with Programming and Software Applications, 3rd ed., WCB/McGraw-Hill, 1998.

[22] H. Cobe, The range of active motion at the wrist of white adults, Journal of Bone Joint Surgery 10 (1928) 763–774.

[23] J. D. Cutnell, K. W. Johnson, Physics, John Wiley & Sons, 1989.

[24] CyberGloveSystems, Cybergloves, URL: http://www.cyberglovesystems.com (2014).

[25] M. da Silva Cameiräo, Virtual reality based stroke neurorehabilitation development and assessment of the rehabilitation gaming system, Ph.D. thesis, Institució Catalana de Recerca i Estudis Avançats (2010).

[26] S. Deterding, D. Dixon, R. Khaled, L. Nacke, From game design elements to gamefulness: Defining ”gamification”, in: Proceedings of the 15th International Academic MindTrek Conference: Envisioning Future Media Environments. ACM, 2011.

[27] R. Duda, P. Hart, D. Stork, Pattern Classification, 2nd ed., John Wiley & Sons, Inc, 2001.

[28] W. Durfee, L. Savard, S. Weinstein, Technical feasibility of teleassessments for rehabilitation, IEEE Transactions on Neural Systems and Rehabilitation Engineering 15 (1) (2007) 23–29.

[29] W. Durfee, S. Weinstein, E. Bhatt, A. Nagpal, J. Carey, Design and usability of a home telerehabilitation ssystem to train hand recovery following stroke, Journal of Medical Devices 3 (2009) 1–8.

[30] J. Edwards, Case study: Denmark's achievements with healthcare information exchange, Tech. rep., Gartner Inc. (2006).
URL http://www-03.ibm.com/industries/ca/en/healthcare/files/gartner-case_study-denmarks_achievementswHIE.pdf

[31] V. A. Efremovič, The geometry of proximity, I, Mat. Sb (31) (1951) 189–200.

[32] M. eHealth, Manitoba ehealth (2012).
URL http://www.manitoba-ehealth.ca

[33] E. Eismann, A. Lucky, R. Cornwall, Hand function and quality of life in children with epidermolysis bullosa, Pediatric Dermatology 31 (2) (2014) 176–182.

[34] S. Ellis, L. Keswick, Medical art studio, URL: http://www.medicalartlibrary.com (2014).

[35] C. Enwemeka, Radiographic verification of knee goniometry, Scandinavian Journal of Rehabilitation Medicine 18 (1986) 47–49.

[36] F. H. Epstein, E. H. Choy, G. S. Panayi, Cytokine pathways and joint inflammation in rheumatoid arthritis, New England Journal of Medicine 344 (12) (2001) 907–916.

[37] G. Ferreiro, S. Vercelli, F. Sartorio, S. M. Lasa, E. Ilieva, E. Brigatti, C. Ruella, C. Foti, Reliability of a smartphone-based goniometer for knee joint goniometry, International Journal of Rehabilitation Research 36 (2013) 146–51.

[38] G. S. Firestein, R. C. Budd, E. D. H. Jr., I. B. McInnes, S. Ruddy, J. S. Sergent, Kelley's Textbook of Rheumatology: Chapter 66 - Clinical Features of Rheumatoid Arthritis, W.B. Saunders, imprint of Elsevier Inc., 2008.

[39] P. Fitts, The information capacity of the human motor system in controlling the amplitude of movement, Journal of Experimental Psychology 47 (6) (1954) 381–391.

[40] S. C. for Telehealth, Telecare, Scottish centre for telehealth and telecare.
URL http://www.sctt.scot.nhs.uk/

[41] I. for Work, Health, The dash outcome measure, PDF (2012).
URL http://www.dash.iwh.on.ca/

[42] M. Fréchet, Sur quelques points du calcul fonctionnel, Rendiconti del Circolo Metematico di Palermo 22 (1906) 1–72.

[43] M. Frize, C. Adea, P. Payeur, G. D. Primio, J. Karsh, A. Ogungbemile, Detection of rheumatoid arthritis using infrared imaging, in: Medical Imaging 2011: Image Processing, 2011.

[44] R. L. Gajdosik, R. W. Bohannon, Clinical measurement of range of motion review of goniometry emphasizing reliability and validity, Physical Therapy 67 (12) (1987) 1867–1872.

[45] L. Gamberini, G. Barresi, A. Majer, F. Scarpetta, A game a day keeps the doctor away: A short review of computer games in mental healthcare, Journal of CyberTherapy & Rehabilitation 1 (2008) 127–145.

[46] M. Genovese, Kelley's Textbook of Rheumatology: Chapter 67 - Treatment of Rheumatoid Arthritis, W.B. Saunders, imprint of Elsevier Inc., 2008.

[47] M. Golomb, S. Warden, E. Fess, B. Rabin, J. Yonkman, B. Shirley, G. Burdea, Maintained hand function and forearm bone health 14 months after an in-home virtual-reality videogame hand telerehabilitation intervention in an adolescent with hemiplegic cerebral palsy, Journal of Child Neurology 26 (2011) 389–393.

[48] R. Gonzalez, R. Woods, Digital Image Processing, 3rd ed., Pearson Prentice Hall, 2008.

[49] U. Grenander, General Pattern Theory. A Mathematical Study of Regular Structures, Clarendon Press Oxford Mathematical Monographs, 1994.

[50] Gyration, Gyration air mouse, URL: http://www.gyration.com (2014).

[51] J. Hamari, J. Koivisto, H. Sarsa, Does gamification work? - a literature review of empirical studies on gamification, in: Proceedings of the 47th Hawaii International Conference on System Sciences, 2014.

[52] G. Hamilton, P. Lachenbruch, Reliability of goniometers in assessing finger joint angle, Physical Therapy 49 (1969) 465–469.

[53] E. Hammond, B. Shay, T. Szturm, Objective evaluation of fine motor manipulation - a new clinical tool, Journal of Hand Therapy 22 (1) (2009) 28–36.

[54] R. M. Haralick, K. Shanmugam, I. Dinstein, Textural features for image classification, IEEE Transactions on Systems, Man and Cybernetics SMC-3 (6) (1973) 610–621.

[55] D. Henriques, J. Soechting, Approaches to the study of haptic sensing, Journal of Neurophysiology 93 (2005) 3036–3043.

[56] C. J. Henry, Near sets: Theory and applications, Ph.D. thesis, University of Manitoba (2010).

[57] A. Heuser, H. Kourtev, S. Winter, D. Fensterheim, G. Burdea, V. Hentz, P. Forducey, Telerehabilitation using the rutgers master ii glove following carpal tunnel release surgery: Proof-of-concept, IEEE Transactions on Neural Systems and Rehabilitation Engineering 15 (2007) 43–49.

[58] W. Hick, On the rate of gain of information, Quarterly Journal of Experimental Psychology 4 (1) (1952) 11–26.

[59] J. Hidler, P. Lum, The road ahead for rehabilitation robotics, Journal of Rehabilitation Research & Development 48 (2011) 7–10.

[60] A. Hoang-Kim, F. Pegreffi, A. Moroni, A. Ladd, Measuring wrist and hand function: Common scales and checklists, Injury, International Journal of the Care of the Injured 42 (2011) 253–258.

[61] K. Huotari, J. Hamari, Defining gamification: a service marketing perspective, in: Proceedings of the 16th International Academic MindTrek Conference. ACM, 2012.

[62] T. M. Inc., Matlab product help, Electronic (2012).
URL http://www.mathworks.com

[63] C. H. Infoway, Telehealth benefits and adoption connecting people and providers across canada, Tech. rep., Canada Health Infoway and Praxia Information Intelligence and Gartner Inc. (2011).
URL https://www2.infoway-inforoute.ca/Documents/telehealth_report_2010_en.pdf

[64] C. H. Infoway, Canada health infoway (2012).
URL https://www.infoway-inforoute.ca/lang-en

[65] T. T. Institute, The telerehabilitation institute.
URL http://www.ti.rutgers.edu/

[66] IntelPR, Ge and intel's telehealth and independent living company is operational today (January 2011).
URL http://newsroom.intel.com/community/intel_newsroom\/blog/2011/01/03/ge-and-intels-telehealth-\and-independent-living-company-is-operational-today

[67] C. Jadhav, P. Nair, V. Krovi, Individualized interactive home-based haptic telerehabilitation, IEEE Multimedia 13 (3) (2006) 32–39.

[68] A. K. Jain, A. Ross, S. Prabhakar, An introduction to biometric recognition, IEEE Transactions on Circuits and Systems for Video Technology 14 (2004) 4–21.

[69] L. Jansen, D. van Schaardenburg, I. van der Horst-Bruinsma, P. Bezemer, B. Dijkmans, Predictors of functional status in patients with early rheumatoid arthritis, Annals of the Rheumatic Diseases 59 (2000) 223–226.

[70] J. Jelsma, M. Pronk, G. Ferguson, D. Jelsma-Smit, The effect of the nintendo wii fit on balance control and gross motor function of children with spastic hemiplegic cerebral palsy, Developmental Neurorehabilitation 16 (1) (2013) 27–37.

[71] A. R. Jensen, Clocking the Mind, Elsevier Ltd., 2006.

[72] M. Johnson, Y. Shakya, E. Strachota, S. Ahamed, Low-cost monitoring of patients during unsupervised robot/computer assisted motivating stroke rehabilitation, Biomedizinische Technik - Biomedical Engineering 56 (2011) 5–9.

[73] M. J. Jones, J. M. Rehg, Statistical color models with application to skin detection, International Journal of Computer Vision 46 (1) (2002) 81–96.

[74] L. Y. Joo, T. S. Yin, D. Xu, E. Thia, P. F. Chia, C. W. K. Kuah, K. K. He, A feasibility study using interactive commercial off-the-shelf computer gaming in upper limb

rehabilitation in patients after stroke, Journal of Rehabilitation Medicine 42 (2010) 437–441.

[75] Joomla!, Joomla! content management system framework, Electronic (2012). URL http://www.joomla.org

[76] E. D. H. Jr., G. S. Firestein, Kelley's Textbook of Rheumatology: Chapter 66 - Clinical Features of Rheumatoid Arthritis, W.B. Saunders, imprint of Elsevier Inc., 2008.

[77] V. Kumar, A. K. Abbas, J. C. Aster, Robbins Basic Pathology, 9th ed., Saunders, an imprint of Elsevier Inc., 2013.

[78] B. Lange, S. Flynn, A. Rizzo, Game-based telerehabilitation, European Journal of Physical and Rehabilitation Medicine 45 (2009) 143–151.

[79] G. Lloyd-Jones, Radiology masterclass: Trauma x-ray - upper limb - hand/finger, URL: http://radiologymasterclass.co.uk (2014).

[80] D. Lockery, J. Peters, S. Ramanna, B. Shay, T. Szturm, Store-and-feedforward adaptive gaming system for hand-finger motion tracking in telerehabilitation, IEEE Transactions on Information Technology in Biomedicine 15 (2011) 467–473.

[81] D. Lockery, J. Peters, C. Taswell, Ctgaming: A problem oriented registry for clinical telegaming rehabilitation and intervention, Journal of Emerging Technologies in Web Intelligence 3 (1) (2011) 28–37.

[82] A. R. Luft, How to gain evidence in neurorehabilitation: a personal view, Biomedizinische Technik - Biomedical Engineering 57 (6) (2012) 427–433.

[83] J. MacQueen, Some methods for classification and analysis of multivariate observations, in: Proceedings of the Berkeley Symposium on Mathematical Statistics and Probability, vol. 1, 1967.

[84] V. Majithia, S. A. Geraci, Rheumatoid arthritis: Diagnosis and management, The American Journal of Medicine 120 (2007) 936–939.

[85] R. G. Marx, C. Bombardier, J. G. Wright, What do we know about the reliability and validity of physical examination tests used to examine the upper extremity?, The Journal of Hand Surgery 24A (1) (1999) 185–193.

[86] M. McLaughlin, R. Zimmermann, L. Liu, Y. Jung, W. Peng, S. Jin, J. Stewart, S. Yeh, W. Zhu, B. Seo, Integrated voice and haptic support for tele-rehabilitation, in: Proceedings of the Fourth Annual IEEE International Conference on Pervasive Computing and Communications Workshops 2006, 2006.

[87] V. Metsis, P. Jangyodsuk, V. Athitsos, M. Iversen, F. Makedon, Computer aided rehabilitation for patients with rheumatoid arthritis, in: 2013 International Conference on Computing, Networking and Communications (ICNC), 2013.

[88] D. Mottet, R. J. Bootsma, The dynamics of goal-directed rhythmical aiming, Biological Cybernetics 80 (1999) 235–245.

[89] S. Naimpally, Near and far. a centennial tribute to frigyes riesz, Siberian Electronic Mathematical Reports 6 (2009) A.1–A.10.

[90] S. Naimpally, B. Warrack, Proximity Spaces, Cambridge University Press, 1970.

[91] J. Nalepa, T. Grzejszczak, M. Kawulok, Real-time wrist localization in hand silhouettes, in: In proceedings of: Computer Recognition Systems, CORES 2013, 2013.

[92] V. Nell, K. Machold, G. Eberl, T. Stamm, M. Uffmann, J. Smolen, Benefit of very early referral and very early therapy with disease-modifying anti-rheumatic drugs in patients with early rheumatoid arthritis, Rheumatology 43 (2004) 906–914.

[93] F. H. Netter, Atlas of Human Anatomy, 5th ed., Saunders, 2010.

[94] K. Nieuwenhuisen, D. Aliakseyeu, J. Martens, Insight into goal-directed movement strategies, in: CHI 2010: Gesturing and Drawing, ACM, ACM, Atlanta, Georgia, USA., 2010.

[95] K. Nieuwenhuisen, J. Martens, L. Liu, R. van Liere, Insights from dividing 3d goal-directed movements into meaningful phases, IEEE Computer Graphics and Applications 29 (6) (2009) 44–53.

[96] N. G. Nijmegen, The disease activity score, Electronic (1980).
URL http://www.das-score.nl/

[97] J. Nirme, A. Duff, P. F. Verschure, Adaptive rehabilitation gaming system: On-line individualization of stroke rehabilitation, in: 33rd Annual International Conference of the IEEE EMBS, 2011.

[98] C. C. Norkin, D. J. White, Measurement of Joint Motion, 3rd ed., F. A. Davis Company, 2003.

[99] A. O'Brien, P. Jones, R. Mullis, D. Mulherin, K. Dziedzic, Conservative hand therapy treatments in rheumatoid arthritis - a randomized controlled trial, Rheumatology 45 (2006) 577–583.

[100] P. Oesch, S. Bachmann, Kelley's Textbook of Rheumatology: Chapter 64 - Introduction to Physical Medicine and Rehabilitation, W.B. Saunders, imprint of Elsevier Inc., 2008.

[101] M. Optics, Thermal imager, URL: www.muoptics.com (2014).

[102] C. Otto, Magnetic motion tracking system, Master's thesis, University of Manitoba (2007).

[103] D. Pani, G. Barabino, A. Dessi, I. Tradori, M. Piga, A. Mathieu, L. Raffo, A device for local or remote monitoring of hand rehabilitation sessions for rheumatic patients, Rehabilitation Devices and Systems 2.

[104] G. Pare, C. Sicotte, M. Chekli, M. Jaana, C. DeBlois, Evaluation of the impacts of a provider-focused telehomecare intervention: A pre-post study, in: the 42nd International Conference on System Sciences, 2009.

[105] H. Park, Q. Peng, L. Zhang, A portable telerehabilitation system for remote evaluations of impaired elbows in neurological disorders, IEEE Transactions on Neural Systems and Rehabilitation Engineering 16 (2008) 245–254.

[106] B. Parmanto, A. Saptono, Telerehabilitation: State-of-the-art from an informatics perspective, International Journal of Telerehabilitation.

[107] M. R. Peres (ed.), The Concise Focal Encyclopedia of Photography: From the First Photo on Paper to the Digital Revolution, 1st ed., Focal Press, 2007.

[108] P. Pergami, N. Seemaladinne, P. Martone, A pc-based motor control task for evaluation and serial monitoring of upper extremity motor function, Neuroinform 10 (2012) 323–328.

[109] J. Peters, Near sets. general theory about nearness of objects, Applied Mathematical Sciences 53 (1) (2007) 2609–2629.

[110] J. Peters, T. Szturm, M. Borkowski, D. Lockery, S. Ramanna, B. Shay, Pervasive Computing: Innovations in Intelligent Multimedia and Applications; Wireless Adaptive Therapeutic TeleGaming in a Pervasive Computing Environment, Springer-Verlag, 2009.

[111] J. F. Peters, Topology of Digital Images, Springer-Verlag, 2014.

[112] J. F. Peters, T. Szturm, M. Borkowski, D. Lockery, S. Ramanna, B. Shay, Pervasive Computing Computer Communication and Networks, chap. Wireless Adaptive Therapeutic TeleGaming in a Pervasive Computing Environment, Springer London, 2010, pp. 3–28.

[113] J. F. Peters, P. Wasilewski, Tolerance spaces: Origins, theoretical aspects and applications, Information Sciences 195 (2012) 211–225.

[114] C. L. Phillips, J. M. Parr, Signals, Systems, and Transforms, 2nd ed., Prentice Hall Inc., 1999.

[115] R. Plamondon, A. Alimi, Speed/accuracy trade-offs in target-directed movments, Behavioral and Brain Sciences 20 (1997) 279–349.

[116] J. Poole, Measures of hand function, Arthritis Care & Research 63 (2011) 189–199.

[117] J. G. Proakis, D. G. Manolakis, Digital Signal Processing. Principles, Algorithms and Applications, 3rd ed., Prentice Hall, Inc., 1996.

[118] D. Prochnow, S. B. i Badia, J. Schmidt, A. Duff, S. Brunheim, R. Kleiser, R. Seitz, P. Verschure, A functional magnetic resonance imaging study of visuomotor processing in a cirtual reality-based paradigm: Rehabilitation gaming system, European Journal of Neuroscience 37 (2013) 1441–1447.

[119] N. A. Punchard, C. J. Whelan, I. Adcock, Editorial: The journal of inflammation, Journal of Inflammation 1 (1).

[120] P. Rego, P. M. Moreira, L. P. Reis, Serious games for rehabilitation a survey and a classification towards a taxonomy, in: 5th Iberian Conference on Information Systems and Technologies, 2010.

[121] W. F. Riley, L. D. Sturges, Engineering Mechanics Statics, 2nd ed., John Wiley & Sons Inc., 1996.

[122] M. Rogante, M. Grigioni, D. Cordella, C. Giacomozzi, Ten years of telerehabilitation: A literature overview of technologies and clinical applications, NeuroRehabilitation 27 (2010) 287–304.

[123] J. Ruitenbeek, Invariants in loaded goal directed movements, Biological Cybernetics 51 (1984) 11–20.

[124] L. A. Ruiz, A. Fdez-Sarria, J. Recio, Evaluation of texture analysis techniques to characterize vegetation, Advances in Quantitative remote sensing (2002) 514–521.

[125] T. G. Russell, Physical rehabilitation using telemedicine, Journal of Telemedicine and Telecare 13 (2007) 217–220.

[126] N. Sattar, D. W. McCarey, H. Capel, I. B. McInnes, Explaining how "high-grade" systemic inflammation accelerates vascular risk in rheumatoid arthritis, Circulation 108 (24) (2003) 2957–2963.

[127] A. Scott, K. Khan, J. Cook, V. Duranio, What is "inflammation"? are we ready to move beyond celsus?, British Journal of Sports Medicine 38 (2004) 248–249.

[128] D. Scott, K. Pugner, K. Kaarela, D. Doyle, A. Woolf, J. Holmes, K. Hieke, The links between joint damage and disability in rheumatoid arthritis, Rheumatology 39 (2000) 122–132.

[129] C. Shannon, A mathematical theory of communication, Bell System Technical Journal 27 (3) (1948) 379–423.

[130] M. Sharma, S. Singh, Evaluation of texture methods for image analysis, in: In proceedings of the 7th Australian and New Zealand Intelligent Information Systems Conference, 2001.

[131] M. Shauver, The michigan hand outcomes questionnaire, Electronic (2012).
URL http://sitemaker.umich.edu/mhq/overview

[132] J.-H. Shin, H. Ryu, S. H. Jang, A task-specific interactive game-based virtual reality rehabilitation system for patients with stroke: a usability test and two clinical experiments, Journal of NeuroEngineering and Rehabilitation 11 (32).

[133] A. K. Singh, A. K. Agrawal, C. B. Pal, Hand geometry verification system: A review, in: International Conference on Ultra Modern Telecommunications & Workshops, 2009.

[134] L. Sledziewski, R. C. Schaaf, J. Mount, Use of robotics in spinal cord injury: A case report, The Ameriacn Journal of Occupational Therapy 66 (2012) 51–58.

[135] R. Smith, J. Dias, A. Ullah, B. Bhowal, Visual and computer software-aided estimates of dupuytren's contractures: Correlation with clinical goniometric measurements, Annals of the Royal College of Surgeons of England 91 (4) (2009) 296–300.

[136] T. A. Society, T. C. R. Society, Rheumatoid arthritis know your options (2011). URL http://www.arthritis.ca/local/files/pdf%20documents/Types%20of%20Arthritis/TAS_RA_eBROCH_ENG.pdf

[137] G. Song, S. Guo, Development of a novel tele-rehabilitation system, in: Proceedings of the 2006 IEEE International Conference on Robotics and Biomimetics, Kunming, China, 2006.

[138] C. S. Srikesavan, B. Shay, D. B. Robinson, T. Szturm, Task-oriented training with computer gaming in people with rheumatoid arthritis or osteoarthritis of the hand: study protocol of a randomized controlled pilot trial, Trials Open Access Journal 14 (69) (2013) 1–12.

[139] A. Stenger, M. V. Leeuwen, P. Houtman, G. Bruyn, F. Speerstra, B. Barendsen, E. Velthuysen, M. V. Rijswijk, Early effective suppression of inflammation in rheumatoid arthritis reduces radiographic progression, British Journal of Rheumatology 37 (1998) 1157–1163.

[140] E. E. Stone, M. Skubic, Unobtrusive, continuous, in-home gait measurement using the microsoft kinect, IEEE Transactions on Biomedical Engineering 60 (10) (2013) 2925–2932.

[141] R. S. Sutton, A. G. Barto, Reinforcement Learning An Introduction, MIT Press Cambridge, Massachusetts, 1998.

[142] A. Technologies, Ascension technologies (2012).
URL http://www.ascension-tech.com/

[143] M. Telehealth, Manitoba telehealth (2012).
URL http://www.mbtelehealth.ca

[144] S. Thorpe, D. Fize, C. Marlot, Speed of processing in the human visual system, Nature 381 (6582) (1996) 520–522.

[145] D. W. Trim, Calculus for Engineers, Prentice Hall Inc., 1998.

[146] J. Trommershauser, L. Maloney, M. Landy, Statistical decision theory and the selection of rapid, goal-directed movements, Journal of the Optical Society of America A 20 (2003) 1419–1433.

[147] T. R. Unit, Telerehabilitation research unit.
URL http://www.uq.edu.au/telerehabilitation/

[148] M. van den Berg, H. Ronday, A. Peters, S. le Cessie, F. van der Giesen, F. Breedveld, T. V. Vlieland, Using internet technology to deliver a home-based physical activity intervention for patients with rheumatoid arthritis: A randomized controlled trial, Arthritis & Rheumatism (Arthritis Care & Research) 55 (2006) 935–945.

[149] E. van Trijffel, R. J. van de Pol, R. A. Oostendorp, C. Lucas, Inter-rater reliability for measurement of passive physiological movements in lower extremity joints is generally low: a systematic review, Journal of Physiotherapy 56 (2010) 223–235.

[150] L. Virtual Realities, Data gloves, URL: http://www.vrealities.com/products/data-gloves (2014).

[151] L. Warren, Encyclopedia of 20th century photography, Routledge, 2006.

[152] J. M. Winters, Telerehabilitation research: Emerging opportunities, Annual Review of Biomedical Engineering 4 (2002) 287–320.

[153] R. Woodworth, The accuracy of voluntary movement, Psychology Review 3 (1899) 1–106.

[154] A. Young, J. Dixey, N. Cox, P. Davies, J. Devlin, P. Emery, S. Gallivan, A. Gough, D. James, P. Prouse, P. Williams, J. Winfield, How does functional disability in early rheumatoid arthritis (ra) affect patients and their lives? results of 5 years of follow-up in 732 patients from the early ra study (eras), Rheumatology 39 (2000) 603–611.

[155] F. Zaal, R. Bootsma, P. van Wieringen, Dynamics of reaching for stationary and moving objects: Data and model, Journal of Experimental Psychology 25 (1999) 149–161.

Index